UNIVERSITY OF CALIFORNIA,
IRVINE

Controllers for Systems with Bounded Actuators: Modeling and control of an F-16 aircraft

THESIS

submitted in partial satisfaction of the requirements
for the degree of

MASTER OF SCIENCE

in Mechanical and Aerospace Engineering

by

Albert Farré Gabernet

Thesis Committee:

Professor Faryar Jabbari, Chair
Professor Kenneth Mease
Professor James E. Bobrow

2007

The thesis of Albert Farré Gabernet is approved:

_____

_____

_____

Committee Chair

University of California, Irvine

2007

Table of Contents

List of Figures vi

List of Tables ix

List of Notations x

Acknowledgements xii

Abstract of the Thesis xiii

1 Introduction 1

2 Modeling of an F-16 aircraft 4

2.1 Nonlinear 6 degree-of-freedom aircraft model 4

2.1.1 Engine model 8

2.2 Longitudinal model 13

2.2.1 Aircraft description 14

2.2.2 Aerodynamic data 15

2.3 Linear model 16

2.3.1 Obtention of an initial condition 16

2.3.2 Linearizing around the initial condition 18

2.4 Validation 18

3 Linear Parameter Varying (LPV) systems 35

3.1 LPV basics 36

3.2 LPV model of the F-16 aircraft 37

4 Controller design 45

4.1 Saturation control background 45

4.2 Anti-saturation LMIs: basic equations 48

4.2.1 LMI introduction 49

4.2.2 Invariant-set LMI 50

4.2.3 Constraint LMI 52

4.2.4 Performance LMI 53

4.3 Scheduling design technique 54

4.3.1 Conservatism associated with the design technique 55

4.3.2 Gain scheduling technique to overcome conservatism 58

4.4 Approach for tracking of general signals 61

5 Simulations 64

5.1 Problems setup 65

5.1.1 Inclusion of the elevator actuator 65

5.1.2 Turbulence model for the altitude hold problem 67

5.1.3 Rearranging the equations for the tracking problem 69

5.1.4 Adjusting the controller design technique 73

5.2 Altitude hold 78

5.3 Tracking 82

6 Conclusions **107**

Bibliography **110**

List of Figures

2.1 Definition of roll, yaw and pitch angles and main control surfaces in a general aircraft 5

2.2 Definition of axes and aerodynamic angles (obtained from [13]) 6

2.3 Scheme of the engine model used with the functions $TGEAR$, $PDOT$ and $THRUST$. Dashed circles show the inputs, plain circles show the outputs. 9

2.4 Relationship between the throttle setting and the engine power level. Note the change in slope around $\delta_{th} = 0.77$ 11

2.5 Scheme of the thrust vectoring and its relevant angles 12

2.6 Relevant angles and axes in the longitudinal model 24

2.7 Scheme of the longitudinal model of the aircraft with and without the thrust vectoring 24

2.8 Nonlinear longitudinal model of the $F-16$ aircraft implemented in Simulink® 25

2.9 Plots of the different aerodynamic coefficients 26

2.10 Perturbation of the input commands used to validate the linear model 27

2.11 Time responses for a perturbation in δ_e at $V = 160ft/s$ and $\alpha = 35.01°$ 28

2.12 Time responses for a perturbation in δ_{th} at $V = 160ft/s$ and $\alpha = 35.01°$ 29

2.13 Perturbation of the input commands used to validate the linear model without engine 30

2.14 Time responses for a perturbation in δ_e at $V = 160ft/s$ and $\alpha = 35.01°$ (linearization without the engine model) 31

2.15 Time responses for a perturbation in T at $V = 160ft/s$ and $\alpha = 35.01°$ (linearization without the engine model) 32

2.16 Time responses for a perturbation in δ_e at $V = 200ft/s$ and $\alpha = 22.46°$ (linearization without the engine model) 33

2.17 Time responses for a perturbation in T at $V = 200ft/s$ and $\alpha = 22.46°$ (linearization without the engine model) 34

3.1 Scheme of the LPV model 38

3.2 Time responses for a perturbation in δ_e at $V = 180ft/s$ and $\alpha = 33.5°$ (linear system obtained using an LPV model) 42

3.3 Time responses for a perturbation in δ_e at $V = 180ft/s$ and $\alpha = 33.5°$ (linear system obtained using an LPV model) 43

3.4 Extended scheme of the LPV model, in which the LPV region consists on different squares with coincident sides 44

4.1 Plot of the saturation effect 46

4.2 Scheme of a plant with an open loop controller and a representation of the actuator. The actuator is represented by a saturation block and a delay transfer function 47

4.3 Estimate for the smallest invariant set associated with ω_{max} without actuator limits (large ellipsoid) and ω_{nom} (small ellipsoid) for K_{nom}. Parallel lines show region where K_{nom} is not saturated (figure obtained from [17]) 56

4.4 Importance of the condition (4.24). On the left, the system may find a way to escape the safe controller and therefore it may become uncontrollable. On the right, this possibility does not exist. 57

4.5 Invariant set associated with ω_{max} and K_{safe} compared to linear case (figure obtained from [17]) 58

5.1 Scheme of the elevator actuator 66

5.2 Bode plot of the elevator actuator 68

5.3 Probability of exceedance of turbulence intensity as a function of altitude 70

5.4 Effect of expanding the saturation limits, showing how $P_{nom,max}$ includes $P_{nom,min}$ ($u_{lim,min} \leq u_{lim,max}$) 75

5.5 Plot of the wind velocity obtained from a moderate disturbance and the open loop response (altitude) of the linear model of the aircraft to this disturbance 80

5.6 Plot of the wind velocity obtained from a moderate disturbance and the closed loop response (altitude) of the linear model of the aircraft to this disturbance 92

5.7 Plot of the wind velocity obtained from an extreme disturbance and the closed loop response (altitude) of the linear model of the aircraft to this disturbance 93

5.8 Effect of the transfer function in (5.27) to the commanded flight path angle γ_{cmd} (the amplitude of γ_{cmd} may vary depending on the case of study) 94

5.9 Nonlinear $\pm 1.5^\circ$ doublet response (stable case) with K_{nom} 95

5.10 Nonlinear $\pm 3^\circ$ doublet response (stable case) with K_{nom} 96

5.11 Nonlinear $\pm 3^\circ$ doublet response (stable case) with K_{nom} and K_{safe} . . 97

5.12 Nonlinear $\pm 3^\circ$ doublet response (stable case) with K_{nom}, K_1, K_2 and K_{safe} 98

5.13 Nonlinear $\pm 5^\circ$ doublet response (stable case) with K_{nom}, K_1, K_2 and K_{safe} 99

5.14 For comparison purposes: nonlinear $\pm 1^\circ$ doublet response (stable case) with an LTI nominal controller (extracted from [13]) 100

5.15 For comparison purposes: nonlinear $\pm 2^\circ$ doublet response (stable case) with/without an LTI antiwindup compensator (extracted from [13]) . 101

5.16 Nonlinear $\pm 1.5^\circ$ doublet response (unstable case) with K_{nom} 102

5.17 Nonlinear $\pm 3^\circ$ doublet response (unstable case) with K_{nom} 103

5.18 Nonlinear $\pm 3^\circ$ doublet response (unstable case) with K_{nom} and K_{safe} 104

5.19 Nonlinear $\pm 3^\circ$ doublet response (unstable case) with K_{nom}, K_1, K_2 and K_{safe} 105

5.20 Nonlinear $\pm 3.5^\circ$ doublet response (unstable case) with K_{nom}, K_1, K_2 and K_{safe} 106

List of Tables

2.1 Mass and geometric properties of the aircraft 15

2.2 Models of the control actuators 15

2.3 Engine thrust saturation limits 21

5.1 Maximum peak values of the disturbance for a $\pm 5^\circ$ doublet 85

5.2 Maximum peak values of the disturbance for a $\pm 3.5^\circ$ doublet 89

List of Notations

U	component of velocity along x body axis (ft/s)
V	component of velocity along y body axis (ft/s)
W	component of velocity along z body axis (ft/s)
P	roll rate about x body axis (rad/s)
Q or q	pitch rate about y body axis (rad/s)
R	yaw rate about z body axis (rad/s)
F_x^G,F_y^G,F_z^G	gravitational forces along x, y, z body axes (lb)
F_x^A,F_y^A,F_z^A	aerodynamic forces along x, y, z body axes (lb)
F_x^T,F_y^T,F_z^T	propulsive forces along x, y, z body axes (lb)
F_x,F_y,F_z	total forces along x, y, z body axes (lb)
m	mass of the aircraft $(slug)$
W	weight of the aircraft (lb)
θ	angle (pitch) of the aircraft body axes relative to a plane normal to the earth radius at the point the aircraft is at(local horizon) (rad)
ϕ	angle (roll) of the aircraft (rad)
ψ	angle (yaw) of the aircraft that corresponds to the true heading of the aircraft (rad)
θ,ϕ,ψ	Euler angles (rad)
J_x	moment of inertia about x body axis $(slug \cdot ft^2)$
J_y	moment of inertia about y body axis $(slug \cdot ft^2)$
J_z	moment of inertia about z body axis $(slug \cdot ft^2)$
J_{xz}	cross product of inertia about x and y axes $(slug \cdot ft^2)$
M_x^T, M_y^T, M_z^T	moments produced by the propulsive forces about the body axes $(slug \cdot ft)$
M_x^A, M_y^A, M_z^T	moments produced by the aerodynamic forces about the body axes $(slug \cdot ft)$
M_x, M_y, M_z	resultant of moments about the body axes $(slug \cdot ft)$
p_N	geographic coordinate (corresponding to the geographic coordinate system) that aligns north (ft)
p_E	geographic coordinate (corresponding to the geographic coordinate system) that aligns east (ft)
h	altitude of the aircraft (ft)
g	constant of gravity (ft/s^2)
$\bar{q}$	dynamic pressure (lb/ft^2)

S	wing area (ft)
T	thrust force (lb)
b	wing span (ft)
$\bar{c}$	mean aerodynamic chord of the wing (ft)
$C_{l,t}$	total rolling moment coefficient
$C_{m,t}$	total pitching moment coefficient
$C_{n,t}$	total yawing moment coefficient
$C_{x,t}$	total force coefficient in x body axis
$C_{y,t}$	total force coefficient in y body axis
$C_{z,t}$	total force coefficient in z body axis
V_T	true velocity of the aircraft (ft/s)
α	angle of attack angle, considered one of the aerodynamic angles (rad)
β	sideslip angle, considered one of the aerodynamic angles (rad)
C_m	pitching moment coefficient about y body axis
C_{mq}	pitching moment derivative with respect to the pitch rate (rad^{-1})
C_x	aerodynamic force coefficient in x body axis
C_{xq}	aerodynamic stability derivative along x axis with respect to pitch rate (rad^{-1})
C_z	aerodynamic force coefficient in z body axis
C_{zq}	aerodynamic stability derivative along z axis with respect to pitch rate (rad^{-1})
δ_{th}	throttle setting (one of the control surfaces of the aircraft)
δ_e	elevator angle (one of the control surfaces of the aircraft) (rad)
δ_{ptv}	angle (pitch) of the thrust force with the xy body plane due to thrust vectoring (rad)
δ_{ytv}	angle (yaw) of the thrust force with the xz body plane due to thrust vectoring (rad)
l_T	distance between the aircraft center of gravity and the point of application of the engine thrust force (ft)
x_{cg}	coordinates of the center of gravity of the aircraft (ft)
$x_{cg,ref}$	reference position of the center of gravity of the aircraft for aerodynamic data (ft)
γ	flight path angle (rad)
Δ	distance between the reference and the actual position of the center of gravity (ft)
x_T	coordinates of the point of application of the engine thrust force (ft)

Acknowledgments

I would like to thank my advisor Professor Faryar Jabbari for his support during my study, his advice and his dedication. Equally, I would like to thank Mr. Pete Balsells for offering me the opportunity to come to the University of California, Irvine to pursue graduate studies through the Balsells Fellowship Program.

Also, I would like to thank Professor Roger Rangel for his support and dedication as the Director of the Balsells Fellowship Program and to the members of the Control Lab for their help and hospitality. Thanks also to the rest of my committee members, Professor Kenneth Mease and Professor James E. Bobrow.

Finally, special thanks to my family for their unconditional support and to all my friends in the US who made my stay in California so special.

Abstract of the Thesis

Controllers for Systems with Bounded Actuators: Modeling and control of an F-16 aircraft

by

Albert Farré Gabernet

Master of Science in Mechanical and Aerospace Engineering

University of California, Irvine, 2007

Professor Faryar Jabbari, Chair

Actuator capacity limitation has been a major topic of control research in recent decades and plays a major role in the flight control system design area, specially in the high angle of attack region. The development of linear matrix inequalities (LMIs) and other optimization techniques provided a new framework that facilitates the design of controllers dealing with saturation, making it easier to obtain stability and performance guarantees for the designed controllers. These saturation techniques can be classified into two groups: anti-windup and direct approach. Recently, a new method combining both groups has been proposed in [17] for the disturbance attenuation problem, although it can be easily extended to include the tracking problem. This thesis will show the potential of this new combined technique applied to common aircraft problems (altitude hold and tracking a reference command) in which saturation problems have been reported.

Chapter 1

Introduction

Actuator capacity limitation has been a major topic of research in recent decades. Saturation occurs when an actuator reaches its maximum magnitude or rate capacity and is not able to provide the desired control demands of the compensator. The result of actuator saturation is a degraded performance of the system and often the system is driven to instability.

One field in which saturation plays a main role is flight control system design, specially in the high angle of attack region. High angle of attack flight is used to reduce the landing distance, to avoid collision with the terrain when following and in evasive maneuvers, among others. The saturation of the control surfaces in this region compromise these desirable properties, often severely, with catastrophic outcomes. Another well known problem related to saturation in aircrafts is the pilot induced oscillation (PIO), attributed to the magnitude and rate limitation of control surface deflectors.

Historically, most of the techniques used to deal with saturation were based on ad hoc techniques, often relying on practical experience. These techniques required extensive simulations and testing, which was both expensive and time consuming, because they did not provide rigorous stability and performance guarantees. Recently,

the development of linear matrix inequalities (LMIs) and other optimization techniques have provided a framework in which the stability and performance guarantees are more rigorous than in the past.

The techniques used to deal with saturation can be classified into two groups. The first group uses the so-called anti-windup scheme, which consists on an augmentation on top of a nominal controller that was designed without taking saturation into account. Once the nominal controller saturates, the anti-windup scheme tries to modify the value of the control signal such that the closed loop system behaves well. It is the most extended approach to avoid saturation problems in control design, specially in cases in which saturation is not likely to occur because the nominal controller is used most of the time. The second group can be called the direct approach method, in which saturation of the controller is taken into account from the beginning of the design process. In this approach, controllers are designed in order to avoid saturation even for the worst-case scenario (e.g. worst case disturbance). Since this worst case may not occur, it is usually a conservative method.

Recently, a new method combining both design schemes has been proposed in [17] for the disturbance attenuation problem. The main advantage of this method is that it can be applied to unstable systems and that it can be extended, in a straightforward fashion, to include some level of controller scheduling in order to reduce conservatism.

Therefore, the objective of this thesis is to demonstrate the potential of this new method applied to flight control system design. Two main maneuvers are simulated with the objective to saturate the control surfaces and check the performance of this new technique: altitude hold (disturbance attenuation problem) and flight path angle tracking (model following problem).

This thesis is organized as follows.

In chapter 2 a longitudinal nonlinear model of an $F-16$ aircraft is developed and implemented using Matlab® and Simulink®. The equations used and the assumptions considered are shown, as well as the linearization and validation processes.

Chapter 3 explains the linear parameter varying systems concept (LPV) and discusses its usefulness to extend the linear models obtained in the previous chapter. Basically, it allows to obtain a model of the airplane not only about one equilibrium point but also about a region delimited by different equlibrium points.

Chapter 4 gives an introduction to linear matrix inequalities (LMIs) and discusses the conservatism of the direct approach. Then, the new technique combining anti-windup and direct approach is shown, extending it with scheduling in order to reduce conservatism. This technique is also extended to include the tracking problem.

Finally, chapter 5 shows the results obtained in the simulations and chapter 6 gives the main conclusions of this thesis.

Chapter 2

Modeling of an F-16 aircraft

Modeling is one of the most important parts in control engineering. It allows to mathematically represent the desired system and simulate it via appropriate simulation programs. This way, computer simulations can be run and the controllers can be tested.

In this section, a nonlinear model of an F-16 aircraft will be studied. First, a general 6 degree-of-freedom (DOF) model is shown and then reduced to a decoupled longitudinal 3 DOF model.

2.1 Nonlinear 6 degree-of-freedom aircraft model

According to [18] and [13], the equations of motion of an aircraft in the body-fixed reference axes can be expressed as:

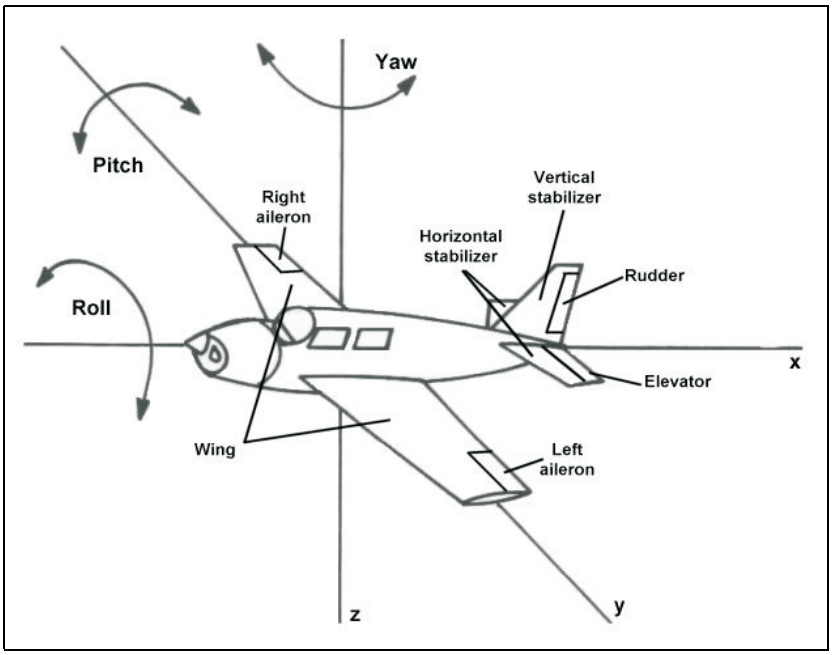

Figure 2.1: Definition of roll, yaw and pitch angles and main control surfaces in a general aircraft

FORCE EQUATIONS

$$\dot{U} = RV - QV - \frac{F_x^G}{m} + \frac{F_x^A}{m} + \frac{F_x^T}{m} \tag{2.1}$$

$$\dot{V} = -RU + PW + \frac{F_y^G}{m} + \frac{F_y^A}{m} + \frac{F_y^T}{m} \tag{2.2}$$

$$\dot{W} = QU - PV + \frac{F_z^G}{m} + \frac{F_z^A}{m} + \frac{F_z^T}{m} \tag{2.3}$$

KINEMATIC EQUATIONS

$$\dot{\phi} = P + Q\,sin\phi\,tan\theta + R\,cos\phi\,tan\theta \tag{2.4}$$

$$\dot{\theta} = Q\,cos\phi - R\,sin\phi \tag{2.5}$$

$$\dot{\psi} = Q\,sin\phi\,sec\theta + R\,cos\phi\,sec\theta \tag{2.6}$$

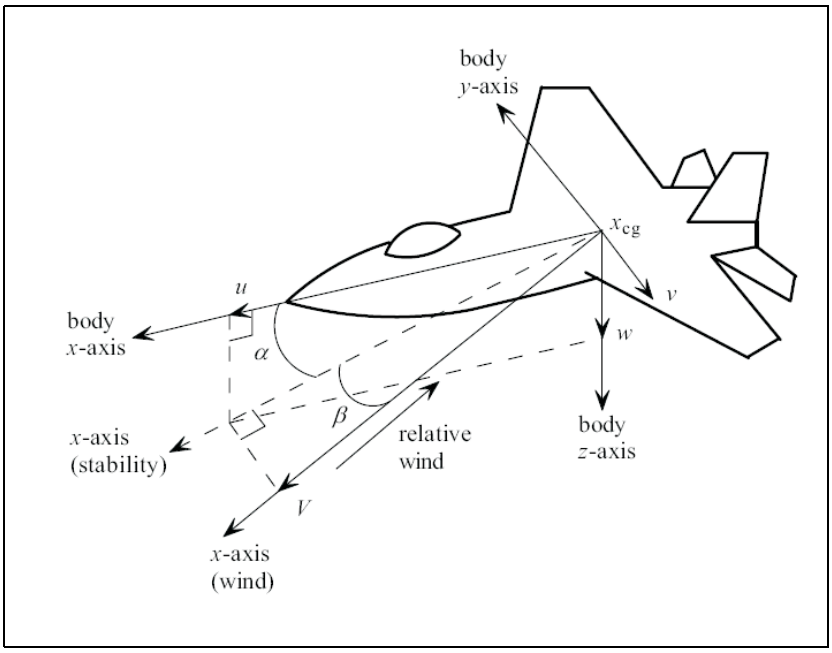

Figure 2.2: Definition of axes and aerodynamic angles (obtained from [13])

MOMENT EQUATIONS

$$\Gamma\dot{P} = J_{xz}(J_x - J_y + J_z)PQ - [J_z(J_z - J_y) + J_{xz}^2]QR + J_z M_x + J_{xz} M_z \tag{2.7}$$

$$J_y\dot{Q} = (J_z - J_x)PR - J_{xz}(P^2 - R^2) + M_y \tag{2.8}$$

$$\Gamma\dot{R} = [(J_x - J_y)J_x + J_{xz}^2]PQ - J_{xz}(J_x - J_y + J_z)QR + J_{xz} M_x + J_x M_z \tag{2.9}$$

$$\Gamma = J_x J_z - J_{xz}^2 \tag{2.10}$$

NAVIGATION EQUATIONS

$$\dot{p}_N = Uc\theta c\psi + V(s\phi s\theta c\psi - c\phi s\psi) + W(s\phi s\psi + c\phi s\theta c\psi) \tag{2.11}$$

$$\dot{p}_E = Uc\theta c\psi + V(c\phi c\psi + s\phi s\theta s\psi) + W(c\phi s\theta s\psi - s\phi c\psi) \tag{2.12}$$

$$\dot{h} = Us\theta - Vs\phi c\theta - Wc\phi c\theta \tag{2.13}$$

The forces acting on the aircraft can be separated into aerodynamic, gravitational and propulsive forces. Same concept applies to the moments acting on the aircraft. The definitions of the forces and moments used in equations (2.1) to (2.13) are:

Gravitational forces

$$\begin{pmatrix} F_x^G \\ F_y^G \\ F_z^G \end{pmatrix} = -mg \begin{pmatrix} sin\theta \\ cos\theta\, sin\phi \\ cos\theta\, cos\phi \end{pmatrix} \tag{2.14}$$

Aerodynamic forces

$$\begin{pmatrix} F_x^A \\ F_y^A \\ F_z^A \end{pmatrix} = \bar{q}S \begin{pmatrix} C_{x,t} \\ C_{y,t} \\ C_{z,t} \end{pmatrix} \tag{2.15}$$

Propulsive forces

$$\begin{pmatrix} F_x^T \\ F_y^T \\ F_z^T \end{pmatrix} = \begin{pmatrix} T \\ 0 \\ 0 \end{pmatrix} \tag{2.16}$$

Total forces

$$\begin{pmatrix} F_x \\ F_y \\ F_z \end{pmatrix} = \bar{q}S \begin{pmatrix} F_x^G + F_x^A + F_x^T \\ F_y^G + F_y^A + F_y^T \\ F_z^G + F_z^A + F_z^T \end{pmatrix} \tag{2.17}$$

Aerodynamic moments

$$\begin{pmatrix} M_x^A \\ M_y^A \\ M_z^A \end{pmatrix} = \begin{pmatrix} bC_{l,t} \\ \bar{c}C_{m,t} \\ bC_{n,t} \end{pmatrix} \tag{2.18}$$

For purposes of linearizing the equations of motion and studying the dynamic behavior, it is recommended to have the velocity equations expressed in wind or stability axes variables, which are the true airspeed and the aerodynamic angles of the aircraft axes with respect to the wind axes (V_T, α and β) (2.19)-(2.21). The stability reference frame is an special frame fixed in the body that is used in the study of small deviations from a nominal flight condition. It differs from the body frame shown in (2.2) because the x-axis is chosen as the projection of the aircraft true velocity into the plane defined by the body axes XZ (the y-axis of this stability frame coincides with the body y-axis). The wind frame has its x-axis in the direction of the aircraft's true velocity and the z-axis is the same as the body z-axis.

$$V_T = \sqrt{U^2 + V^2 + W^2} \tag{2.19}$$

$$\alpha = tan^{-1}\Big(\frac{W}{U}\Big) \tag{2.20}$$

$$\beta = sin^{-1}\Big(\frac{V}{V_T}\Big) \tag{2.21}$$

Using the definitions (2.19) to (2.21), we can rewrite the force equations (2.1) to (2.3) with the new states:

$$\dot{V_T} = \frac{1}{m}(F_x c\alpha\, c\beta + F_y s\beta + F_z c\beta\, s\alpha) \tag{2.22}$$

$$\dot{\beta} = \frac{1}{mV_T}(-F_x c\alpha\, s\beta + F_y c\beta - F_z s\alpha\, s\beta) + P\, s\alpha - R\, c\alpha \tag{2.23}$$

$$\dot{\alpha} = \frac{1}{mV_T}\Big(- Fx\frac{s\alpha}{c\beta} + F_z\frac{c\alpha}{c\beta}\Big) - P\, c\alpha\, tan\beta + Q - R\, s\alpha\, tan\beta \tag{2.24}$$

2.1.1 Engine model

The engine of an F-16 aircraft is an afterburning turbofan engine. A model of this engine is included in [12] and can be also found in [18]. A scheme of this model is

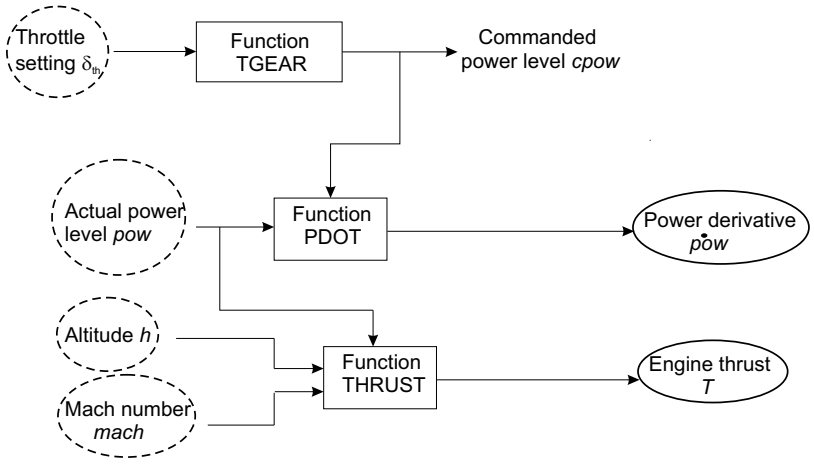

Figure 2.3: Scheme of the engine model used with the functions $TGEAR$, $PDOT$ and $THRUST$. Dashed circles show the inputs, plain circles show the outputs.

represented in figure (2.3). It consists on three different functions ($TGEAR$, $PDOT$ and $THRUST$) that will be explained next. The inputs to the model are the desired thrust setting δ_{th} (set by the pilot), the altitude h, the mach number $mach$ (function of velocity) and the actual state of the engine pow.

First, the control command from the pilot to the engine enters the function $TGEAR$. This command is the throttle setting δ_{th}, which can take values between 0 and 1 ($0 \leq \delta_{th} \leq 1$). This function establishes a linear relationship between the throttle setting and the commanded engine power level, with a change in slope when the engine reaches the military power level at $\delta_{th} = 0.77$ (see figure (2.4)).

The response of the aircraft to this commanded engine power level is modeled as a first-order lag with a time constant (tau) that depends on the actual power level of the engine (pow) and on the commanded power ($cpow$). This is modeled in function $PDOT$, which output is the derivative of the actual power of the engine $\dot{pow}$, that is, the rate of change of power. The function $PDOT$ is shown next together with the auxiliary function TC in the next page.

Finally, the function $THRUST$ calculates the actual engine thrust T (in lb) resulting from the actual power of the engine. This final thrust depends on the actual power level pow, the Mach number and the altitude. There are three lookup tables

containing this data, depending on the power level at which the engine is working: idle, military or maximum. These tables can be found in [18].

Since the final thrust depends on the actual power level, the actual power level has to be included in the state vector of the system. This state is called pow, is dimensionless and ranges from 0 to 100. The variations in time of pow depend on the thrust setting δ_{th} set by the pilot and the algorithm in function $PDOT$.

$FUNCTION \quad PDOT \quad (\, cpow\,,\, pow\,)$

if $(cpow \geq 50.0)$ **then**
  if $(pow \geq 50.0)$ **then**
    $tau = 5.0$
    $paux = cpow$
  else
    $paux = 60.0$
    $tau = tc(paux - pow)$
  end
else
  if $(pow \geq 50.0)$ **then**
    $tau = 5.0$
    $paux = 40.0$
  else
    $paux = cpow$
    $tau = tc(paux - pow)$
  end
end

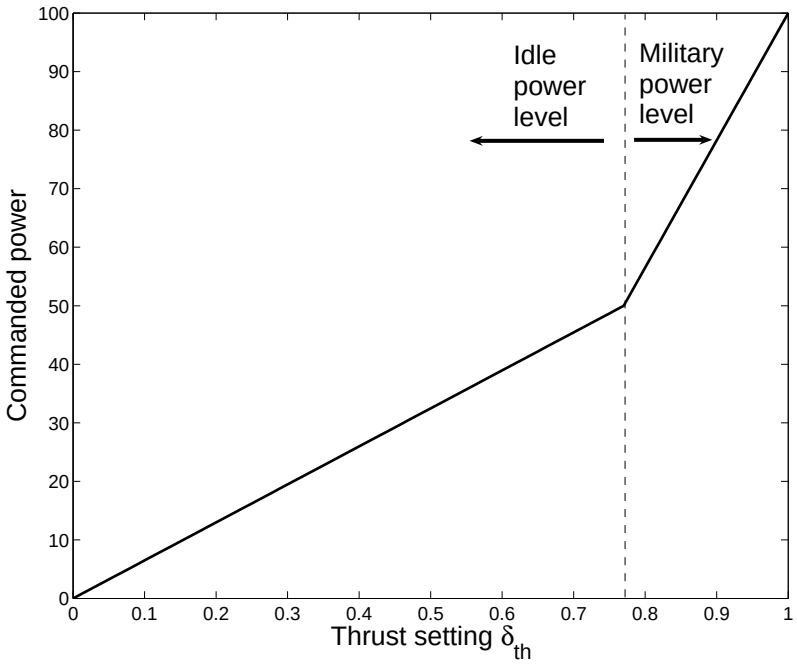

Figure 2.4: Relationship between the throttle setting and the engine power level. Note the change in slope around $\delta_{th} = 0.77$

$$FUNCTION \quad TC \quad (\, pow\_diff \,)$$

if $(pow\_diff \leq 25.0)$ **then**

$tau\_aux = 1.0$

else if $(pow\_diff \geq 50.0)$ **then**

$tau\_aux = 0.1$

else

$tau\_aux = 1.9 - 0.036 * pow\_diff$

end

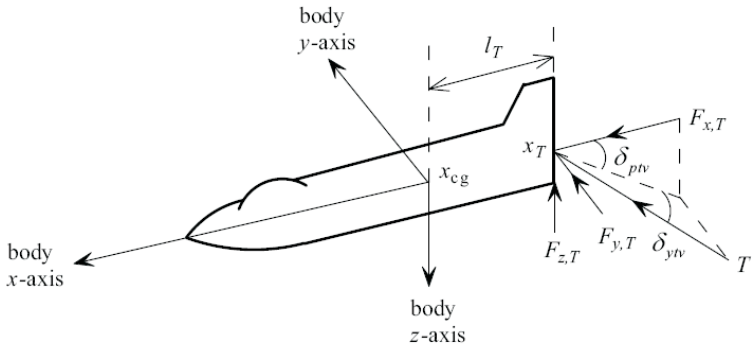

Figure 2.5: Scheme of the thrust vectoring and its relevant angles

Thrust vectoring model

In the high angle of attack region, the usual control surfaces of the aircraft may not be sufficient to control the aircraft and obtain the desired performance. Vectoring the thrust is one option to extend the capabilities of the aircraft in this region.

Usually, the thrust of the engine is directed through the body x-axis. Therefore, the propulsive force of the engine has only one component in this axis, having no effect on the other axes (check equation (2.16)). By vectoring the thrust, we are able to direct this propulsive thrust into any direction. The main benefit is that now the propulsive force of the engine has components in all the body axes, obtaining a better performance of the engine for the same amount of thrust.

Considering a deflection of the thrust vector in the pitch (δ_{ptv}) and yaw (δ_{ytv}) planes as in figure (2.5), the new propulsive forces can be written as (2.25)(according to [13]). These new components of the propulsive forces also produce moments along the yaw and pitch axes, with a moment arm of $l_T = x_{cg} - x_T$ (2.26).

Propulsive forces with thrust vectoring become

$$\begin{pmatrix} F_x^T \\ F_y^T \\ F_z^T \end{pmatrix} = T \begin{pmatrix} cos\delta_{ptv}\, sin\delta_{ytv} \\ sin\delta_{ytv} \\ -sin\delta_{ptv}\, cos\delta_{ytv} \end{pmatrix} \tag{2.25}$$

Propulsive moments due to thrust vectoring become

$$\begin{pmatrix} M_x^T \\ M_y^T \\ M_z^T \end{pmatrix} = \begin{pmatrix} 0 \\ l_T\, F_z^T \\ l_T\, F_y^T \end{pmatrix} \tag{2.26}$$

2.2 Longitudinal model

In this section we will present the actual model that we implemented for the simulations. It is based on the fact that, under certain conditions, the equations of motion can be decoupled a longitudinal mode (motion in the vertical plane) and into a lateral mode (motion in the horizontal plane). These conditions are:

- The aircraft is on a wings-level steady-state flight condition (implies $\phi = 0$).
- The sideslip angle is very small ($\beta \simeq 0$).
- the roll and yaw rates (P and R) are small.

Assuming these assumptions hold and including the thrust vectoring system seen before ($\delta_{ytv} = 0$ due to the longitudinal assumptions), the state variables are

$$x = [\, V_T \;\; \alpha \;\; q \;\; \theta \;\; pow \;\; h \,]^T$$

and the equations of motion can be rewritten as follows:

$$\begin{aligned}
\dot{V_T} &= \frac{\bar{q}S\bar{c}}{2mV_T}[C_{xq}(\alpha)cos(\alpha) + C_{zq}(\alpha)sin(\alpha)]q - gsin(\theta-\alpha) + \\
&\quad + \frac{\bar{q}S}{m}(C_x(\alpha,\delta_e)cos(\alpha) + C_z(\alpha,\delta_e)sin(\alpha)) + \frac{T}{m}cos(\alpha+\delta_{ptv}) \qquad (2.27)\\
\dot{\alpha} &= [1 + \frac{\bar{q}S\bar{c}}{2mV_T^2}(C_{zq}(\alpha)cos(\alpha) - C_{xq}(\alpha)sin(\alpha))]q + \frac{g}{V_T}cos(\theta-\alpha) + \\
&\quad + \frac{\bar{q}S}{mV_T}(C_z(\alpha,\delta_e)cos(\alpha) - C_x(\alpha,\delta_e)sin(\alpha)) - \\
&\quad - \frac{T}{mV_T}sin(\alpha+\delta_{ptv}) \qquad (2.28)\\
\dot{q} &= \frac{\bar{q}S\bar{c}}{2J_yV_T}[\bar{c}C_{mq}(\alpha) + \Delta C_{zq}(\alpha)]q + \\
&\quad + \frac{\bar{q}S\bar{c}}{J_y}[C_m(\alpha,\delta_e) + \frac{\Delta}{\bar{c}}C_z(\alpha,\delta e)] - \frac{l_TT}{J_y}sin(\delta_{ptv}) \qquad (2.29)\\
\dot{\theta} &= q \qquad (2.30)\\
\dot{h} &= V_Tcos\alpha\, sin\theta - V_Tsin\alpha\, cos\theta \qquad (2.31)
\end{aligned}$$

The time derivative of the state *pow* has been presented in section 2.1.1, where the function $PDOT$ calculates the time derivative of *pow* as a function of itself and the commanded power level set by the pilot. Information about the engine can obtained from a more detailed model of the engine, available in [12]. Figure (2.8) shows the implemented $F-16$ aircraft model in Simulink®.

2.2.1 Aircraft description

The parameters used to implement the model of the F-16 aircraft are shown in table (2.1).

The aircraft longitudinal model uses three different actuators. The first one corresponds to the elevator angle δ_e, which mainly affects the value of the aerodynamic coefficients. The second one is the thrust setting δ_{th}, that affects the value of the motor thrust T. The third one, δ_{ptv} is the vectoring angle of the thrust. Table (2.2)

Table 2.1: Mass and geometric properties of the aircraft

Parameter	Value
Weight W (lb)	20500
Wing area S (ft^2)	300
Mean aerodynamic chord $\bar{c}$ (ft)	11.32
Reference cg location $x_{cg,ref}$ (ft)	$0.35\bar{c}$
Moment of inertia J_y $(slug\, ft^2)$	55814

Table 2.2: Models of the control actuators

Actuators	Position limit	Rate limit	Time constant
Elevator δ_e	$\pm 25^\circ$	$60^\circ/s$	0.0495s
Thrust vectoring δ_{ptv}	$\pm 17^\circ$	$60^\circ/s$	0.07s

shows the relevant parameters of these actuators. The response of the elevator and the thrust vectoring actuators is modeled in both cases as first-order systems.

In this master's thesis, the delay in the response of the elevator (with a time constant of 0.0495 s) is considered in the simulations and the design of the controllers. However, the thrust vectoring actuator will not be considered, although it is introduced in the model for further simulations and investigations.

2.2.2 Aerodynamic data

The aerodynamic data used in this thesis was obtained in a series of wind tunnel tests on a subscale model of an F-16 airplane ([12]). This data consists on 50 look-up tables and covers a wide range of angle of attack and of sideslip angle ($-20\circ \leq \alpha \leq 90^\circ$ and $-30\circ \leq \beta \leq 30^\circ$). However the actual techniques for modeling in the poststall region are not accurate, so the reduced data presented in [18] is used.

This reduced data (10 look-up tables) covers a range for the angle of attack between -10 and 45 degrees and the dependence on β has been approximated in some cases. The number of look-up tables is finally reduced to 4 by considering only the

relevant data for the longitudinal model of the aircraft.

This aerodynamic data can be seen in figure (2.9). The equations to obtain the total aerodynamic coefficients $C_{x,t}$, $C_{z,t}$ and $C_{m,t}$ are shown next.

$$C_{x,t} = C_x(\alpha, \delta_e) + \frac{q\bar{c}}{2V_T} C_{xq}(\alpha) \tag{2.32}$$

$$C_{z,t} = C_z(\alpha, \delta_e) + \frac{q\bar{c}}{2V_T} C_{zq}(\alpha) \tag{2.33}$$

$$C_{m,t} = C_m(\alpha, \delta_e) + C_{z,t}(x_{cg,ref} - x_{cg}) + \frac{q\bar{c}}{2V_T} C_{mq}(\alpha) \tag{2.34}$$

$$C_z(\alpha, \delta_e) = C_z(\alpha, 0) - 0.19\frac{\delta_e}{25} \tag{2.35}$$

2.3 Linear model

In order to design the desired controllers, the nonlinear model needs to be linearized. Due to the complexity of the aircraft's equations, linearization must be done numerically instead of analytically. This linearization process requires two steps: obtention of an equilibrium condition (initial condition) and linearizing around this condition. These two steps have been implemented using Matlab® routines.

2.3.1 Obtention of an initial condition

We obtain an initial condition by considering that the aircraft is on a steady wings-level flight, which means that the control inputs are constant and that the states are

in equilibrium. Therefore, obtaining an initial conditions requires finding the values of the state and control vectors that satisfy equations (2.36) and (2.27) - (2.31).

$$\dot{V_T} = \dot{\alpha} = \dot{q} = \dot{\theta} = \dot{pow} = \dot{h} = 0 \tag{2.36}$$

One important aspect is which variables we have to use to specify the initial condition. The control inputs enter the equations mainly through look-up tables (aerodynamic coefficients or engine) and therefore it is better to determine them numerically when solving the equations and not to use them to specify the initial condition.

That leaves us with the state variables. We know that velocity and angle of attack are related (through the amount of lift necessary to support the weight of the aircraft). Also, α and θ are interrelated through the rate-of-climb constraint, which has the form (2.37) in wings-level, non-sideslipping flight, where γ is the flight path angle. Therefore, we choose to first specify true velocity, flight path angle and altitude (V_T, γ and h) and calculate the rest of the variables from them.

$$\gamma = \theta - \alpha \tag{2.37}$$

To solve the system of equations (2.27) - (2.31), we use an iterative method minimizing the value of a cost function of the form:

$$J = c_1\dot{x_1} + c_2\dot{x_2} + c_3\dot{x_3} + c_4\dot{x_4} + c_5\dot{x_5} \tag{2.38}$$

where $\dot{x_i}$ corresponds to a state derivative.

2.3.2 Linearizing around the initial condition

Once the trim condition is obtained, the system is linearized around this trim condition using a linearization function included in Matlab®. The result of this linearization is a system of the form

$$\begin{cases} \dot{x} = Ax + Bu \\ z = Cx + Du \end{cases} \tag{2.39}$$

that is valid around the equilibrium point determined in the first part.

2.4 Validation

Before using the linear model in the controller design process, we have to validate it, i.e. we have to make sure that the linear model represents accurately enough the nonlinear one. In order to do this, we compare the response of both models to small perturbations in the input commands. This is done around different trim conditions to check in which regions the linearization correctly represents the nonlinear model.

The following perturbations in the input commands were used to compare the response of the two models:

$$\delta_e = \begin{cases} \delta_{e,0} & \text{if } t \leq 1s \\ \delta_{e,0} + 1^\circ & \text{if } 1s \leq t < 11s \\ \delta_{e,0} - 2^\circ & \text{if } 11s \leq t < 21s \\ \delta_{e,0} & \text{if } t > 21s \end{cases} \tag{2.40}$$

$$\delta_{th} = \begin{cases} \delta_{th,0} & \text{if } t \leq 1s \\ \delta_{th,0} + 0.1 & \text{if } 1s \leq t < 11s \\ \delta_{th,0} - 0.1 & \text{if } 11s \leq t < 21s \\ \delta_{th,0} & \text{if } t > 21s \end{cases} \tag{2.41}$$

The first trim condition checked was:

$$x_{trim} = \begin{pmatrix} V_{T,0} = 160 ft/s \\ \alpha_0 = 35.01^\circ \\ q_0 = 0^\circ/s \\ \theta_0 = 35.01^\circ \\ pow_0 = 44.62 \\ h_0 = 3420 ft \end{pmatrix} \tag{2.42}$$

with input commands

$$u_{trim} = \begin{pmatrix} \delta_{e,0} = -11.31^\circ \\ \delta_{ptv,0} = 0^\circ \\ \delta_{th,0} = 0.6871 \end{pmatrix} \tag{2.43}$$

and we can see the response in figures (2.11) and (2.12).

Although the response to a perturbation on the elevator angle is almost the same for both the nonlinear and the linear model, we cannot say the same for the response to a perturbation in the thrust setting: the linear model does not respond to a perturbation in δ_{th}. The flat line in the different plots of figure (2.12) represents the fact that the states in the linear model remain constant, i.e. they are not perturbed from the equilibrium condition when changing the δ_{th} command. On the contrary, it can be seen that changes in the δ_{th} command do affect the nonlinear model.

The reason of this discrepancy between the nonlinear model and the linear model can be found by checking the linearized equation obtained at the corresponding trim condition. The resulting matrices A and B_2 of this linearization can be found in equations (2.44) and (2.45) respectively.

$$A = \begin{pmatrix} -0.1656 & -10.7137 & -7.2815 & -32.1740 & 0 & 3.951e-4 \\ -0.0018 & -0.0981 & 0.9276 & 0 & 0 & 4.2663e-6 \\ 0 & -0.6252 & -0.4673 & 0 & 0 & 0 \\ 0 & 0 & 1.0000 & 0 & 0 & 0 \\ 0 & 0 & 0 & 0 & -1.0000 & 0 \\ 0 & -160.0000 & 0 & 160.0000 & 0 & 0 \end{pmatrix} \tag{2.44}$$

$$B_2 = \begin{pmatrix} -4.0478 & -9.2839 & 0 \\ -0.0253 & -0.0828 & 0 \\ -0.8992 & -1.8471 & 0 \\ 0 & 0 & 0 \\ 0 & 0 & 64.9400 \\ 0 & 0 & 0 \end{pmatrix} \tag{2.45}$$

From the B matrix we can see that the thrust setting δ_{th} (3rd column) only affects the *pow* state (4th row). Then, by checking the A matrix, it can be seen that the *pow* state (4th column and row) only affects itself, having no effect on the other states. Therefore, a change in the thrust setting produces a change in the *pow* state, but this change does not translate into changes in the other states. The *pow* state is decoupled and this is the reason why the linear model does not follow the nonlinear model for changes in δ_{th}.

In order to avoid this problem, the engine model has to be removed from the general nonlinear aircraft model. Then, the control input δ_{th} disappears and is substituted by T (engine thrust). This means that our control signal is directly the output of the engine. Table (2.3) shows the physical limitations of the engine thrust T [18], that will be used in the simulations chapters to determine whether the thrust actuator is saturated or not. We will not consider any delay effects in the thrust, since we interpret that they depend on the engine model.

Table 2.3: Engine thrust saturation limits

Actuator	Minimum limit	Maximum limit
Engine thrust T	$-3600\ lb$	$28886\ lb$

Once the engine is removed, we return to the validation of the model. The perturbations to the inputs commands are then:

$$\delta_e = \begin{cases} \delta_{e,0} & \text{if } t \leq 1s \\ \delta_{e,0} + 1^\circ & \text{if } 1s \leq t < 11s \\ \delta_{e,0} - 2^\circ & \text{if } 11s \leq t < 21s \\ \delta_{e,0} & \text{if } t > 21s \end{cases} \tag{2.46}$$

$$T = \begin{cases} T & \text{if } t \leq 1s \\ T + 500lb & \text{if } 1s \leq t < 11s \\ T - 500lb & \text{if } 11s \leq t < 21s \\ T & \text{if } t > 21s \end{cases} \tag{2.47}$$

Using these perturbation in the input commands, we repeat the validation of the linear model by comparing its response with the nonlinear model around different trim conditions.

First, we repeat the same trim condition shown in equation (2.42) removing the *pow* state. Note that the input command vector has changed (due to the removal of the engine) to:

$$u_{trim} = \begin{pmatrix} \delta_{e,0} = -11.31^\circ \\ \delta_{ptv,0} = 0^\circ \\ T_0 = 1.0309e4 \end{pmatrix} \tag{2.48}$$

Figures (2.14) and (2.15) show the compared response of the linear and nonlinear model to perturbations of the input commands. It can be seen that the linear model behaves very similar to the nonlinear model, and therefore the linear model can be

considered a good approximation around the equilibrium conditions of (2.42).

Finally, we compare the behavior of both models around another equilibrium condition:

$$x_{trim} = \begin{pmatrix} V_{T,0} = 200ft/s \\ \alpha_0 = 22.46^\circ \\ q_0 = 0^\circ/s \\ \theta_0 = 22.46^\circ \\ h_0 = 3000ft \end{pmatrix} \tag{2.49}$$

with input commands

$$u_{trim} = \begin{pmatrix} \delta_{e,0} = -6.97^\circ \\ \delta_{ptv,0} = 0^\circ \\ T_0 = 6.1259e3 \end{pmatrix} \tag{2.50}$$

Figures (2.16) and (2.17) show the results. Although the response to the perturbation in the thrust force T is similar in both models, we cannot say the same for the response to an elevator perturbation.

As seen in (2.16), the response of the nonlinear and the linear model are quite different. This difference is due to the fact that the linearization point in this case is around $\alpha = 21^\circ$. In this region, there is a major change in the aerodynamic behavior of the aircraft: it changes from low-angle of attack to high-angle of attack. This change can be seen in the aerodynamic data presented in figure (2.9): there is a major change in the slope of the some aerodynamic coefficients (C_x, C_{xq} and C_z) around this region.

Consequently, after linearizing the nonlinear model around different points, we can determine that the linear model is a good representation of the nonlinear model as long as

- changes in the angle of attack α are small, and
- the model stays away from the region around $\alpha \simeq 21^\circ$ or other regions where there is a significant change in the aerodynamic behavior of the aircraft (i.e.

regions where there is a major change in the slope of the aerodynamic coefficients)

Two regions in which there are not significant changes in the aerodynamic coefficients and that are representative of the behavior of the aircraft when linearized about them are:

- $-5^\circ \leq \alpha \leq 15^\circ$
- $25^\circ \leq \alpha \leq 40^\circ$

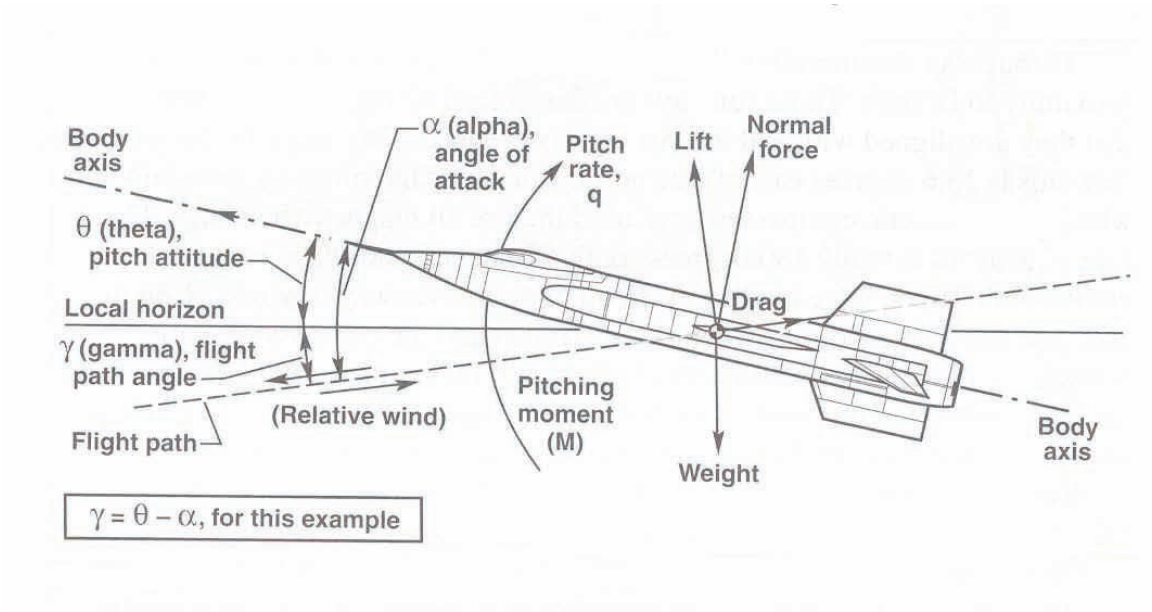

Figure 2.6: Relevant angles and axes in the longitudinal model

(a) Original F-16 model

(b) F-16 model augmented with thrust vectoring

Figure 2.7: Scheme of the longitudinal model of the aircraft with and without the thrust vectoring

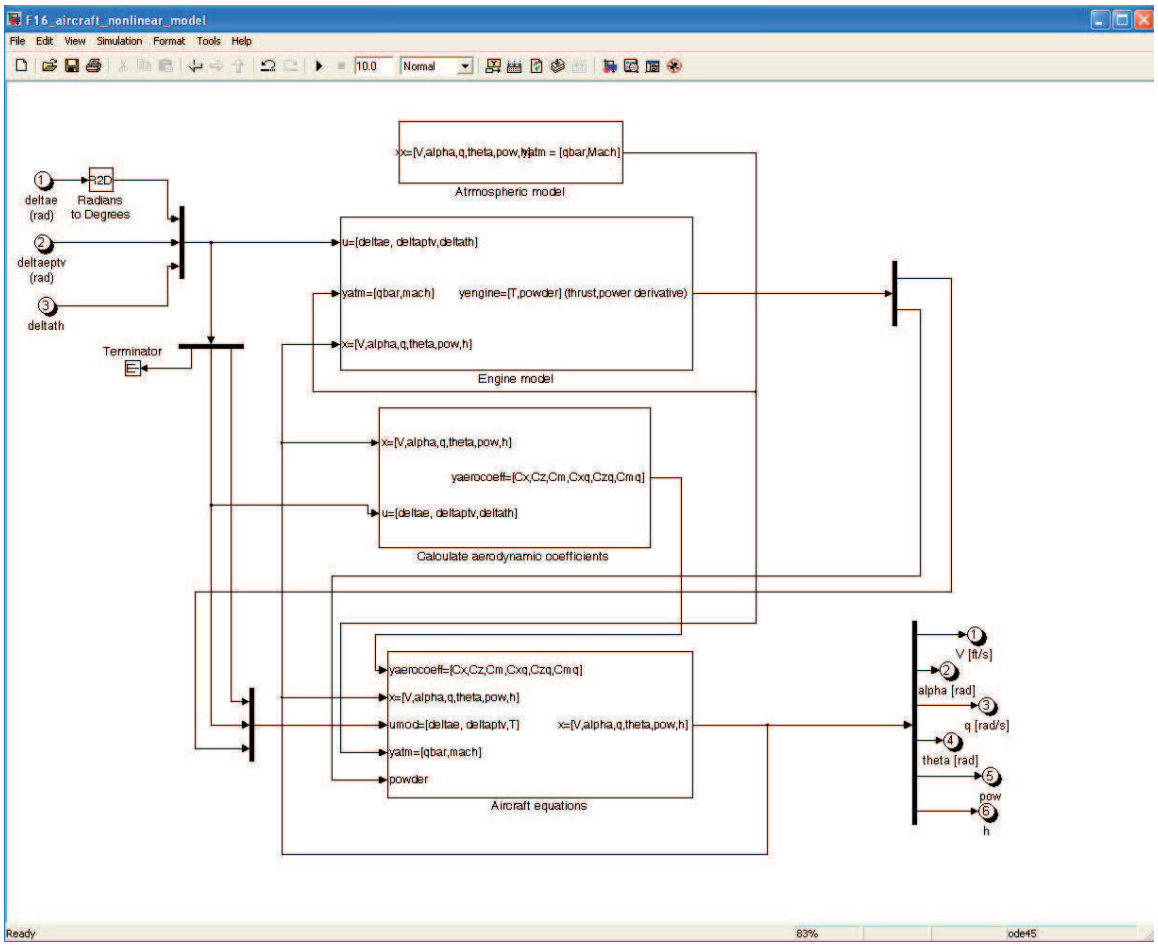

Figure 2.8: Nonlinear longitudinal model of the $F-16$ aircraft implemented in Simulink®

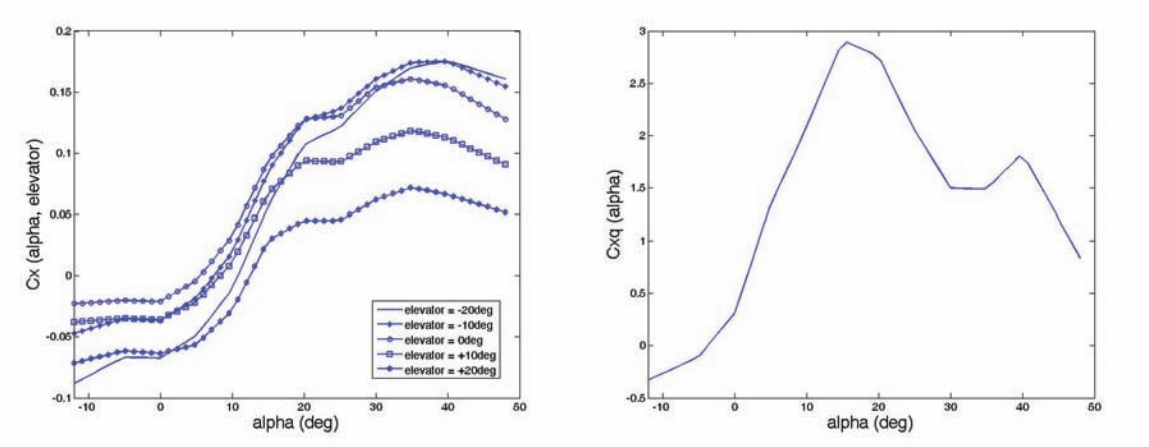

a) x-axis force coefficient C_x b) Damping coefficient C_{xq}

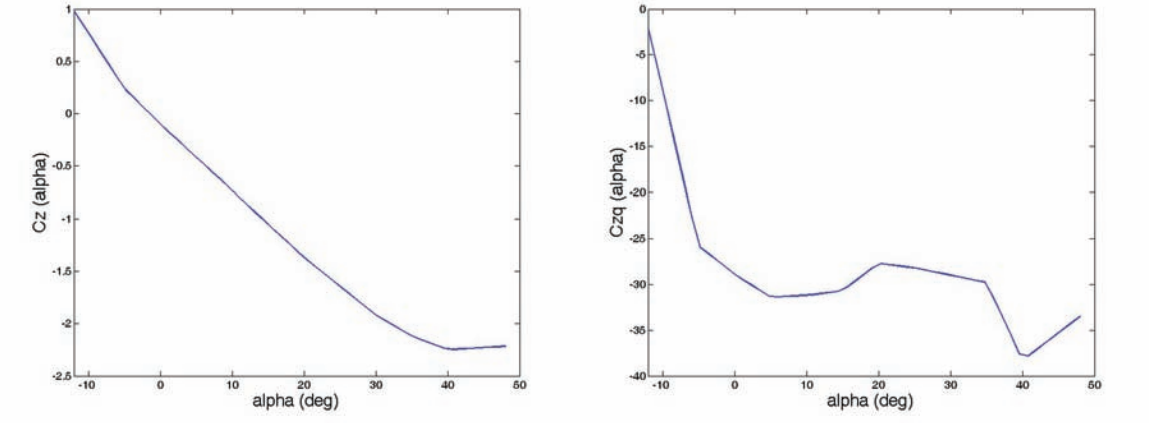

c) z-axis force coefficient C_z d) Damping coefficient C_{zq}

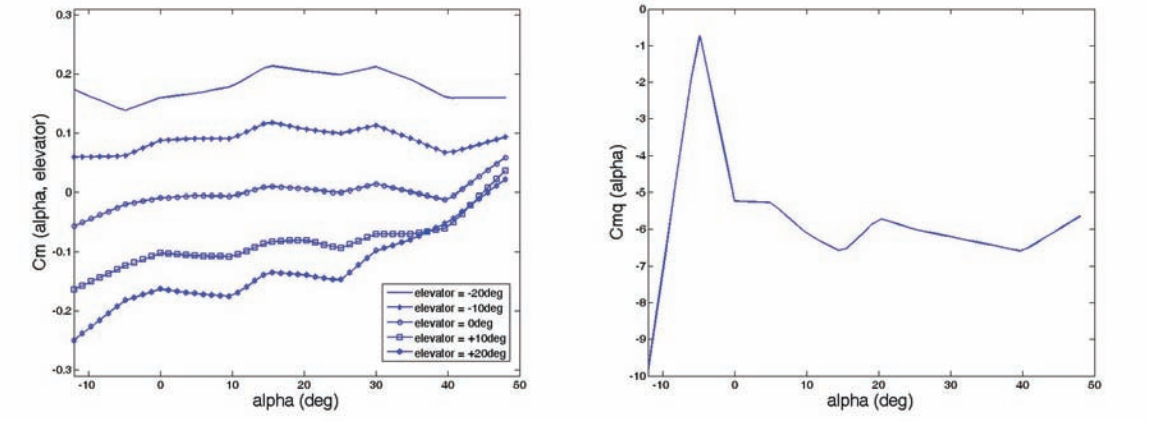

e) Pitching moment coefficient C_m f) Damping coefficient C_{mq}

Figure 2.9: Plots of the different aerodynamic coefficients

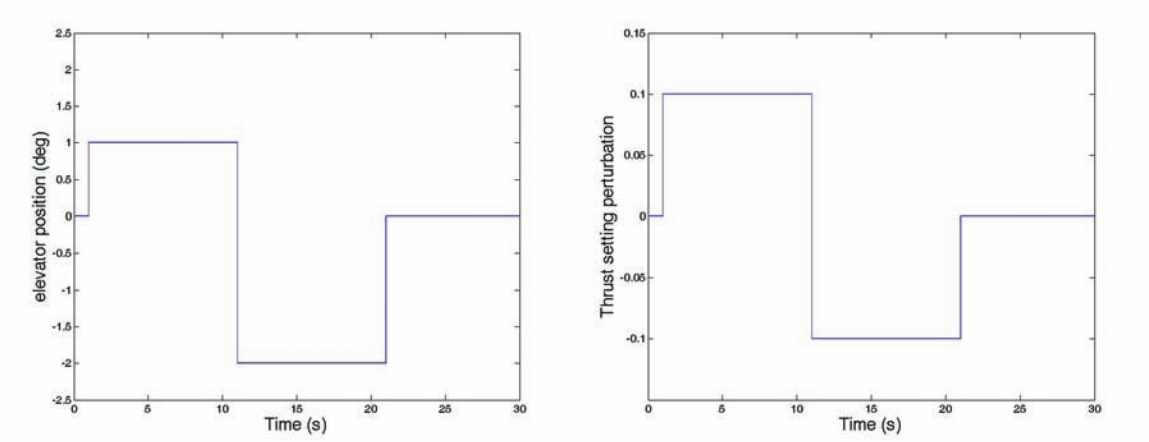

a) Elevator perturbation δ_e (deg)

b) Throttle setting perturbation δ_{th}

Figure 2.10: Perturbation of the input commands used to validate the linear model

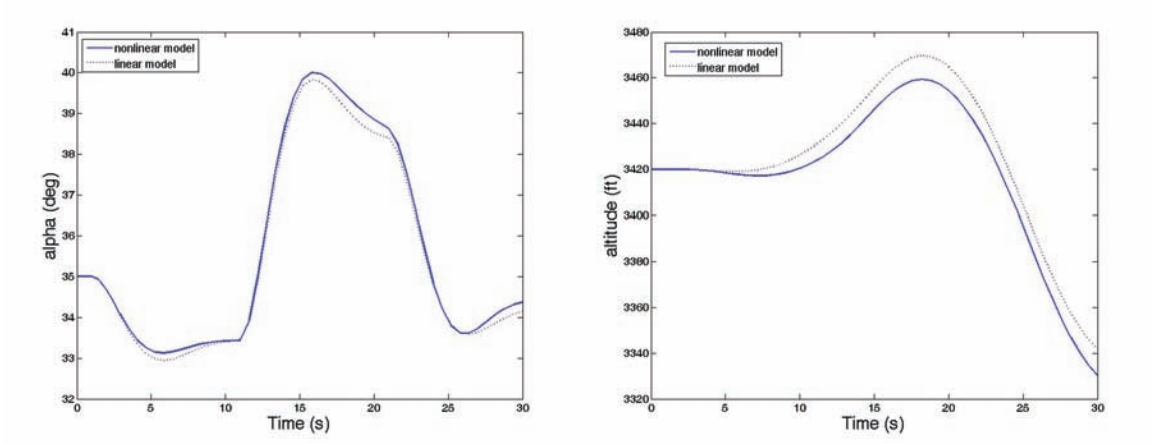

a) Angle of attack α b) Altitude *h*

c) Pitch angle θ d) Velocity *V*

Figure 2.11: Time responses for a perturbation in δ_e at $V = 160 ft/s$ and $\alpha = 35.01°$

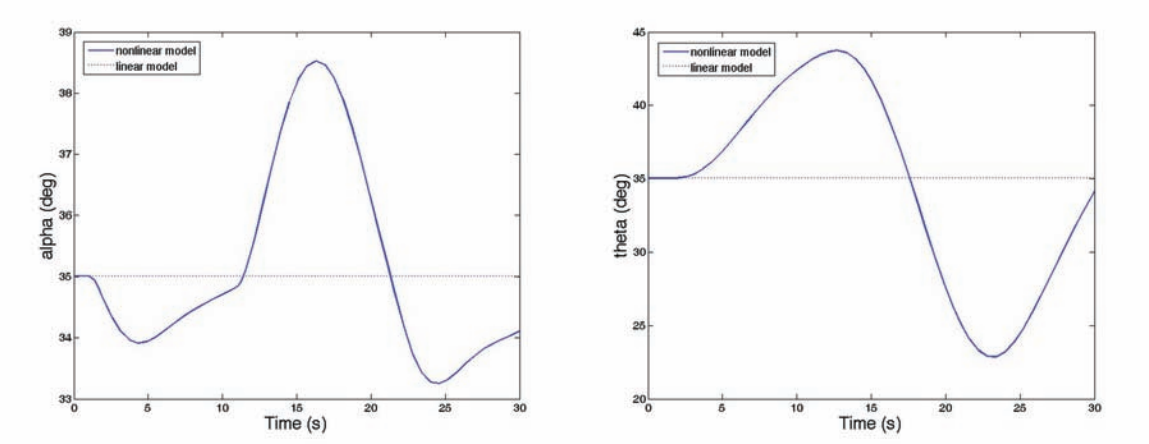

a) Angle of attack α

b) Velocity V

c) Pitch angle θ

Figure 2.12: Time responses for a perturbation in δ_{th} at $V = 160 ft/s$ and $\alpha = 35.01°$

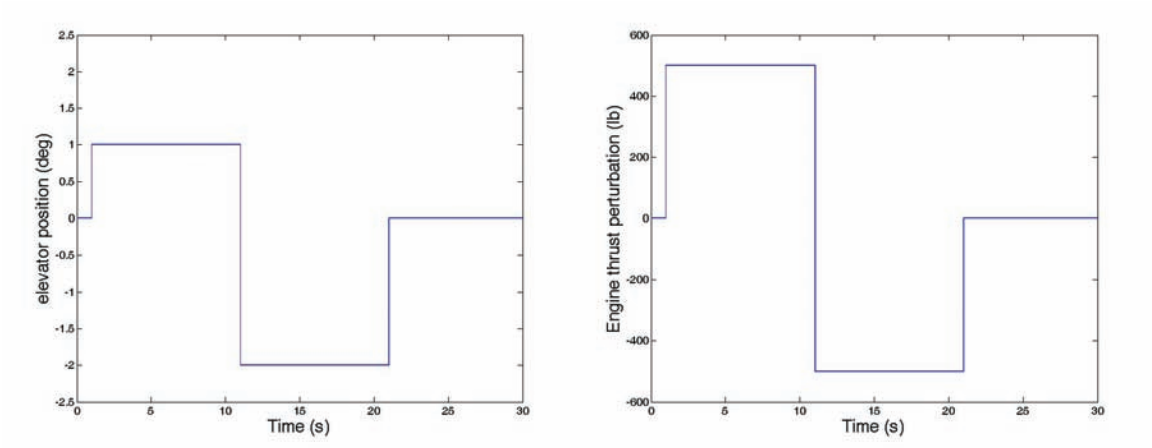

a) Elevator perturbation δ_e (deg)

b) Engine throttle perturbation T (lb)

Figure 2.13: Perturbation of the input commands used to validate the linear model without engine

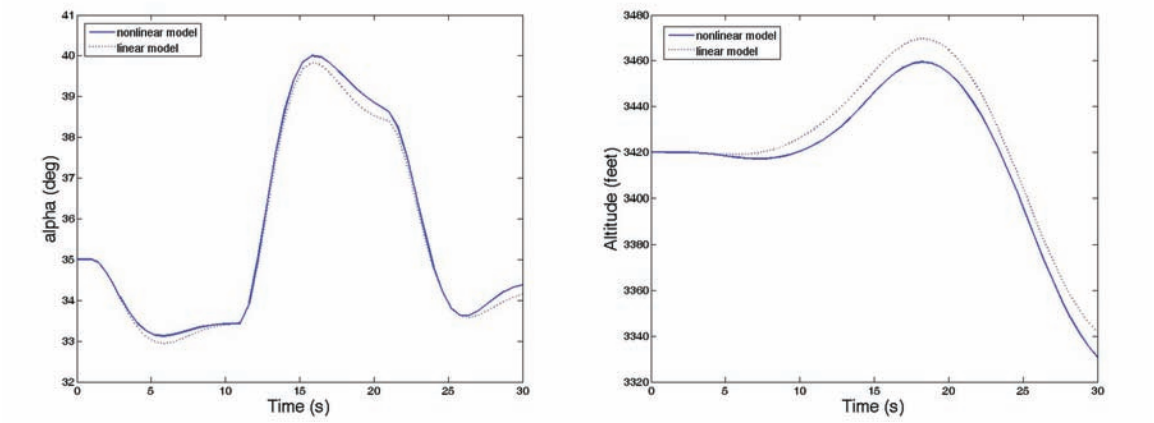

a) Angle of attack α

b) Altitude *h*

c) Pitch angle θ

d) Velocity *V*

Figure 2.14: Time responses for a perturbation in δ_e at $V = 160 ft/s$ and $\alpha = 35.01°$ (linearization without the engine model)

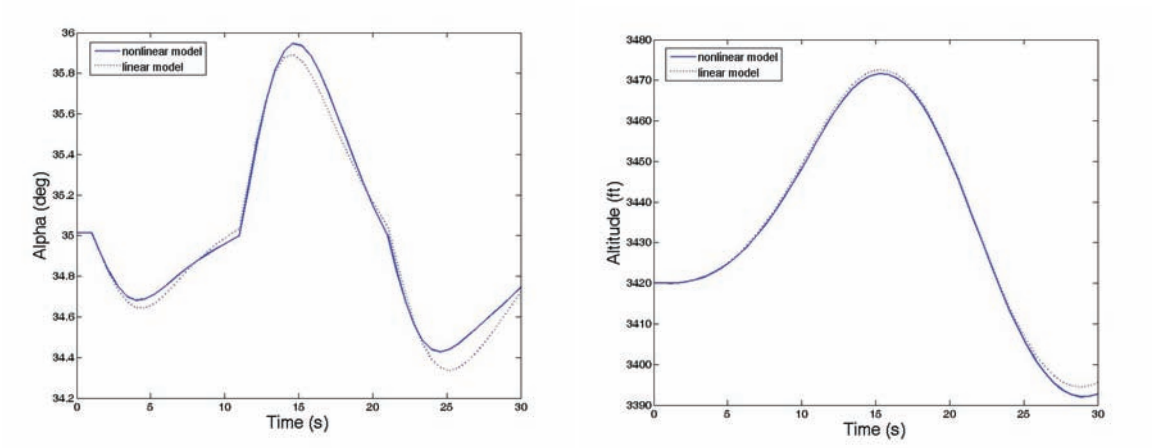

a) Angle of attack α

b) Altitude *h*

c) Pitch angle θ

d) Velocity *V*

Figure 2.15: Time responses for a perturbation in T at $V = 160ft/s$ and $\alpha = 35.01°$ (linearization without the engine model)

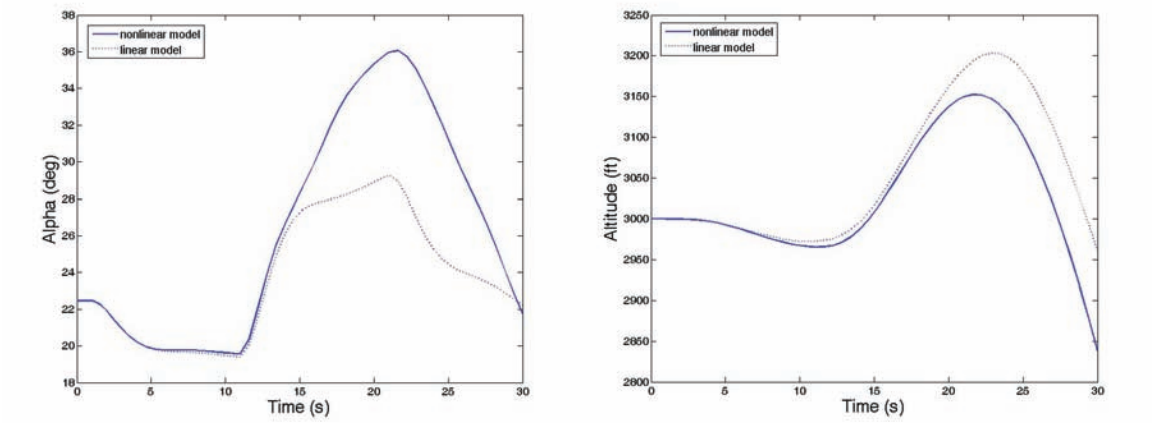

a) Angle of attack α

b) Altitude *h*

c) Pitch angle θ

d) Velocity *V*

Figure 2.16: Time responses for a perturbation in δ_e at $V = 200ft/s$ and $\alpha = 22.46°$ (linearization without the engine model)

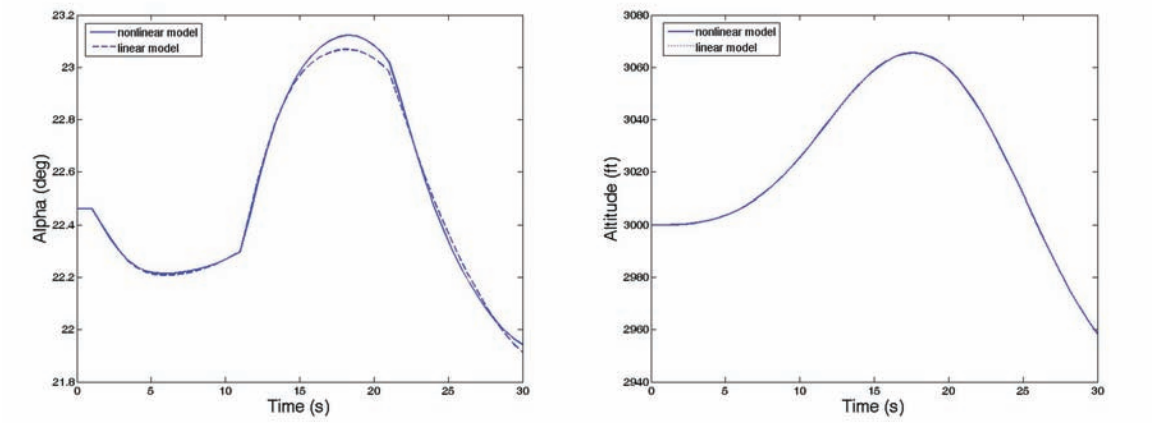

a) Angle of attack α

b) Altitude *h*

c) Pitch angle θ

d) Velocity *V*

Figure 2.17: Time responses for a perturbation in T at $V = 200ft/s$ and $\alpha = 22.46°$ (linearization without the engine model)

Chapter 3

Linear Parameter Varying (LPV) systems

One of the main problems in modeling real life systems is the presence of uncertainties because it affects the validity of the model. Out of the two main families of linear systems uncertainties (dynamical input-output and state space uncertainties, [1]), state space uncertainties are particularly interesting.

State space uncertainties arise due to the fact that the physical parameters on which the system depends may vary with time, and they directly affect the state space matrices. The wider the operating envelope of the system, the more the parameter (and consequently the system matrices) change. This often makes the system nonlinear, since the variation depends on the value of the states.

An example of state space uncertainty would be the weight of an aircraft. During flight, fuel is burned and the weight of the airplane is reduced, changing the state space matrices.

One of the most popular methods to overcome this nonlinearities in controller design is gain scheduling. This technique constructs a nonlinear controller by interpolating in some manner (e.g. switching or linear combination) between a set of linear time invariant controllers. Each linear controller is designed to meet the requirements of stability and performance about an equilibrium point in which the system may operate.

This technique linearizes the plant around different equilibrium points (corresponding to different values of the uncertain physical parameters) and then uses linear techniques to design controllers in these different conditions. These controllers are designed separately and the final controller is either a linear combination of them or a switching law involving them (that is, use each controller in a region around its design point and switch to another controller when it leaves this region).

Gain scheduling, however, has one main drawback: it can not guarantee overall performance or stability of the overall system of controllers other than at the design points. For example, switching from one controller to another can drive the system unstable even though were dealing with an stable system. This is specially critical when the systems parameters change quickly and typically requires a great deal of simulations to check if the resulting closed loop system is stable.

The desire of being able to guarantee performance and stability over all the performance envelope of the system lead to the development of linear parameter varying (LPV) control techniques.

3.1 LPV basics

A Linear Parameter Varying (LPV) system is a class of finite dimensional linear systems of the form

$$\begin{cases} \dot{x(t)} = A(\rho(t))x(t) + B(\rho(t))u(t) \\ z(t) = C(\rho(t))x(t) + D(\rho(t))u(t) \end{cases} \tag{3.1}$$

where $A \epsilon \Re^{nxn}$, $B \epsilon \Re^{mxn}$ and $\rho(t)$ is a time-varying parameter vector (scheduling vector) not known in advanced although it can be measured in real time and it moves inside a certain bounded region P known a priori. If the scheduling vector $\rho(t)$ includes some of the states of the system, then we have a quasi-LPV (qLPV) system. The LPV framework takes advantage of the fact that although the future evolution of the scheduling vector is unknown, the relationship between $\rho(t)$ and the system matrices is known. The LPV controller can be then designed according to this relationship.

The LPV controller design technique allows us to design the controllers only in the corner points of the scheduling region P with its corresponding stability and performance requirements and then it guarantees that these requirements will be fulfilled in all the performance envelope [1], [11].

One of the main difficulties in using the LPV controller design techniques is that the system must be written in an LPV form (equation 3.1). There are three main methods to obtain approximated LPV models:

- Jacobian Linearization
- State Transformation
- Function Substitution

More information on the advantages and disadvantages of the different methods and how they work can be found in [3].

3.2 LPV model of the F-16 aircraft

Obtaining an LPV model of the longitudinal model of the F-16 aircraft following the directions in [3] is very complicated because of the complexity of the equations of motion. In this section, we show how we obtained an approximated LPV model of the aircraft and its validation through simulation.

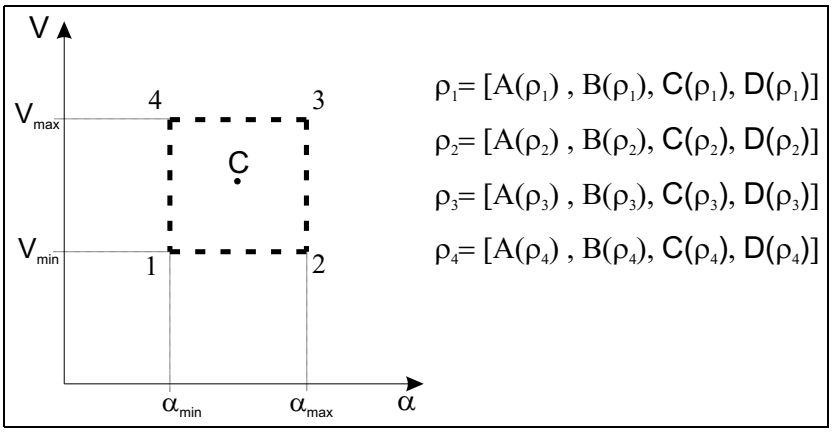

Figure 3.1: Scheme of the LPV model

First, the scheduling vector $\rho(t)$ must be specified. For the F-16 aircraft model, velocity V_T and angle of attack α are chosen, which are the most common choices for the longitudinal motion of an aircraft ([3], [13]). Then, the envelope of interest (call it $\wp$ region) is chosen, that is, maximum and minimum values for $\rho(t) = [V_T, \alpha]^T$ are specified.

Let's consider that

$$V_{T,min} \leq V_T(t) \leq V_{T,max}$$

$$\alpha_{min} \leq \alpha \leq \alpha_{max}$$

and therefore $\wp$ is a convex region with the following corners (see figure 3.1)

$$\begin{aligned}
\rho_1 &= [V_{T,min} \;\; \alpha_{min}]^T \\
\rho_2 &= [V_{T,min} \;\; \alpha_{max}]^T \\
\rho_3 &= [V_{T,max} \;\; \alpha_{max}]^T \\
\rho_4 &= [V_{T,max} \;\; \alpha_{min}]^T
\end{aligned}$$

The nonlinear model is then linearized around the corner points (that is, linearized around the trim conditions specified by ρ_1, ρ_2, ρ_3 and ρ_4), obtaining 4 different linear systems with its corresponding state space matrices ($[A_i, B_i, C_i, D_i]$ for $i = 1, \ldots, 4$).

Once this is done, we consider that inside this square convex region the aircraft can be represented by a linear combination of the 4 linear systems obtained in the corners, as long as $\wp$ is small enough. In other words, we can represent the behavior of the aircraft in any point $z \, \epsilon \, \wp$ as follows

$$A_z = \tau_1 A_1 + \tau_2 A_2 + \tau_3 A_3 + \tau_4 A_4 \tag{3.2}$$

$$B_z = \tau_1 B_1 + \tau_2 B_2 + \tau_3 B_3 + \tau_4 B_4 \tag{3.3}$$

$$C_z = \tau_1 C_1 + \tau_2 C_2 + \tau_3 C_3 + \tau_4 C_4 \tag{3.4}$$

$$D_z = \tau_1 D_1 + \tau_2 D_2 + \tau_3 D_3 + \tau_4 D_4 \tag{3.5}$$

with

$$\tau_1 = \frac{\alpha_{max} - \alpha_z}{\alpha_{max} - \alpha_{min}} \cdot \frac{V_{T,max} - V_{T,z}}{V_{T,max} - V_{T,min}} \tag{3.6}$$

$$\tau_2 = \frac{\alpha_z - \alpha_{min}}{\alpha_{max} - \alpha_{min}} \cdot \frac{V_{T,max} - V_{T,z}}{V_{T,max} - V_{T,min}} \tag{3.7}$$

$$\tau_3 = \frac{\alpha_z - \alpha_{min}}{\alpha_{max} - \alpha_{min}} \cdot \frac{V_{T,z} - V_{T,min}}{V_{T,max} - V_{T,min}} \tag{3.8}$$

$$\tau_4 = \frac{\alpha_{max} - \alpha_z}{\alpha_{max} - \alpha_{min}} \cdot \frac{V_{T,z} - V_{T,min}}{V_{T,max} - V_{T,min}} \tag{3.9}$$

$$\sum_{i=1}^{4} \tau_i = 1 \tag{3.10}$$

We can easily show that equations (3.6)-(3.9) satisfy the condition (3.10) by direct substitution (to simplify the notation, the T subscript in the velocity is dropped and subscripts a and b are used to substitute max and min respectively):

$$
\begin{aligned}
\sum_{i=1}^{4}\tau_i &= \tau_1+\tau_2+\tau_3+\tau_4 = \tfrac{1}{\alpha_a-\alpha_b}\cdot\tfrac{1}{V_a-V_b}[(\alpha_a-\alpha_z)(V_a-V_z)+ \\
&\quad +(\alpha_z-\alpha_b)(V_a-V_z)+(\alpha_z-\alpha_b)(V_z-V_b)+(\alpha_a-\alpha_z)(V_z-V_b)] = \\
&= \tfrac{1}{\alpha_a-\alpha_b}\cdot\tfrac{1}{V_a-V_b}[\alpha_aV_a-\alpha_aV_z-\alpha_zV_a+\alpha_zV_z+\alpha_zV_a-\alpha_zV_z-\alpha_bV_a+ \\
&\quad +\alpha_bV_z+\alpha_zV_z-\alpha_zV_b-\alpha_bV_z+\alpha_bV_b+\alpha_aV_z-\alpha_aV_b-\alpha_zV_z+\alpha_zV_b] = \\
&= \tfrac{1}{\alpha_a-\alpha_b}\cdot\tfrac{1}{V_a-V_b}[(\alpha_a-\alpha_b)\cdot(V_a-V_b)] = 1
\end{aligned}
$$

Similarly, it can be shown that on each corner of the LPV region (figure (3.1)) the value of τ_i corresponding to that corner is 1 while the rest of them have a 0 value.

To validate this method to obtain an LPV model, we have to compare the behavior of the nonlinear model inside the selected LPV region with the behavior of the approximated system (3.2)-(3.5). For this validation, we use the same method as in section 2.4, that is, check the response of both systems to perturbations in the input commands (δ_e and T).

To check the region bounded by

$$160ft/s \leq V_T(t) \leq 200ft/s \tag{3.11}$$

$$32^\circ \leq \alpha \leq 35^\circ \tag{3.12}$$

we simulate the behavior of the nonlinear model in the middle of this zone, that is, in the trim condition obtained by imposing

$$V_{T,Z} = 180ft/s \tag{3.13}$$

$$\alpha_Z = 33.5^\circ \tag{3.14}$$

and compare it to the behavior of the plant represented in (3.2)-(3.5) with

$$\tau_1 = 0.25$$
$$\tau_2 = 0.25$$
$$\tau_3 = 0.25$$
$$\tau_4 = 0.25$$

Note that this point is located in the middle of the square defined by ρ_1, ρ_2, ρ_3 and ρ_4, that is, it corresponds to the point C in figure (3.1). Figures 3.2 and 3.3 show the results.

We can see that the approximated linear system behaves quite similar to the nonlinear system, and therefore this method is validated. The same method has been used to validate the LPV concept in the region bounded by (3.15) and (3.16), obtaining similar results.

$$500ft/s \leq V_T(t) \leq 550ft/s \tag{3.15}$$

$$3^\circ \leq \alpha \leq 8^\circ \tag{3.16}$$

It is important, however, to keep in mind the linearization restrictions commented in section 2.4 and also that the LPV region has to be small enough for the method to be valid. This fact may present a problem: the region may be too small to include the movements of the aircraft. In other words, if the region defined by the LPV corners is small, the aircraft may leave it during its trajectory. An option to solve this is to expand the LPV model as in figure (3.4). Inside each square we use its four corners to obtain the LPV approximated model, so when the aircraft moves from one square to the other we just need to change two of the corners and the model will still be valid [20].

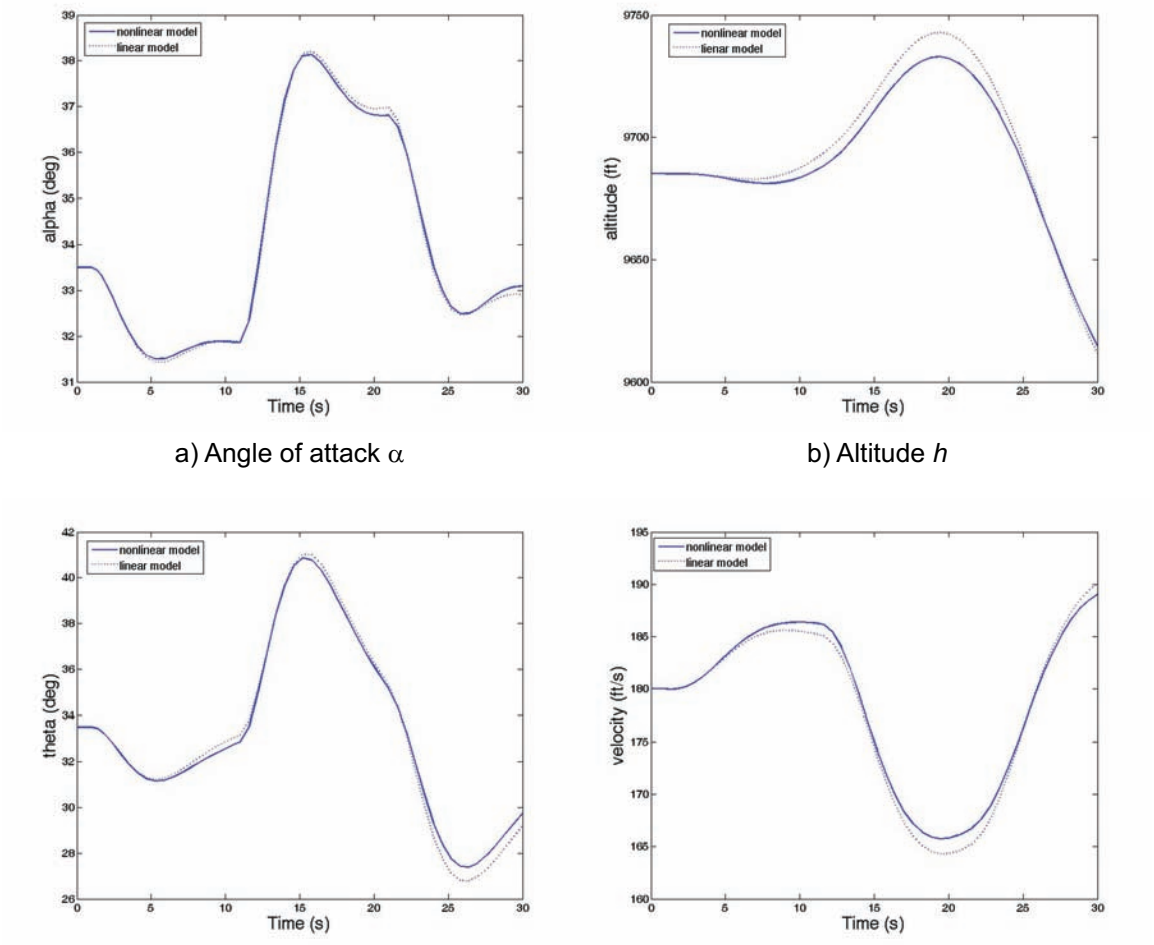

a) Angle of attack α

b) Altitude *h*

c) Pitch angle θ

d) Velocity *V*

Figure 3.2: Time responses for a perturbation in δ_e at $V = 180ft/s$ and $\alpha = 33.5°$ (linear system obtained using an LPV model)

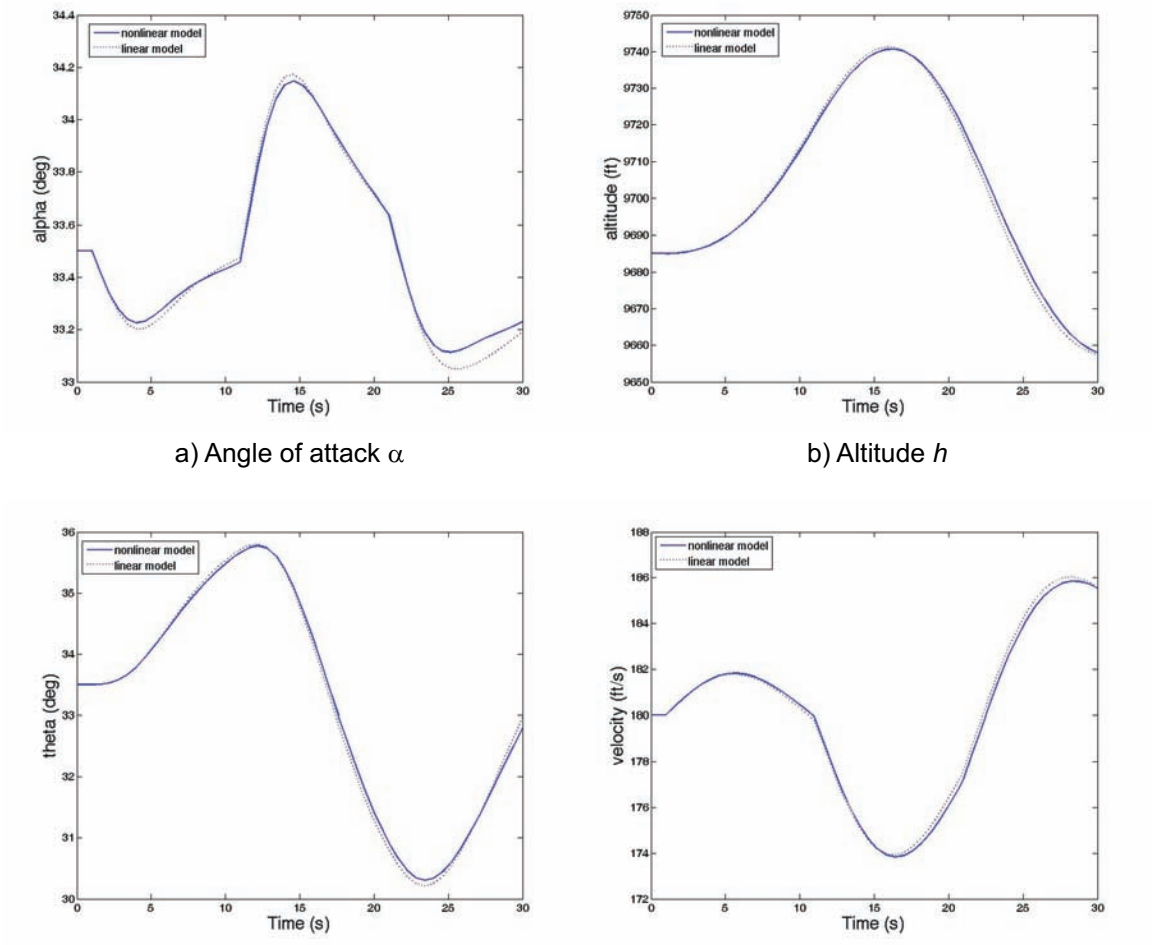

Figure 3.3: Time responses for a perturbation in δ_e at $V = 180ft/s$ and $\alpha = 33.5°$ (linear system obtained using an LPV model)

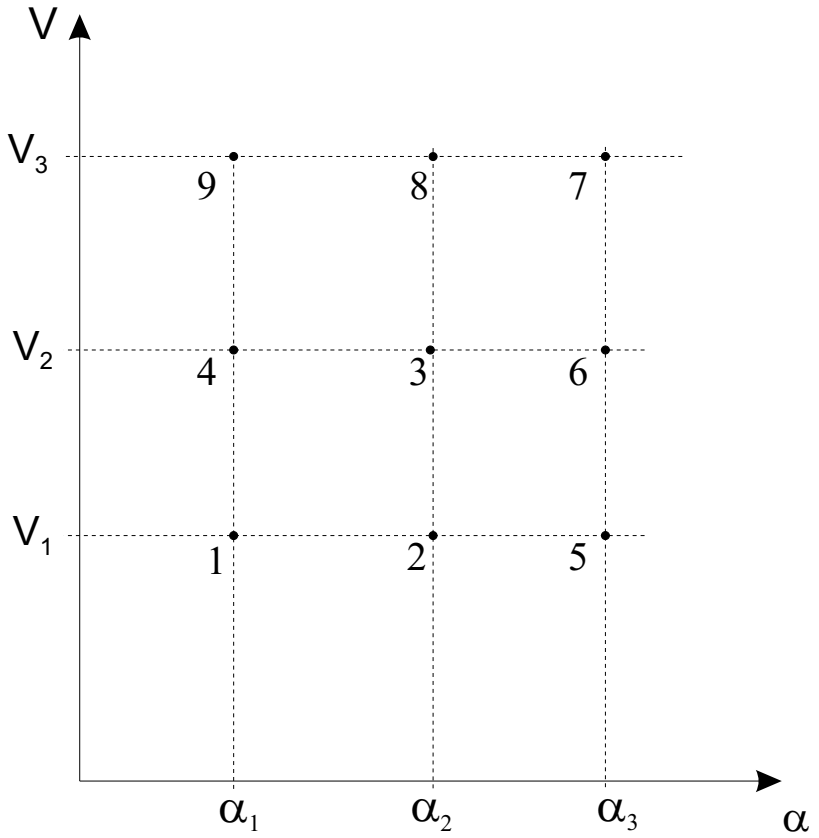

Figure 3.4: Extended scheme of the LPV model, in which the LPV region consists on different squares with coincident sides

Chapter 4

Controller design

4.1 Saturation control background

Actuator saturation has always been a main issue in all engineering fields [9]. It is probably the most important and dangerous nonlinearity present in any system with actuators and there are many research projects trying to avoid the problems it causes. Forgetting to consider it in the controller design can lead to a major degradation of the system's performance or, in the worst case, can drive the system unstable (even for open-loop stable systems).

Saturation occurs often in real life problems because actuators have an inherent limited capacity and therefore they cannot always provide the action that is required from them. In other words, actuator saturation means that there is a difference between the input command to the actuator and its output, that is, when the actuator reaches its capacity limitation. This limitation can lead to instability.

Equation (4.1) and figure (4.1) show the usual characterization of saturation effects, being y the actuator input, u the actuator output and u_{max} (u_{min}) the maximum (minimum) capacity of the actuator.

$$u = \begin{cases} u_{max} & \text{if } u_{max} \leq y \\ y & \text{if } u_{min} \leq y < u_{max} \\ u_{min} & \text{if } y \leq u_{min} \end{cases} \tag{4.1}$$

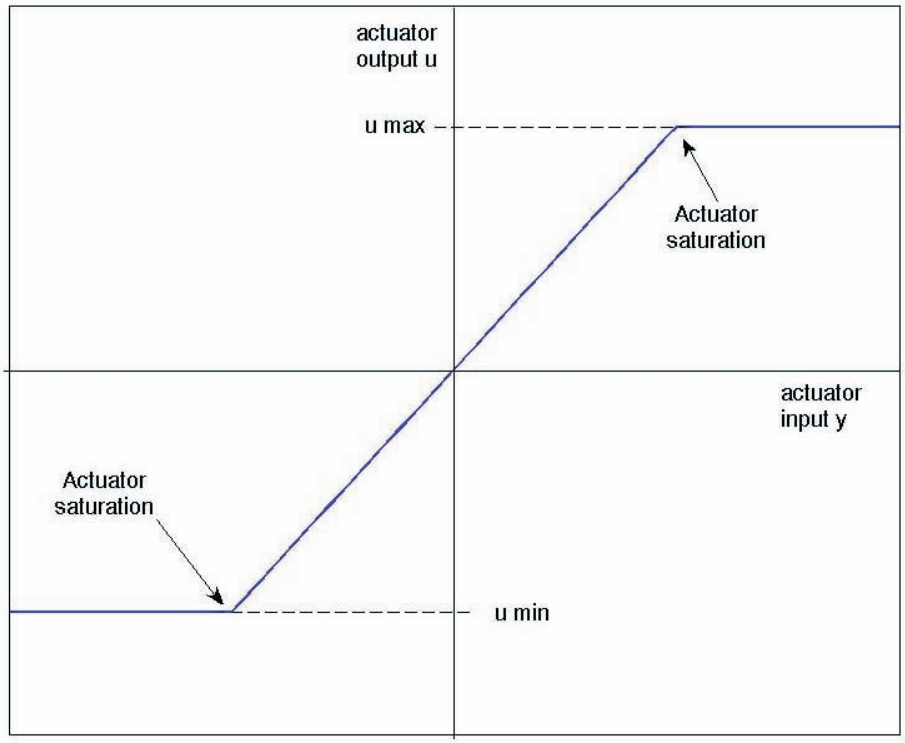

Figure 4.1: Plot of the saturation effect

Figure (4.2) shows the scheme of a plant with an open loop controller and a representation of the actuator. This representation includes a delay (usually due to mechanical limitations) and a saturation block. This block introduces the saturation effects described in (4.1). The delay is often modeled as a first order transfer function.

In the flight control world, saturation has been linked to the failure of several aircrafts [4],[13]. Also, saturation plays a main role in the pilot in-the-loop oscillations (PIO) [2] and in manual flight control situations, specially in high angle of attack conditions [4], [15]. Usually, there have been two main approaches to the design of

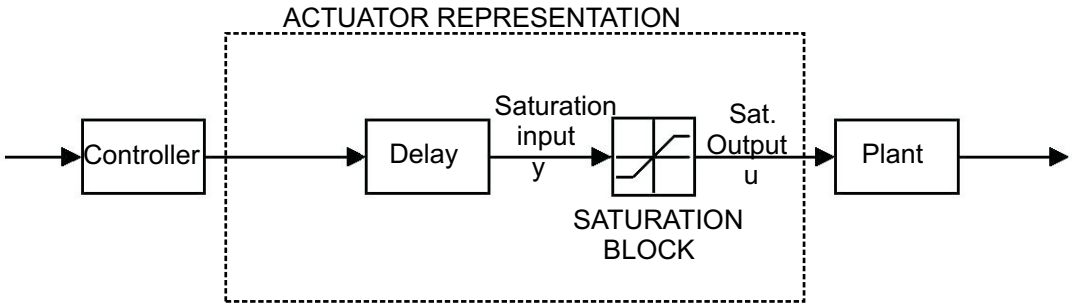

Figure 4.2: Scheme of a plant with an open loop controller and a representation of the actuator. The actuator is represented by a saturation block and a delay transfer function

controllers dealing with saturation.

The first approach takes saturation into account for the design of the controllers from the beginning of the design process. Usually, this means designing a controller that is guaranteed not to saturate under any conditions. It is a rather conservative approach, since the controller will be designed for the worst-case scenario (although this scenario may never occur) and it involves the combination of various requirements [10], [17].

The second approach (known as anti-windup) focuses on the design of the best possible controller even though it may saturate. Once saturation occurs, modifications to this controller are applied in order to return the system to the non-saturated status. The main advantage is that is less conservative than the previous method, since a more aggressive controller is used most of the time. One drawback of this method is the fact that most anti-windup techniques require an stable open-loop plant, which is not always the case [4], [14].

For more information on saturation, the reader is referred to [9].

4.2 Anti-saturation LMIs: basic equations

Consider the following open loop system

$$\begin{cases} \dot{x} = Ax + B_1\omega + B_2u \\ z = Cx + D_1\omega + D_2u \end{cases} \tag{4.2}$$

where x is the state vector, z is the controlled output, u is the control input and ω is the disturbance. The state space matrix A can be stable or unstable, depending on the points about which the model is linearized.

In this thesis only state feedback is considered (4.3), which implies that all the states can be measured. Assuming that all the states are available is not unusual in research in flight control [18]. The gain of the controller is represented by K. Using state feedback, equation (4.2) can be rewritten as (4.4).

$$u = Kx \tag{4.3}$$

$$\begin{cases} \dot{x} = (A + B_2K)x + B_1\omega = A_{CL}x + B_1\omega \\ z = (C + D_2K)x + D_1\omega \end{cases} \tag{4.4}$$

For the disturbance ω, different bounds can be used. In this thesis, we will consider that we known its peak value (4.5). This is a rather conservative bound, because it refers to the maximum possible peak value that might occur, but most probably the disturbance value will be considerably less than this peak value during most or all of the time. How to reduce this conservatism using a scheduling technique will be discussed later (section 4.3).

$$\omega^T(t)\omega(t) \leq \omega_{max}^2 \tag{4.5}$$

There are three basic constraints to consider when designing controllers that take saturation nonlinearity into account while responding to a disturbance:

- **Invariant-set**

  This is the set that the state vector can not leave given any initial conditions inside it, considering the above limits on the disturbance applied.

- **Constraint (actuator saturation)**

  Inside the invariant set, the controller can not be saturated.

- **Performance**

  The effects of the disturbance on the controlled output have to be as small as possible (i.e. the performance has to be as good as possible).

Next, we will express these three constraints mathematically in the form of linear matrix inequalities (LMIs). In order to do that we will use the Lyapunov function (4.6), where P is a positive definite matrix and x is the system's state vector. Although P can be any positive definite matrix, in this thesis we will consider P to be constant.

$$V = x^T P x \tag{4.6}$$

Also, we will use the concept of ellipsoids to define the shape of the different sets in which the state vector can move. An ellipsoid is defined by two parameters: a matrix P and a constant C, such that

$$\varepsilon\{P, C\} = \{x \mid x^T P x < C^2\} \tag{4.7}$$

4.2.1 LMI introduction

A Linear Matrix Inequality (LMI) is any constraint that has the following form

$$F(x) = F_0 + \sum_{i=1}^{N} x_i F_i = F_0 + x_1 F_1 + \ldots + x_N F_N < 0 \tag{4.8}$$

where $x = (x_1, \ldots, x_N)^T \, \epsilon \, \Re^N$ is a vector of unknown variables (the decision or optimization variables) and $F_i \; for \; i \; = \; 0, \ldots, N$ are known symmetric matrices. As long as x enters linearly or affinely in (4.8), the search for a solution is convex. That means that (4.8) can be solved numerically using very efficiently using optimization methods, having the guarantee that a solution will be found if it exists.

The importance of Linear Matrix Inequalities and LMI techniques in the control design area is that a variety of analysis and synthesis problems can be manipulated until they are in the form of (4.8), or its related form

$$minimize \quad c^T x \quad subject \quad to \quad F(x) > 0 \tag{4.9}$$

One example of this manipulation is shown next (corresponds to the basic Lyapunov stability problem): the system (4.10) is stable if and only if there exists a positive definite matrix $P > 0$ such that (4.11) is verified. Equation (4.11) corresponds to a simple convex search in P, easily done with the software available nowadays.

$$\begin{cases} \dot{x} = Ax \\ x(0) = x_0 \end{cases} \tag{4.10}$$

$$PA + A^T P < 0 \tag{4.11}$$

For more information on LMIs and the software used to solve them, the reader is referred to [7] [5].

4.2.2 Invariant-set LMI

Remember that we want the state vector to always remain inside an invariant set, which we define using the ellipsoid $\varepsilon(P, \omega_{max})$ (4.7). This will happen if we can find a $P > 0$ such that $\dot{V} \leq 0$ for all states outside of the invariant set. We want to

stay inside the invariant set even when there is a perturbation applied to the system, which can be written mathematically as

$$\dot{V} + \alpha(V - \omega_{max}^2) < 0 \tag{4.12}$$

It can be seen that $V \leq \omega_{max}^2$ is an attractive invariant set. The boundary of the region corresponds to $V = \omega_{max}^2$. Outside this boundary, we've got $\dot{V} < 0$ and therefore if you start outside you are attracted to the invariant set. If you are inside, $\dot{V}$ can be positive but in the boundary $\dot{V} = 0$, which means that we can not leave the ellipsoid.

So the problem of finding an invariant-set becomes the problem of finding a constant $P > 0$ matrix (recall that $V = x^T P x$) that satisfies (4.12). We can rewrite (4.12) as a linear matrix inequality and then as a matrix expression as follows:

$$\dot{V} + \alpha(V - \omega_{max}^2) < 0$$

$$\dot{x}^T P x + x^T P \dot{x} + \alpha(x^T P x - \omega_{max}^2) < 0$$

$$\left[(A + B_2 K)x + B_1 \omega\right]^T P x + x^T P[(A + B_2 K)x + B_1 \omega] + \alpha(x^T P x - \omega_{max}^2) < 0$$

$$x^T(A^T P + PA)x + x^T(K^T B_2^T P + P B_2 K)x + \omega^T B_1^T P x + x^T P B_1 \omega - \alpha\omega_{max}^2 < 0$$

$$\begin{pmatrix} A^T P + PA + K^T B_2^T P + P B_2 K + \alpha P & PB_1 \\ B_1^T P & -\alpha I \end{pmatrix} < 0 \tag{4.13}$$

However, P and K do not show up linearly in the equation (4.13), which makes it difficult to solve. We can transform it into a convex search by pre and post multiplying by

$$\begin{pmatrix} P^{-1} & 0 \\ 0 & I \end{pmatrix}$$

and by considering

$$Q = P^{-1}, F = KQ$$

The final LMI form of the invariant-set equation is shown in (4.14). This linear matrix inequality guarantees that the states will remain inside the ellipsoid defined by P as long as the maximum peak of the disturbance is ω_{max}^2. Given a value for ω_{max}^2, hence, the objective would be to minimize P such that the value of the control input is as small as possible (and therefore we avoid saturation).

$$\begin{pmatrix} (\boldsymbol{A^TQ + QA + F^TB_2^T + B_2F + \alpha Q}) & \boldsymbol{B_1} \\ \boldsymbol{B_1^T} & \boldsymbol{-\alpha I} \end{pmatrix} < \mathbf{0} \tag{4.14}$$

4.2.3 Constraint LMI

We do not want the controller to saturate inside the ellipsoid $\varepsilon(P, \omega_{max})$ that defines the previous invariant set. Mathematically, this condition is expressed by

$$\mid u \mid^2 < u_{lim}^2$$

$$\omega_{max}^2 \mid u \mid^2 < \omega_{max}^2 u_{lim}^2$$

$$u^T \frac{\omega_{max}^2}{u_{lim}^2} u < \omega_{max}^2 \tag{4.15}$$

Recalling from the previous sections that $V \leq \omega_{max}^2$ and that $u = Kx$, we can rewrite (4.15) in an LMI form:

$$u^T \frac{\omega_{max}^2}{u_{lim}^2} u < V$$

$$x^T [K^T \frac{\omega_{max}^2}{u_{lim}^2} K] x < x^T P x$$

$$K^T \frac{\omega_{max}^2}{u_{lim}^2} K < P$$

$$\begin{pmatrix} P & K^T \\ K & \frac{u_{lim}^2}{\omega_{max}^2} I \end{pmatrix} > 0$$

Repeating the last steps of last section, we obtain the final LMI for non saturation:

$$\begin{pmatrix} \boldsymbol{Q} & \boldsymbol{F^T} \\ \boldsymbol{F} & \frac{\boldsymbol{u_{lim}^2}}{\boldsymbol{\omega_{max}^2}} \end{pmatrix} > \mathbf{0} \tag{4.16}$$

Given a positive definite P matrix, the objective is to maximize the value of ω_{max}^2 inside the ellipsoid created by P, making sure that at all times the control input is non saturated.

4.2.4 Performance LMI

Not only we want our controller not to saturate inside a determined region, we want the best possible response to the perturbation applied. There are different ways to consider the performance of the system. In this thesis, we will use the L_2 or H_∞ gain. The idea is that we want to find the smallest γ (energy gain of the system or L_2) such that

$$\int_0^\infty z^T z dt < \Gamma^2 \int_0^\infty \omega^T \omega dt \tag{4.17}$$

By means of the Lyapunov matrix, equation (4.17) converts into (4.18). One can go from (4.18) to (4.17) by simply integration. Then, we can convert (4.18) into an LMI expression resulting in (4.19).

$$\dot{V}(x) + z^T z - \Gamma^2 \omega^T \omega < 0 \tag{4.18}$$

$$\dot{x}^T P x + x^T P \dot{x} - \Gamma^2 \omega^T \omega + z^T z < 0$$

$$[A_{CL}x + B_1\omega]^T Px + x^T P[A_{CL}x + B_1\omega] - \Gamma^2\omega^T\omega + \\ + [(C + D_2K)x + D_1\omega]^T[(C + D_2K)x + D_1\omega] < 0 \tag{4.19}$$

Considering it as a product of a matrix with two vectors and applying the Schur complement, we get the expression in (4.20). Again, we apply the steps of the end of section 4.2.2 in order to obtain the final form of the performance linear matrix inequality (4.21).

$$\begin{pmatrix} P^{-1}A_{CL}^T + A_{CL}P^{-1} & B_1 & P^{-1}(C^T + K^T D_2^T) \\ B_1^T & -\Gamma I & D_1^T \\ (C + D_2K)P^{-1} & D_1 & -\Gamma I \end{pmatrix} < 0 \tag{4.20}$$

$$\begin{pmatrix} \boldsymbol{QA^T + AQ + B_2F + F^TB_2^T} & \boldsymbol{B_1} & \boldsymbol{QC^T + F^TD_2^T} \\ \boldsymbol{B_1^T} & \boldsymbol{-\Gamma I} & \boldsymbol{D_1^T} \\ \boldsymbol{CQ + D_2F} & \boldsymbol{D_1^T} & \boldsymbol{-\Gamma I} \end{pmatrix} < \mathbf{0} \tag{4.21}$$

So, by minimizing the variable Γ we are minimizing the effect of the disturbance on the controlled output, that is, we are maximizing the performance.

4.3 Scheduling design technique

As mentioned in the previous sections of this chapter, the main problem of considering the saturation effects at the beginning of the design problem is conservatism, that is, the obtention of a controller that is valid when the maximum disturbance is applied but probably will have a poor performance during the rest of the time.

In this section, the causes of this conservatism are briefly shown and a gain-scheduling technique to overcome it is presented. The reader can find detailed explanations of this technique in [17].

4.3.1 Conservatism associated with the design technique

Lets consider that a nominal state-feedback controller K_{nom} is available for the open loop system (4.22). Also, lets consider that the maximum peak bound value of the disturbance is known (equation (4.23)). Although it is very unlikely, this maximum peak value could occur and therefore a controller that does not saturate under ω_{max} must be designed.

$$\begin{cases} \dot{x} = Ax + B_1\omega + B_2u \\ z = Cx + D_1\omega + D_2u \\ y = x \end{cases} \tag{4.22}$$

$$\omega^T(t)\omega(t) \leq \omega_{max}^2 \tag{4.23}$$

Using system analysis LMIs, we can determine the invariant set ellipsoid associated with ω_{max}^2 and K_{nom}, which is $\varepsilon(P_{nom}, \omega_{max}) = \{x \mid x^T P_{nom} x \leq \omega_{max}^2\}$. This ellipsoid includes all the possible values that the state vector can take under ω_{max}^2 and the controller K_{nom}. Figure (4.3) shows an scheme of this invariant set ellipsoid together with the region in which $u = K_{nom}x$ avoids saturation (region between the parallel lines). Also, a smaller invariant set is shown, which represents the maximum peak value of the disturbance (ω_{nom}) that K_{nom} can stand without saturating.

The objective is then to design a controller K_{safe} that provides a safe override for the nominal controller. Providing a safe override means that:

- K_{safe} does not saturate even for the worst case disturbance

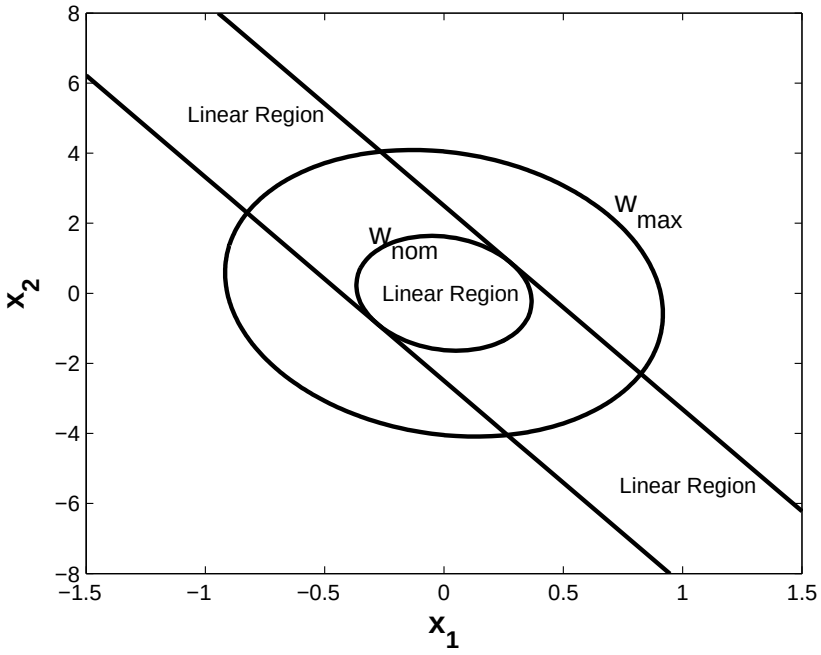

Figure 4.3: Estimate for the smallest invariant set associated with ω_{max} without actuator limits (large ellipsoid) and ω_{nom} (small ellipsoid) for K_{nom}. Parallel lines show region where K_{nom} is not saturated (figure obtained from [17])

- The invariant set associated with K_{safe} and ω_{max} ($\varepsilon(P_{safe}, \omega_{max})$) completely includes the invariant set associated with K_{nom} and ω_{max} ($\varepsilon(P_{nom}, \omega_{max})$), that is,

$$P_{safe} < P_{nom} \tag{4.24}$$

Condition (4.24) is necessary because otherwise the state vector may follow some trajectories which lead outside the safe invariant set (see figure (4.4))and therefore we have no stability guarantee K_{safe} (it may saturate). If we consider $Q = P^{-1}$, condition (4.24) converts into

$$Q_{safe} > Q_{nom} \tag{4.25}$$

Using then LMIs (4.14), (4.16) and (4.21) together with the inclusion condition (4.25) we obtain a safe controller K_{safe} with guarantee that it will not saturate even for the worst possible disturbance and therefore guaranteeing that the system will always remain stable.

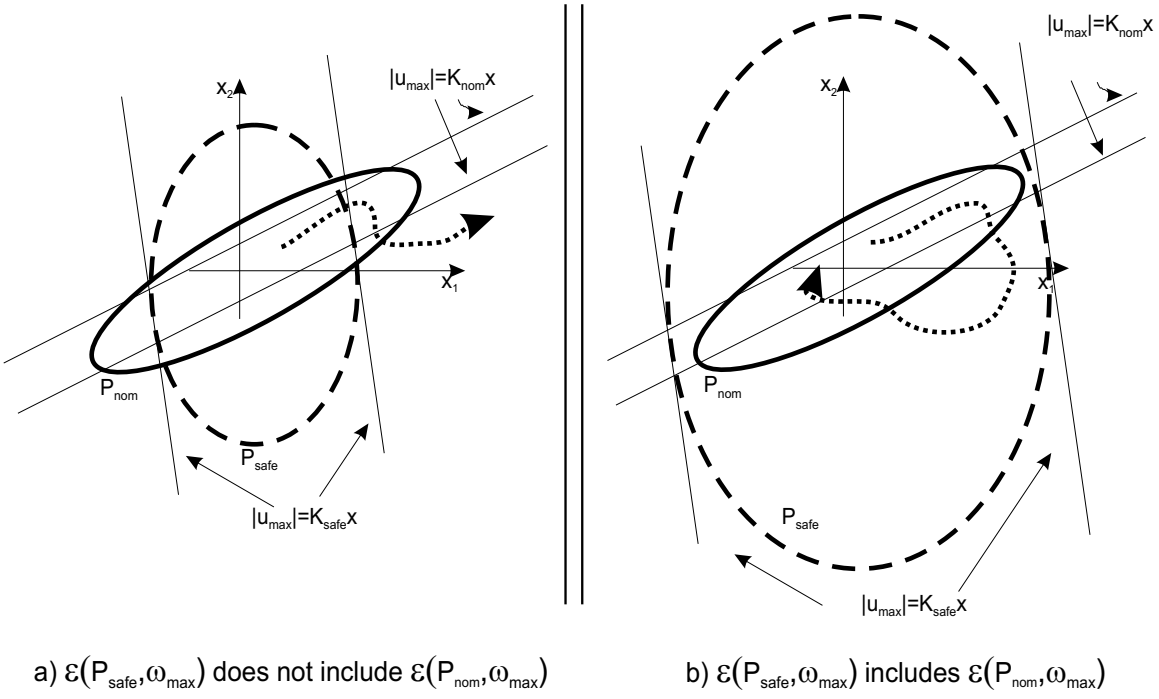

Figure 4.4: Importance of the condition (4.24). On the left, the system may find a way to escape the safe controller and therefore it may become uncontrollable. On the right, this possibility does not exist.

The main problem of this approach, as said before, is conservatism. The invariant-set ellipsoid $\varepsilon(P_{safe}, \omega_{max})$ obtained from solving the LMIs system can be much larger than necessary (see figure (4.5)). The bigger the ellipsoid, the lower the gain of K_{safe} and therefore the lower the performance of the controller.

Basically, using this technique we may end up with a stability guarantee but with a very low performance for values of the disturbance lower than ω_{max}. Since ω_{max} is very unlikely to occur, most of the time we may be using a controller much more conservative than necessary. How to improve the overall performance is an important issue shown next.

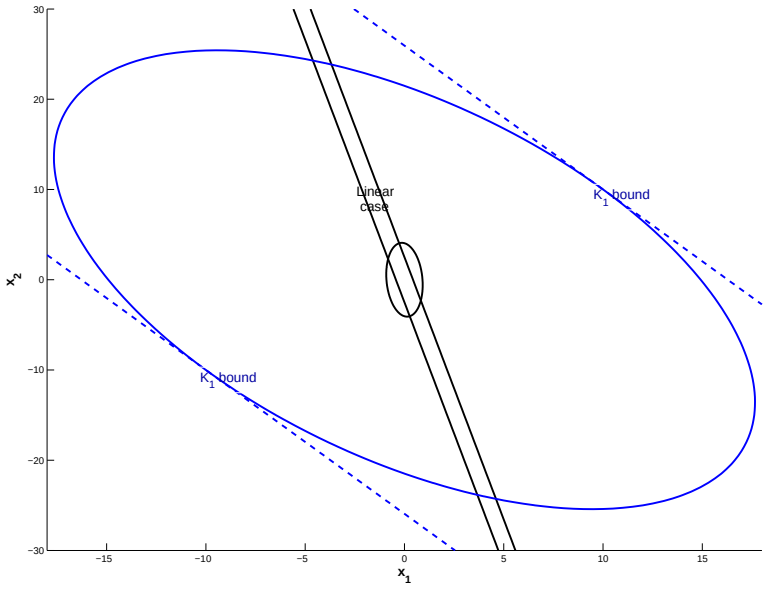

Figure 4.5: Invariant set associated with ω_{max} and K_{safe} compared to linear case (figure obtained from [17])

4.3.2 Gain scheduling technique to overcome conservatism

To overcome the conservatism seen in the previous subsection, controller scheduling is introduced. Consider first a nominal controller (K_{nom}), which in this thesis is designed solving the following system of LMIs:

$$\begin{pmatrix} AQ + QA^T + B_2F_{nom} + F_{nom}^TB_2^T & B_1 & Q_iC_1^T + F_{nom}^TD_2^T \\ B_1^T & -\Gamma_i I & D_1^T \\ CQ + D_2F_{nom} & D_1 & -\Gamma_i I \end{pmatrix} \tag{4.26}$$

$$Q > 0 \tag{4.27}$$

$$\Gamma > \Gamma_{min} \tag{4.28}$$

The objective of equations (4.26) and (4.27) is to obtain a controller (remember that $F_{nom} = K_{nom}Q$) that minimizes the L_2 gain of the system. However, sometimes the nominal controller obtained using this method has an unrealistic gain. In order to decrease the gain, the performance is limited to be higher than a minimum value (equation (4.28)).

Define then the maximum peak value of the disturbance that K_{nom} can stand without saturating as ω_{nom}, as in section 4.3.1. Then, instead of directly designing a safe low-gain controller that does not saturate even for the worst possible disturbance ω_{max}, the idea is to introduce intermediate controllers that are more aggressive (have a better performance) while assuring that the system remains stable for any disturbance up to ω_{max}. We can define four main objectives to accomplish:

- The nominal controller should be used as long a it is not saturated, that is, as long as $u = K_{nom}x \leq u_{lim}$, because it offers the best possible performance
- Performance and stability must be guaranteed for different values of the disturbance, including the case with peak disturbance equal to ω_{max}
- Always use the most aggressive controller available (i.e. the non-saturated controller with a higher gain)
- Maximize the performance for a certain range of disturbances that are more frequent or more likely to saturate the nominal controller.

To address these objectives, we can define intermediate values for the peak disturbance between ω_{nom} and ω_{max}, where n is the total number of controllers that we want to design:

$$\omega_{nom} = \omega_0 < \omega_1 < \ldots < \omega_n = \omega_{max} \tag{4.29}$$

Considering each ω_i to be the worst possible disturbance, we can design a family of controllers K_i with non saturation guarantee for each peak disturbance ω_i. Also, we can expect a better performance (higher gain controller) as i gets smaller.

The way this family of controllers works is that the controller with a higher gain (lower i) that is not saturated is the one to be used. If the disturbance gets worse and K_i saturates, then we switch to the following available lower gain controller (we increase i) that is not saturated, until we reach $K_n = K_{safe}$. The controller K_{safe} is designed using ω_{max} and therefore will never saturate. By contrary, if at any time there are higher gain controllers (smaller i than the one we are using) that are not saturated, we switch back to them. That guarantees that we are always using the most aggressive controller available.

The last thing to do is guarantee that the switching is safe, that is, that the changing from K_i to K_j does not drive the system unstable. To do that, we have to make sure that the invariant set associated with each intermediate controller includes the previous ellipsoids (the ellipsoids corresponding to lower i controllers), as explained at the end of the previous subsection.

Expressing everything mathematically, we can find the set of controllers by minimizing

$$J = \sum_{1}^{N} c_i \Gamma_i \tag{4.30}$$

subject to the following constraints:

$$\begin{pmatrix} A^T Q_i + Q_i A + F_i^T B_2^T + B_2 F_i + \alpha_i Q_i & B_1 \\ B_1^T P & -\alpha_i I \end{pmatrix} < 0 \tag{4.31}$$

$$\begin{pmatrix} Q_i & F_i^T \\ F_i & \frac{u_{lim}^2}{\omega_i^2} I \end{pmatrix} > 0 \tag{4.32}$$

$$\begin{pmatrix} Q_i A^T + A Q_i + B_2 F_i + F_i^T B_2^T & B_1 & Q_i C^T + F_i^T D_2^T \\ B_1^T & -\Gamma_i I & D_1^T \\ C Q_i + D_2 F_i & D_1 & -\Gamma_i I \end{pmatrix} < 0 \tag{4.33}$$

$$Q_{i-1} < Q_i \tag{4.34}$$

From this system of equations we can obtain Q_i and K_i ($F_i = K_i Q_i$) for the disturbance values in (4.29). That means that we have a family of controllers that guarantee stability up to ω_{max} with an overall performance equal to J.

This method solves all the controllers at the same time and allows to maximize the performance for a desired range of disturbances (because they are more common for example) by adequately changing the parameters c_i in equation (4.30). If this constraint in the performance is not needed, we can solve individually for each controller (making sure that its ellipsoid includes the previous ellipsoids). For example, if we want to design the fourth scheduled controller K_4, the LMIs to solve are (4.31) to (4.34) with $i = 4$. Note that Q_{i-1} (Q_3 in this example) includes all the previous Q matrices (Q_{nom}, Q_1 and Q_2) and so does Q_i because of LMI (4.34).

Once all the controllers are obtained, the following algorithm is used to decide which one is actually giving feedback to the system:

if	$\mid K_{nom}\, x \mid \leq u_{lim}$	**then**
	$u = K_{nom}\, x$	
else if	$\mid K_1\, x \mid \leq u_{lim}$	**then**
	$u = K_1\, x$	
$\vdots$	$\vdots$	$\vdots$
else if	$\mid K_{n-1}\, x \mid \leq u_{lim}$	**then**
	$u = K_{n-1}\, x$	
else		
	$u = K_n\, x = K_{safe}\, x$	
end		

4.4 Approach for tracking of general signals

A common problem in aircraft control design is tracking of an unknown time-varying signal, such as the pilot command. It is a very interesting problem because it usually involves some degree of actuator saturation, specially when flying under high angle

of attack conditions, and therefore it will be considered in this thesis.

To use the controller design method presented in the previous sections, however, some changes need to be made, because it is based on the disturbance attenuation problem, not in the tracking one (see section 4.2). To address this problem, we will use the method proposed in [8], that re-writes the tracking problem in a disturbance attenuation way by reducing the norm of the error between the tracking signal (reference) and the controlled output.

As it will be shown next, this method introduces the tracking error into the state vector and considers the tracking reference as a disturbance. By using L_2 gain, it minimizes the effect of the disturbance on the states, and therefore it minimizes the tracking error independently of the disturbance (reference signal).

Let's consider the following system, where x_d is the vector we want to track (reference signal):

$$\begin{cases} \dot{\hat{x}} = \hat{A}\hat{x} + \hat{B}_2 u \\ \hat{y} = C\hat{x} + \hat{D}_{12}u = [I \quad 0]\hat{x} = \hat{x}_1 \\ e = \hat{y} - x_d = \hat{x}_1 - x_d \end{cases} \tag{4.35}$$

Considering the error as a state,

$$\bar{x} = \begin{bmatrix} \hat{x}_1 \\ \hat{x}_2 \end{bmatrix} - \begin{bmatrix} \hat{x}_d \\ 0 \end{bmatrix} = \begin{bmatrix} \hat{x}_1 - \hat{x}_d \\ \hat{x}_2 \end{bmatrix} = \begin{bmatrix} e \\ \hat{x}_2 \end{bmatrix} \tag{4.36}$$

we get the following system

$$\dot{\bar{x}} = \hat{A}\bar{x} + \hat{B}_2 u - \begin{bmatrix} \dot{x}_d \\ 0 \end{bmatrix} + \begin{bmatrix} \hat{A}_{11} \\ \hat{A}_{21} \end{bmatrix} x_d \tag{4.37}$$

$$= \hat{A}\bar{x} + \hat{B}_2 u + \begin{bmatrix} \hat{A}_{11} & -I \\ \hat{A}_{21} & 0 \end{bmatrix} \begin{bmatrix} x_d \\ \dot{x}_d \end{bmatrix} \tag{4.38}$$

$$= \hat{A}\bar{x} + \hat{B}_2 u + \hat{B}_1 \omega \tag{4.39}$$

that has the general form seen in equation (4.2) with the disturbance vector defined

as $\omega = [x_d \quad \dot{x}_d]^T$. Therefore, the maximum peak value for the disturbance can be defined as

$$\omega^T \omega \leq \omega_{max}^2$$

$$[x_d \quad \dot{x}_d] \begin{bmatrix} x_d \\ \dot{x}_d \end{bmatrix} \leq \omega_{max}^2$$

$$x_d^2 + \dot{x}_d^2 \leq \omega_{max}^2$$

Considering then $x_{d,max}$ and $\dot{x}_{d,max}$ to be the maximum values for x_d and $\dot{x}_d$ respectively for all $t > 0$, we obtain the following estimate for the maximum peak value:

$$x_{d,max}^2 + \dot{x}_{d,max}^2 \leq \omega_{max}^2 \tag{4.40}$$

Chapter 5

Simulations

In the previous chapters, we have validated the model of the F-16 aircraft and we have presented the method we will use to avoid saturation. In this chapter, we want to apply the anti-saturation methods seen in chapter 4 to the aircraft model. In order to do that, we need to design a maneuver that involves saturation of the control inputs. Two different maneuvers have been considered:

- Altitude hold autopilot
- Tracking a desired trajectory for the flight path angle

In section 5.1 we will specify some aspects of the work previous to the design of the controllers and the simulations, which include some adjustments made to the technique shown in 4.3.2. In section 5.2 we will apply this method to the altitude hold problem and in section 5.3 we will show the application to the tracking problem.

5.1 Problems setup

In this section we introduce some aspects that required special attention during the preparation of the aircraft simulations.

5.1.1 Inclusion of the elevator actuator

As explained in the modeling section 2.2.1 (specifically in table (2.2)), the elevator is considered as a saturation block plus a first order system, which represents the delay due to physical limitations. The time constant of this first order system is $0.0495\,sec$ [13] and the corresponding transfer function and state space representation of the elevator is:

$$G_{act}(s) = \frac{20.2}{s + 20.2} \tag{5.1}$$

$$\begin{cases} \dot{x}_{act} = A_{act}x_{act} + B_{2,act}u_{act} = -20.2x_{act} + 20.2u_{\delta_e} \\ y_{act} = \delta_e = C_{act}x_{act} = x_{act} \end{cases} \tag{5.2}$$

where u_{δ_e} is the control command referring to the elevator (output of the controller) and δ_e is the actual input to the aircraft's plant. Note that the state space representation has been chosen in order to have δ_e equal to the state of the actuator. This has been done in order to include the elevator actuator state (x_{act}) in the aircraft's state vector, shown next. First, we show the initial aircraft's plant, then we change the state vector including x_{act} and finally we show the equations of the augmented system.

$$\begin{cases} \dot{x} = Ax + [B_{21}\ B_{22}] \begin{pmatrix} \delta_e \\ T \end{pmatrix} \\ y = Cx \end{cases} \tag{5.3}$$

$$x_{aug} = \begin{pmatrix} x \\ x_{act} \end{pmatrix} \tag{5.4}$$

$$\begin{cases} \dot{x}_{aug} = \begin{pmatrix} A & B_{21}C_{act} \\ 0 & A_{act} \end{pmatrix} \begin{pmatrix} x \\ x_{act} \end{pmatrix} + \begin{pmatrix} 0 & B_{22} \\ B_{act} & 0 \end{pmatrix} \begin{pmatrix} u_{\delta_e} \\ u_T \end{pmatrix} \\ y_{aug} = Cx_{aug} \end{cases} \tag{5.5}$$

The reason to include the actuator state into the plant model is to be able to represent the actuator dynamics and therefore obtaining a more realistic model.

Another consequence of including the elevator actuator delay in the model is that we have to consider which signal we are going to bound: the input to the actuator transfer function or the input to the plant. Saturation takes places between the delay block and the system's plant, so the signal δ_e is the one that cannot exceed the saturation limits. However, we decide to bound the signal entering the actuator delay, that is, we decide to bound u_{δ_e} (see figure (5.1)).

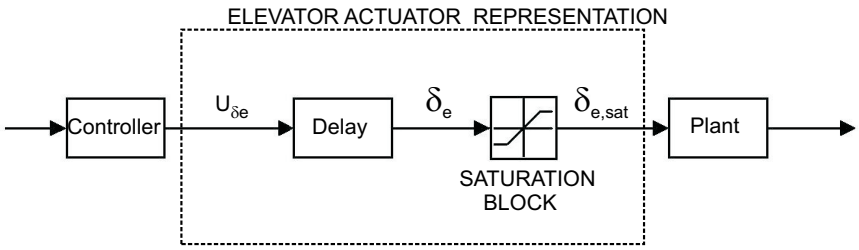

Figure 5.1: Scheme of the elevator actuator

To do that, the peak to peak gain if the delay associated with the actuator must be one (maximum value of the output equals the input) or less than one (in which case we are introducing some conservatism). It cannot be greater than one because then, even though the input to the actuator delay is bounded, the output can be larger than the input and therefore greater than the saturation limits. The peak to

peak gain is checked next.

$$G_{act}(s) = \frac{20.2}{s + 20.2} \rightarrow g(t) = 20.2e^{-20.2t}$$

$$\begin{aligned} \text{Peak to peak gain : } \int_0^\infty \mid g(t) \mid dt &= \int_0^\infty 20.2e^{-20.2t}dt \\ &= 20.2\frac{-1}{20.2}e^{-20.2t}|_0^\infty \\ &= 1. \end{aligned}$$

We can see that the peak to peak gain is 1 and therefore we can limit the signal before the actuator delay without the risk of getting unstable. However, when checking the Bode plot of the elevator's transfer function (figure (5.2)) we can see that the energy gain is 0 dB for low frequencies but it diminishes for higher frequencies. This means that for higher frequencies the output of the actuator delay is smaller than the input, and therefore we are adding some conservatism.

5.1.2 Turbulence model for the altitude hold problem

For the first simulation (altitude hold), we need to model the effects of wind disturbance. According to [16], the effects of the turbulence are introduced to the equations of motion of the aircraft by means of its velocity components: longitudinal, horizontal and vertical. Also according to [16], the effect of the turbulence velocities produces changes in the aerodynamic forces and moments acting on the airplane. Therefore, they enter the equations of motion of the aircraft only through the aerodynamic terms and not the inertial terms.

For altitude hold purposes, the component that mostly affects the response of the aircraft is the vertical velocity (w_g). Since the three gust components can be considered separately due to the linearity of the system, we will only consider the vertical component of the gust.

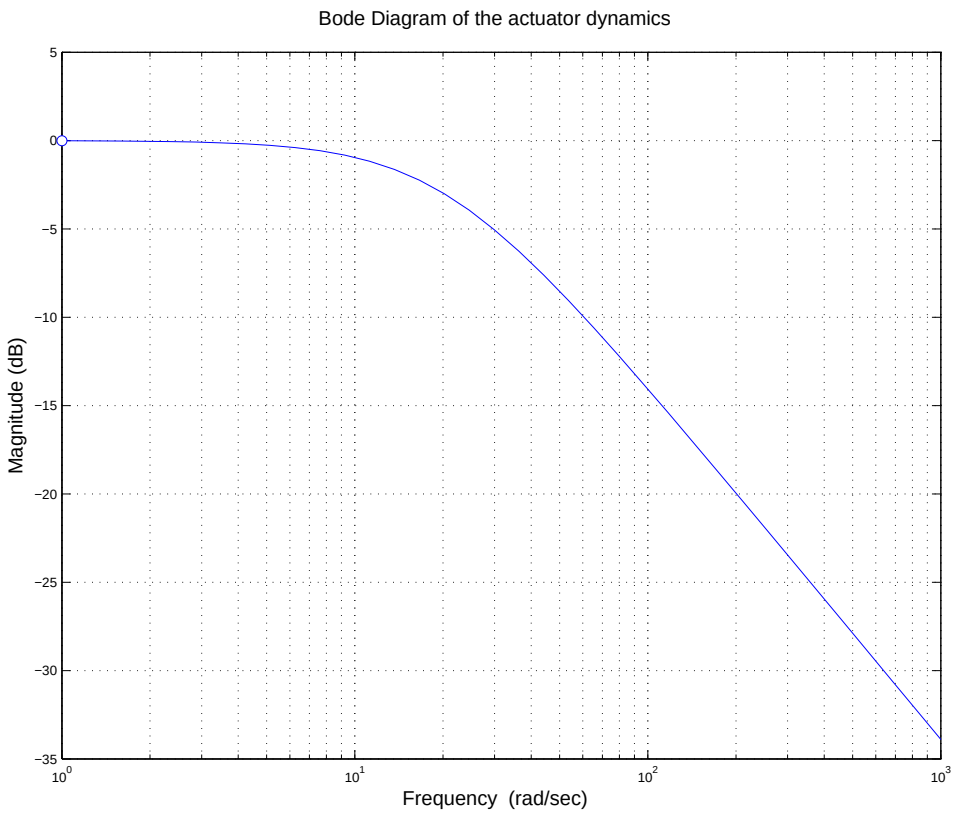

Figure 5.2: Bode plot of the elevator actuator

Using small-angle approximation, the angle of attack to be used in the aerodynamic terms of the equations of motion is:

$$\alpha_A = \alpha + \alpha_g \tag{5.6}$$

with

$$\alpha_g = -\frac{w_g}{V} \tag{5.7}$$

where w_g is the vertical component of the wind velocity, V is the ground velocity of the aircraft and α_g is the effect of turbulence in the angle of attack for aerodynamic purposes.

The wind turbulence model is obtained from [6]. In the military references, both the Dryden and the Von Karman spectral representations are used in order to generate turbulence. Band-limited white noise is filtered by filters derivated from both spectral representations, obtaining the desired component of the wind turbulence.

In this thesis, the Von Karman representation will be used in order to obtain the vertical component of the wind turbulence w_g. The Von Karman spectra is

$$\Phi_{w_g}(\omega) = \sigma_w^2 \frac{L_w}{\pi} \frac{1 + \frac{8}{3}(1.339 L_w \frac{\omega}{V})^2}{[1 + (1.339 L_w \frac{\omega}{V})^2]^{\frac{11}{6}}} \tag{5.8}$$

and the continuous filter obtained from it is

$$H_{w_g}(s) = \frac{\sigma_\omega \sqrt{\frac{L_\omega}{V}}(1 + 2.7478 \frac{L_\omega}{V} s + 0.3398 (\frac{L_\omega}{V})^2 s^2)}{1 + 2.9958 \frac{L_\omega}{V} s + 1.9754 (\frac{L_\omega}{V})^2 s^2 + 0.1539 (\frac{L_\omega}{V})^3 s^3} \tag{5.9}$$

where L_w is the scale of vertical turbulence, σ_w is the vertical gust intensity and ω is the frequency. For an altitude greater than 2000 ft the length of the vertical turbulence is $L_w = 2500\ ft$ [6].

The turbulence intensities are defined in the diagram shown in figure (5.3) [6]. This diagram shows the probability of exceeding a determinate value of turbulence amplitude intensity as a function of altitude. For example, for an altitude around 15000 ft there is a slight probability (10^{-2}) of having a turbulence amplitude larger than 5 ft/s.

5.1.3 Rearranging the equations for the tracking problem

In order to use the controller design approach to the tracking problem presented in 4.4, the variable that we want to follow the tracking command must be part of the state vector. The state vector and state space model of the $F-16$ that we will initially consider for the tracking problem is

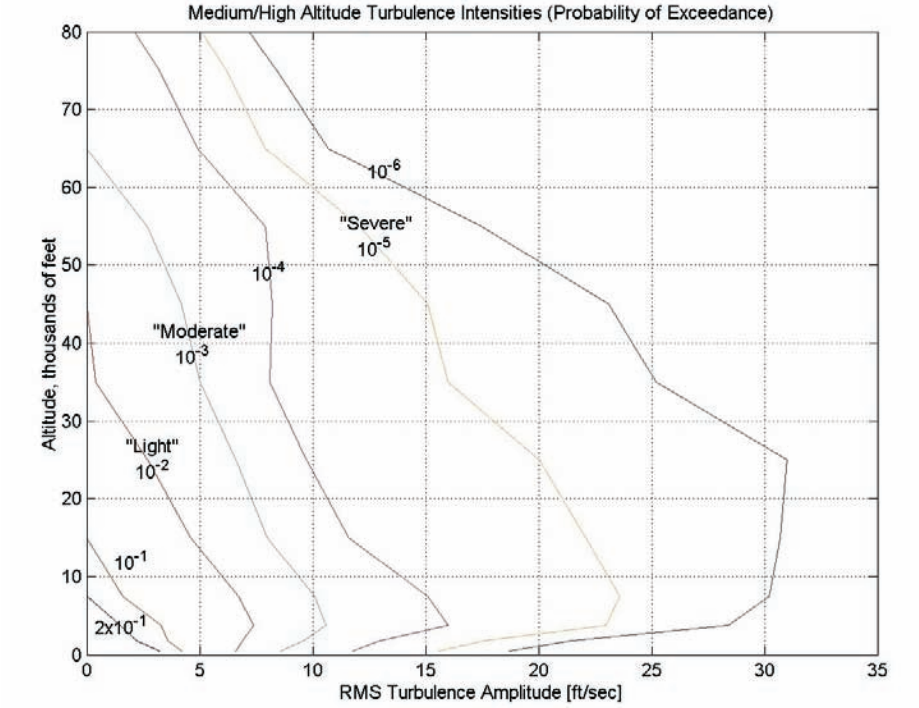

Figure 5.3: Probability of exceedance of turbulence intensity as a function of altitude

$$\begin{cases} \dot{x} = Ax + B_2 u \\ y = Cx + D_{12} u \end{cases} \tag{5.10}$$

$$x = \begin{bmatrix} V \\ \alpha \\ q \\ \theta \\ x_{act} \end{bmatrix} \tag{5.11}$$

Note that we have incorporated the state of the actuator (as explained in section 5.1.2) and that we no longer consider altitude as a state, which is a common assumption in aircraft tracking problems [13] because its effect on the rest of states is very small. Also, in the initial simulations altitude remained almost constant so it was removed from the states for the sake of simplicity of the model.

In this thesis we will work on tracking the flight path angle γ, defined as

$$\gamma = \theta - \alpha \tag{5.12}$$

However, the flight path angle doesn't appear explicitly on the state vector (equation 5.11), so we cannot directly apply the controller design approach presented in 4.4. To apply it, we need to do a coordinate transformation in order to introduce γ into the state vector. This coordinate transformation is done by means of the transformation matrix M.

$$\mathbf{M} = \begin{bmatrix} 0 & -1 & 0 & 1 & 0 \\ 1 & 0 & 0 & 0 & 0 \\ 0 & 0 & 1 & 0 & 0 \\ 0 & 0 & 0 & 1 & 0 \\ 0 & 0 & 0 & 0 & 1 \end{bmatrix} \tag{5.13}$$

$$\hat{x} = Mx = \begin{bmatrix} 0 & -1 & 0 & 1 & 0 \\ 1 & 0 & 0 & 0 & 0 \\ 0 & 0 & 1 & 0 & 0 \\ 0 & 0 & 0 & 1 & 0 \\ 0 & 0 & 0 & 0 & 1 \end{bmatrix} \begin{bmatrix} V \\ \alpha \\ q \\ \theta \\ x_{act} \end{bmatrix} = \begin{bmatrix} \gamma \\ V \\ q \\ \theta \\ x_{act} \end{bmatrix} \tag{5.14}$$

The initial state space system in (5.10) is then transformed into the system in (5.15), which has the same form as in equation (4.35) of section 4.4.

$$\begin{cases} \dot{\hat{x}} = M\dot{x} = MAM^{-1}\hat{x} + MB_2u = \hat{A}\hat{x} + \hat{B}_2u \\ \hat{y} = \hat{C}\hat{x} + \hat{D}_{12}u \end{cases} \tag{5.15}$$

Consequently, now we can use the scheduling design technique to obtain the different controllers to correctly track the reference signal without saturating. Remember

that this design technique required the transformation of the state vector in order to include the error in the tracking variable. To avoid confusion with the notation, the 3 different states vector are shown next:

$$x = \begin{bmatrix} V \\ \alpha \\ q \\ \theta \\ x_{act} \end{bmatrix} \longrightarrow \hat{x} = \begin{bmatrix} \gamma \\ V \\ q \\ \theta \\ x_{act} \end{bmatrix} \longrightarrow \bar{x} = \begin{bmatrix} \gamma - \gamma_{desired} \\ V \\ q \\ \theta \\ x_{act} \end{bmatrix} \tag{5.16}$$

The problem of this rearrangement, however, is that we have changed the state vector and therefore we cannot apply the obtained controllers directly to the nonlinear model because the states of the nonlinear model are still $x = (V, \alpha, q, \theta)^T$. To solve that, another rearrangement has to be made in order to simulate the system with the controllers obtained.

Starting from equation (4.37), multiplying by M on both sides and taking into account the matrix changes introduced in equation (5.15), we can see how to apply both the controller and the reference signal to the nonlinear model (equation (5.17)). The structure of the controller is state feedback, so in the following equations the input command has already been replaced by $u = K\bar{x}$

$$\dot{\bar{x}} = \hat{A}\bar{x} + \hat{B}_2 K\bar{x} + \hat{B}_1\omega$$

$$\dot{\hat{x}} - \dot{x}_d = \hat{A}(\hat{x} - x_d) + \hat{B}_2 K(\hat{x} - x_d) + \hat{A}x_d - \dot{x}_d$$

$$\dot{\hat{x}} = \hat{A}\hat{x} + \hat{B}_2 K\hat{x} - \hat{B}_2 K x_d$$

$$M^{-1}\dot{\hat{x}} = M^{-1}\hat{A}\hat{x} + M^{-1}\hat{B}_2 K\hat{x} - M^{-1}\hat{B}_2 K x_d$$

$$\dot{x} = M^{-1}(MAM^{-1})Mx + M^{-1}(MB_2)KMx - M^{-1}(MB_2)Kx_d$$

$$\boldsymbol{\dot{x} = Ax + B_2 KMx - B_2 Kx_d} \tag{5.17}$$

5.1.4 Adjusting the controller design technique

When applying the controller design technique shown in 4.3.2 to the aircraft problems two main problems showed up: one involving conservatism and the other one involving the switching between controllers. In order to solve them, we had to adjust the technique as follows.

The first problem is associated with conservatism of the controllers and is due to the fact that the saturation limits in the aircraft problems are not symmetric due to the trim values of the actuators. In other words, imagine that we linearize the aircraft around a certain equilibrium condition and the trim value for the elevator is $\delta_{e,0} = 10°$. The elevator has a saturation limit of $25°$, which means that we have non-symmetric bounds for the saturation of the elevator: we have a positive limit of $15°$ ($u_{lim,min}$ in this case) and a negative limit of $-35°$ ($u_{lim,max}$ in this case).

In the constraint LMI (equation (4.16)), however, there is only one possible value for the saturation limit (u_{lim}), that is, the saturation limits must be symmetric (the absolute value of the negative limit and the positive one must be the same).

The objective of the scheduling method is to avoid saturation at all costs and consequently it seems logic to choose u_{lim} to be the smallest value (in absolute terms) so that we can guarantee that if the disturbance stays between the appropriate limits (ω_i for K_i) the controller K_i will not saturate. Doing so, however, we are introducing an important amount of conservatism because we are reducing the actual limits of the actuator.

Continuing with the example above, choosing $u_{lim} = 15°$ means that we are reducing the elevator signal to

$$-5° \leq \delta_e \leq 25°$$

and therefore we are not using its full capacity because we switch to a lower gain controller when $\delta_e < -5°$ even though the elevator is not saturated.

To avoid this conservative effect and use all the capacity of the actuators, we slightly change the design of the controllers as follows:

- The design of the nominal controller is not affected, because it is designed without taking saturation into account. However, in the analysis part we will solve the constraint and invariant-set LMIs with the two different values for u_{lim} ($u_{lim,min}$ and $u_{lim,max}$). We obtain then two values for the maximum peak value disturbance that the nominal controller can stand without saturating ($\omega_{nom,min}$ and $\omega_{nom,max}$). The guaranteed peak value for which the nominal controller will never saturate is $\omega_{nom,min}$. We calculate then the ellipsoid associated with K_{nom} and $\omega_{nom,max}$ ($P_{nom,max}$), which will be used in the next step. We do not need to calculate the ellipsoid associated with K_{nom} and $\omega_{nom,min}$ because it will be included inside $P_{nom,max}$ (since we are just expanding the saturation limits, see figure (5.4)).

- To design the first scheduled controller K_1, we have to impose the ellipsoid associated with K_1 and ω_1 (P_1) to include $P_{nom,max}$. This way we are making sure that when the elevator reaches saturation (with the real values) the system will still be inside P_1: even though K_{nom} may saturate inside $P_{nom,max}$ when reaching $u_{lim,min}$, the system will still be inside P_1 and we will still have control of the system.

- To design the controllers from K_2 to K_{n-1}, we will use the largest limit (in the example would be 35°) as u_{lim}. No matter where we saturate then, the system will always be inside the following ellipsoid (there is no need to switch controllers on the edge of the ellipsoid, we can change inside its limits).

- The design of the last controller ($K_n = K_{safe}$), however, must be conservative because we have to guarantee that it will never saturate even for the worst case. Therefore, u_{lim} must be the smallest value (in the example would be 15°). If the largest value were chosen, there is a possibility that we may saturate inside the ellipsoid associated with K_n and ω_{max}. Since this is the last controller, we can't switch anymore and the system may go out of control.

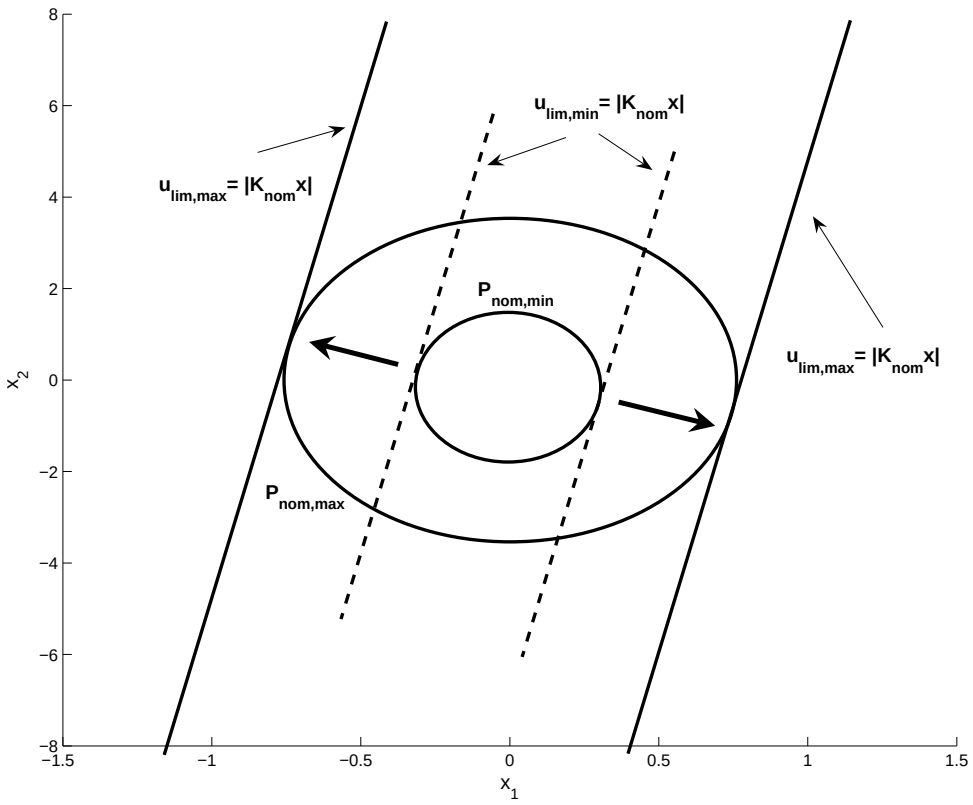

Figure 5.4: Effect of expanding the saturation limits, showing how $P_{nom,max}$ includes $P_{nom,min}$ ($u_{lim,min} \leq u_{lim,max}$)

The result of designing the controllers this way is that we can use the whole capacity of the actuators except for the last controller. Since the objective of the last controller is to guarantee stability in any condition without paying much attention to performance, this reduction in the saturation limits for the last controller is not relevant.

The second problem affects the switching between controllers. In some cases these switchings result in a very abrupt and steep elevator control signal (depending on the differences between the gains of consecutive controllers). In some others the system keeps on switching between consecutive controllers for some time because it is working at the edge of saturation for one of the controllers. This continuous changes also result in a steep control signal and degrade the results of the simulations (they introduce

numerical problems too).

To avoid this problem, two changes are introduced in the switching algorithm shown in section 4.3.2. This changes apply when the system is switching from a low-gain controller to a higher-gain controller (that is, decreasing i). The reason to apply this changes only in this case is because when we switch from a high-gain controller (K_{high}) to a lower-gain controller (K_{low}) we are avoiding the system to saturate, that is, to leave the corresponding ellipsoid. It is an emergency situation to avoid the possibility of the system going out of control.

On the contrary, when switching from K_{low} to a K_{high} we are still inside the ellipsoid associated with the low-gain controller and therefore the system is always under control. We can delay the switch between the controllers to make sure the system enters the ellipsoid associated with the higher gain controller instead of the system getting stuck in the edge of the ellipsoid. Therefore, the objective of the changes introduced is to delay the switching:

- First, we want to make sure that we switch when the system is inside the higher-gain ellipsoid instead of just being on the edge. To accomplish this, we reduce the saturation limit for the higher gain controller when working with the lower gain one. In other words, instead of switching when $K_{high}\, x < 25^\circ$ (for the elevator) we switch when $K_{high}\, x < (25 - \epsilon)^\circ$.

- Second, we want to avoid abrupt changes between controllers. To accomplish it, we limit the rate of change of the elevator control signal when switching from K_{low} to K_{high}. We limit this rate as follows (all the matrices and vectors are available in real time):

$$\dot{u} = K\,\dot{x} = K\,[Ax + B_2 K x + B_1 \omega] < tan(\varrho)$$

In the simulations of this thesis, we used a value of $\epsilon = 0.5^\circ$ for the elevator and of $\epsilon = 100\ lb$ for the thrust. Also, we used a value of $\varrho = 86^\circ$. Taking into account this changes, the switching algorithms were changed. Next we can see the algorithm used

when only the elevator is used (no thrust), which is the case for the altitude problem. The *cnt* variable contains information about the actual controller being used ($cnt = 0$ when we are using the nominal controller, $cnt = n$ when we use the safe controller).

FOR ALTITUDE HOLD (only ELEVATOR is used)

if $(\mid K_{nom}\, x + \delta_{e,0} \mid \leq 25^\circ)$ & $cnt = 0$ **then**
$u = K_{nom}\, x$
$cnt = 0$
else if $(\mid K_{nom}\, x + \delta_{e,0} \mid \leq 24.5^\circ)$ & $\dot{u} < tan(86^\circ)$ & $cnt > 0$ **then**
$u = K_{nom}\, x$
$cnt = 0$
else if $(\mid K_1\, x + \delta_{e,0} \mid \leq 25^\circ)$ & $cnt < 2$ **then**
$u = K_1\, x$
$cnt = 1$
else if $(\mid K_1\, x + \delta_{e,0} \mid \leq 24.5^\circ)$ & $\dot{u} < tan(86^\circ)$ & $cnt > 1$ **then**
$u = K_1\, x$
$cnt = 1$
$\vdots$ $\vdots$ $\vdots$
else if $(\mid K_{n-1}\, x + \delta_{e,0} \mid \leq 25^\circ)$ & $cnt < n$ **then**
$u = K_{n-1}\, x$
$cnt = n - 1$
else if $(\mid K_{n-1}\, x + \delta_{e,0} \mid \leq 24.5^\circ)$ & $\dot{u} < tan(86^\circ)$ & $cnt > n - 1$ **then**
$u = K_{n-1}\, x$
$cnt = n - 1$
else
$u = K_n\, x = K_{safe}\, x$
$cnt = n$
end

5.2 Altitude hold

The first maneuver that we will use to check the performance of the scheduling controller design technique consists on an altitude hold autopilot. Some examples of controller design for this autopilot maneuver can be found in [18].

The objective is that the controller must maintain the same altitude independently of the wind conditions (turbulence). This turbulence basically effects the aerodynamic coefficients of the airplane, as explained in section 5.1.2 together with the turbulence model used. According to the design guidelines provided in [18], this altitude hold is designed also trying to keep the value of θ constant.

The first step is to choose a trim condition in which we want to work. A pilot usually wants to use the autopilot for altitude hold in cruise flight conditions, that is, in low angle of attack conditions. It would not make sense to try to keep altitude constant when flying in a high angle of attack position, mainly because there would be a huge drag force and it would result in a waste of fuel. The trim condition chosen, together with the matrices resulting from the linearization and used in the controller design are shown next.

$$x_0 = \begin{bmatrix} V = 600 ft/s \\ \alpha = 2.68^\circ \\ q = 0\ rad/s \\ \theta = 2.68^\circ \\ h = 20000 ft \\ x_{act} = 0 \end{bmatrix} \tag{5.18}$$

$$u_0 = \begin{bmatrix} \delta_e = 3.88^\circ \\ \delta_{ptv} = 0^\circ \\ T = 2207.8\ lb \\ \omega = 0\ ft/s \end{bmatrix} \tag{5.19}$$

$$\dot{x} = 10^{-1}\begin{pmatrix} -9.968e-2 & -8.378 & -7.546 & -321.7 & 1.013e-3 & 64.50 \\ -1.778e-3 & -6.502 & 9.483 & 0 & 1.806e-5 & -7.881e-1 \\ \simeq 0 & 62.84 & -6.884 & 0 & \simeq 0 & -76.57 \\ 0 & 0 & 10 & 0 & 0 & 0 \\ \simeq 0 & -5999 & 0 & 5999 & 0 & 0 \\ 0 & 0 & 0 & 0 & 0 & -202 \end{pmatrix} x + \\ + 10^{-3}\begin{pmatrix} 1.396 \\ 1.084 \\ -1.047 \\ 0 \\ 0 \\ 0 \end{pmatrix}\omega + \begin{pmatrix} 0 \\ 0 \\ 0 \\ 0 \\ 0 \\ 20.2 \end{pmatrix} u_{\delta_e} \tag{5.20}$$

$$y = \begin{pmatrix} \theta \\ h \end{pmatrix} = \begin{pmatrix} 0 & 0 & 0 & 1 & 0 & 0 \\ 0 & 0 & 0 & 0 & 1 & 0 \end{pmatrix} x \tag{5.21}$$

This condition is obtained using a relative position of the center of gravity of $x_{cg} = 0.35\bar{c}$, which coincides with the reference value $x_{cg,ref} = 0.35\bar{c}$. This position is chosen because we assume the aircraft to be on a cruise flight with no changes in the load that could move the center of gravity from its reference position. Also, in the altitude hold maneuver only the elevator is considered [18]. We assume that on a cruise flight the engine is working at the maximum performance level in order to save fuel and therefore it will not be used to attenuate wind disturbances in order to keep altitude constant (instead, it would be used to change altitudes for example).

Initially, we check the response of the linear model of the aircraft without any controller to a moderate disturbance (probability of exceedance of high-altitude intensity = $10e^{-3}$). To obtain the disturbance, a Von Karman wind turbulence model included in the Simulink Aerospace Blockset® is used. The resulting wind velocity (disturbance signal) and the altitude response are shown in figure (5.5). We can clearly see that the airplane goes unstable, so there is a need of a controller that deals

with the wind disturbance applied.

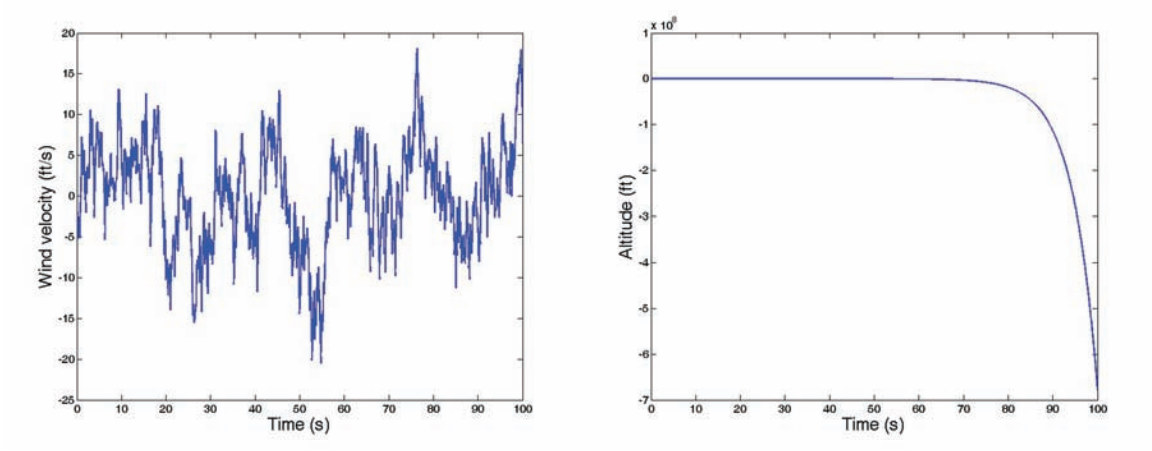

a) Disturbance ω b) Altitude *h*

Figure 5.5: Plot of the wind velocity obtained from a moderate disturbance and the open loop response (altitude) of the linear model of the aircraft to this disturbance

A very high-gain nominal controller is then designed. Although the values may be somewhat higher than usual, the objective is to saturate so there is a need for a safe controller to guarantee stability. Also, in case the safe controller is too conservative the objective is to check the scheduling approach presented in section 4.3.2 to improve the overall performance of the system. The values of the nominal controller K_{nom} (obtained using the LMI system (4.26)-(4.28) without taking saturation into consideration), its performance ($Perf_{nom}$) and the maximum peak value of the disturbance (ω_{nom}) that it can stand without saturating (theoretically, obtained from solving the LMIs) are shown in (5.22), (5.23) and (5.24), respectively.

$$K_{nom} = [\, 8.0831 \cdot 10^{-3} \quad -299.8368 \quad 6.4759 \quad 333.4070 \quad 1.6589 \quad 0\,] \tag{5.22}$$

$$\Gamma_{nom} = 0.06244 \tag{5.23}$$

$$\omega_{nom} = 0.1308\ ft/s \tag{5.24}$$

The response of the aircraft with the nominal controller to the same disturbance applied before (for a longer period of time, exactly 100 seconds) can be checked in figure (5.6). Note that the values for the states shown include the trim values of

(5.18) and (5.19) in order to make them physically meaningful. In figure (5.6) we can see that the response of the aircraft is quite good, with a maximum change in θ of approximately $\pm 2^\circ$ and in altitude h of approximately $\pm 1\ ft$. Also, we can observe that the elevator takes values between -9° and 6°, which is far from the saturation limit of $\mid u_{max} \mid = 25^\circ$.

Therefore, we need to use a worse disturbance in order to saturate the elevator. We decide to use the worst possible case, that is, a probability of exceedance of high-altitude intensity equal to 10^{-6}. Figure (5.7) shows the results obtained. Altitude remains again almost constant, with a maximum change of $\pm 3\ ft$, while θ has a maximum change of $\pm 9^\circ$. This change in θ is probably too high, but we can see that the elevator signal does not saturate (it reaches the saturation limits a few times but does not seem to saturate).

Another important aspect to take into account is the difference between the theoretical value of the maximum peak disturbance ω_{nom} that the nominal controller can stand without saturating and the real value at which it saturates. The analysis of the nominal controller predicted that the maximum peak disturbance value that the nominal controller could stand without saturating is $\omega_{nom} = 0.1308 ft/s$ (equation (5.24)), while simulations showed that the controller is about to saturate for a disturbance with a maximum peak value of $\omega \simeq 80 ft/s$. This is a clear example of the conservatism associated with using the worst-case scenario guarantee: there might be a signal with a maximum value of $\omega_{nom} = 0.1308 ft/s$ that saturates the nominal controller (e.g. a constant disturbance of value equal to ω_{nom}) but the wind model used to obtain the disturbance signal is not this worst scenario case and therefore the controller is able to stand a higher maximum peak value of the disturbance.

Due to these facts, we decide not to apply the scheduling controller design approach to the altitude hold problem and apply it to the tracking problem, shown in next section.

5.3 Tracking

In the previous section we have seen that saturation is not a big issue in the altitude hold autopilot problem. However, research has been done about saturation of the actuators of an aircraft during the tracking of trajectories [13]. Therefore, the next step is to design a tracking maneuver for the flight path angle ($\gamma = \theta - \alpha$) following the scheduling design method discussed in 4.3. The changes in the equations in order to apply this method have been discussed in 4.4 and 5.1.3.

In this tracking problem, altitude will no longer be considered a state of the system [13]. It will be considered a constant input to the system, and therefore the state vector from now on is (including the actuator state):

$$x = \begin{bmatrix} V \\ \alpha \\ q \\ \theta \\ x_{act} \end{bmatrix} \tag{5.25}$$

The objective is to track the flight path angle reference command with a maximum steady state error of 1.25%. This tracking problem is often formulated as a model-following problem, according to [13], where an ideal second order model is to be followed,where γ_{cmd} is the reference command and γ_{ideal} is the ideal response that should be obtained from the aircraft model.

$$\frac{\gamma_{ideal}}{\gamma_{cmd}} = \frac{w_{ideal}^2}{s^2 + 2\zeta_{ideal} w_{ideal} s + w_{ideal}^2} \tag{5.26}$$

The parameters in 5.26 must be chosen according to the desired flying qualities. A natural frequency of $1.5 rad/s$ and a damping ratio of 0.8 are chosen [13], obtaining

the following ideal model:

$$\frac{\gamma_{ideal}}{\gamma_{cmd}} = \frac{2.25}{s^2 + 2.4s + 2.25} \tag{5.27}$$

The control inputs used for the simulations are the elevator and the engine thrust, i.e. $u = [\delta_e \quad T]^T$. The saturation limits for the elevator can be seen in table 2.2. The saturation limits for the thrust are deduced from the engine model presented in [18], and presented in table 2.3. Although the engine model shows that the engine can provide negative thrust, this is only possible in specific conditions: relatively low altitude (below 30000/; ft), high Mach number (higher than 0.6) and the engine working on the *idle* regime. Since during the tracking of a reference flight path angle the engine is more likely to be working on the *military* or *maximum* regime and the conditions chosen for the simulations have a low Mach number (around 0.1) we will consider that the engine cannot provide negative thrust, that is, we cannot obtain negative values for T. Therefore the actual saturation limits for the thrust actuator are the ones in (5.28).

$$0\ lb \leq T \leq 28886\ lb \tag{5.28}$$

The controller design method that we will use requires the setting of the maximum peak value of the disturbance, for which we will guarantee that the aircraft will not saturate and will remain stable. The reference signal to track is γ_{ideal}, which is the output of the second order system in (5.27). Assuming that the input to this filter is a step of amplitude A, we can easily obtain the time expression for both γ_{ideal} and $\dot{\gamma}_{ideal}$ and its maximum value given the input step:

$$\gamma_{ideal} = A[1 - e^{-\xi\omega_n t}(cos\omega_d t + \frac{\xi}{\sqrt{(1-\xi^2)}} sin\omega_d t)] \tag{5.29}$$

$$\dot{\gamma_{ideal}} = A[sin\omega_d t \frac{\omega_n}{\sqrt{1-\xi^2}} e^{-\xi\omega_n t}] \tag{5.30}$$

Two different cases will be shown: an stable and an unstable case. The reason is to show that this technique can be applied independently of the stability of the open loop system (which depends on the linearization conditions). In both cases, the equilibrium conditions have been obtained using a center of gravity position of $x_{cg} = 0.3\bar{c}$ (the same one used in [13]) and the nonlinear model has been used in the simulations. Also, in order to compare the results with [13] a doublet will be used as the reference signal (γ_{cmd}). The response of the second order system (5.27) to this doublet will be the ideal signal to track (γ_{ideal}). The differences between γ_{cmd} and γ_{ideal} can be checked in figure (5.8).

Case 1: Stable plant (V=160 ft/s, $\alpha = 35.01°$)

The equilibrium conditions for this case are:

$$x_0 = \begin{bmatrix} V = 160\ ft/s \\ \alpha = 35.01° \\ q = 0\ rad/s \\ \theta = 35.01° \\ x_{act} = 0 \end{bmatrix} \tag{5.31}$$

$$u_0 = \begin{bmatrix} h = 3420\ ft \\ \delta_e = -11.31° \\ \delta_{ptv} = 0 rad/s \\ T = 10309\ lb \end{bmatrix} \tag{5.32}$$

In this example the objective will be to track a $\pm 3°$ flight path angle doublet, although we want to guarantee that the aircraft will remain stable up to a maximum peak disturbance in the flight path angle of $\pm 5°$. Table (5.1) shows the maximum values of γ_{ideal} and $\dot{\gamma}_{ideal}$ for a $\pm 5°$ doublet, which are then used to calculate the maximum peak value of the disturbance/tracking reference signal. These values were obtained by manually inspecting their plots.

Table 5.1: Maximum peak values of the disturbance for a $\pm 5^{\circ}$ doublet

Variable	Maximum value
$\mid \gamma_{ideal,max} \mid$	0.0899
$\mid \dot{\gamma}_{ideal,max} \mid$	0.1077
ω_{max}	$\sqrt{0.0899^2 + 0.1077^2} = 0.14\ rad$

Four different controllers (K_{nom}, K_1, K_2 and K_{safe}) are designed. Equations (5.33)-(5.36) show the values of these controllers and their maximum peak disturbance values. It can be noted that the safe controller (K_{safe}) is designed such that there is a guarantee that it will not saturate for a value greater or equal than the maximum disturbance peak value that we are expecting (ω_{max} in table (5.1)). The intermediate values for the maximum peak disturbances ω_1 and ω_2 are chosen by trial and error method in order to obtain a good tracking. Note that K_{nom} is designed without considering the state of the actuator (i.e. the last column of (5.33) is 0). Since the objective of the thesis is to design the safer controllers (K_1, K_2 and so on) on top of K_{nom} (which is considered to be given) this assumption does not affect the results.

$$\begin{cases} K_{nom} &= \begin{bmatrix} 1.814 \cdot 10^3 & -7.775 \cdot 10^{-1} & 2.221 \cdot 10^1 & 3.233 \cdot 10^1 & 0 \\ -1.9491 \cdot 10^6 & 8.339 \cdot 10^2 & -4.318 \cdot 10^4 & -6.542 \cdot 10^4 & 0 \end{bmatrix} \\ \omega_{nom} &= 1.211 \cdot 10^{-3}\ rad \end{cases} \tag{5.33}$$

$$\begin{cases} K_1 &= \begin{bmatrix} 1.693 \cdot 10^2 & -1.370 \cdot 10^{-2} & -6.681 \cdot 10^{-2} & -6.059 \cdot 10^{-1} & -1.333 \cdot 10^{-1} \\ -4.922 \cdot 10^6 & -3.608 \cdot 10^2 & -2.967 \cdot 10^4 & -3.670 \cdot 10^4 & -2.676 \cdot 10^3 \end{bmatrix} \\ \omega_1 &= 5 \cdot 10^{-3}\ rad \end{cases} \tag{5.34}$$

$$\begin{cases} K_2 &= \begin{bmatrix} -1.583 \cdot 10^{1} & -4.070 \cdot 10^{-3} & 5.562 \cdot 10^{-1} & 1.979 \cdot 10^{-1} & -4.212 \cdot 10^{-2} \\ -7.089 \cdot 10^{5} & -2.578 \cdot 10^{2} & -1.670 \cdot 10^{4} & -1.636 \cdot 10^{4} & -7.886 \cdot 10^{1} \end{bmatrix} \\ \omega_2 &= 2 \cdot 10^{-2}\ rad \end{cases} \tag{5.35}$$

$$\begin{cases} K_{safe} &= \begin{bmatrix} -1.937 \cdot 10^{-2} & -3.571 \cdot 10^{-4} & 2.362 \cdot 10^{-2} & 1.322 \cdot 10^{-2} & -9.976 \cdot 10^{-4} \\ -2.541 \cdot 10^{3} & -1.488 \cdot 10^{1} & 5.110 \cdot 10^{2} & 5.585 \cdot 10^{2} & -2.245 \cdot 10^{1} \end{bmatrix} \\ \omega_2 &= 1.45 \cdot 10^{-1}\ rad \end{cases} \tag{5.36}$$

Different conditions are checked in this case by tracking reference signals of different amplitude. We start by introducing a reference signal of $\pm 1.5°$ to check the performance of the nominal controller K_{nom}. The results are shown in figure (5.9). The tracking is accurate and there is no saturation of the nominal controller, therefore there is no need to switch to the lower-gain controllers.

Since we want to saturate the controller to be able to check the scheduling controller design technique, we have to increase the amplitude of the reference signal. Around an amplitude of $\pm 1.8°$ the nominal controller starts to saturate, but this saturation does not affect the quality of the tracking. We choose then a reference signal with an amplitude of $\pm 3°$. Figure (5.10) shows the response of the aircraft using only the nominal controller: saturation occurs and the performance gets worse because of that. Since we are working on an stable equilibrium condition the system does not get unstable in this simulation, but there is no guarantee of this fact: we need to use other controllers that guarantee stability.

At this point, figures (5.11) and (5.12) justify the use of intermediate controllers instead of just switching between the K_{nom} and K_{safe} (the one designed to stand the predicted worst case disturbance). On one hand, figure (5.11) shows the nonlinear response of the aircraft by only switching between K_{nom} and K_{safe}. On the other

hand, figure (5.12) shows the nonlinear response by using the 4 controllers introduced before (the variable *controller* on the bottom plot shows which controller is active, i.e. the non saturated controller with a higher gain). Although saturation does not occur in any of the two situations, it can be clearly seen that the tracking in the second situation is much better than in the first one, which is the key aspect of this new technique being tested.

In the first situation, only the nominal controller and the safe controller are available, therefore when the nominal controller saturates we must switch to the safe controller, no matter the level of the disturbance and if the nominal controller is highly or just slightly saturated. This controller has a low gain and its performance is not optimal, since it is designed to guarantee stability even for the worst-case scenario and in that case performance is not the main concern. Instead, in the second situation we do not have to only switch between the nominal and the safe controller because there are the intermediate controllers also available. These controllers are designed considering different levels of disturbance, and have intermediate gains and performances between the nominal and the safe controller. For a low level of disturbance we can continue using high gain controllers (e.g. K_1 or K_2) with a very good performance while we still have the safe controller on top of them to guarantee stability in case the worst-case scenario shows up.

Finally, figure (5.13) shows the response of the nonlinear aircraft to a $\pm 5^\circ$ doublet as the reference flight path angle, which is the worst-case scenario considered in the controller design. The objective is to show that stability is guaranteed even in this worst-case scenario, although the tracking is not optimal. However, this is not a big concern since the priority in a high angle of attack situation is to guarantee stability and not tracking quality, which is a priority in the low angle of attack region [19].

The results from [13] in the same equilibrium condition can be seen in figures (5.14) and (5.15) in order to compare them with the results from this thesis. It can be seen that when the tracking signal has a small amplitude ($\pm 1^\circ$ doublet in [13], $\pm 1.5^\circ$ in this thesis) the nominal controllers do not saturate and the performances are practically the same (compare figures (5.9) and (5.14)). Then a $\pm 2^\circ$ doublet is used in [13] to check the performance of their anti-windup controller, while in this thesis the

response to a $\pm 3^\circ$ doublet is shown. In both cases the quality of the tracking is very similar (compare figures (5.12) and (5.15)) when usually the larger the disturbance the poorer the quality of the tracking. This shows the potential of the scheduling approach discussed in section 4.3.2: we can provide accurate tracking for larger levels of the disturbance/reference tracking signal because we have intermediate controllers available designed to stand different levels of disturbance.

Case 2: Unstable plant (V=165 ft/s, $\alpha = 29.92^\circ$)

The equilibrium conditions for this case are:

$$x_0 = \begin{bmatrix} V = 165\ ft/s \\ \alpha = 29.92^\circ \\ q = 0\ rad/s \\ \theta = 29.92^\circ \\ x_{act} = 0 \end{bmatrix} \tag{5.37}$$

$$u_0 = \begin{bmatrix} h = 400\ ft \\ \delta_e = -7.95^\circ \\ \delta_{ptv} = 0 rad/s \\ T = 8699\ lb \end{bmatrix} \tag{5.38}$$

Again, the objective will be to track a $\pm 3^\circ$ flight path angle doublet but we want to guarantee that the aircraft will remain stable up to a maximum peak disturbance in the flight path angle of $\pm 3.5^\circ$. Table (5.2) shows the maximum values of γ_{ideal} and $\dot{\gamma}_{ideal}$ obtained from a $\pm 3.5^\circ$ doublet reference signal as well as the maximum peak value of the disturbance/reference tracking signal that results from them. These values were obtained by manually inspecting their plots.

In this case, five different controllers (K_{nom}, K_1, K_2, K_3 and K_{safe}) are designed. Equations (5.39)-(5.43) show the values of these controllers and their maximum peak

Table 5.2: Maximum peak values of the disturbance for a $\pm 3.5^{\circ}$ doublet

Variable	Maximum value
$\mid \gamma_{ideal,max} \mid$	0.0629
$\mid \dot{\gamma}_{ideal,max} \mid$	0.0747
ω_{max}	$\sqrt{0.0629^2 + 0.0747^2} = 0.098\ rad$

disturbance values. It can be noted that the safe controller (K_{safe}) is designed such that there is a guarantee that it will not saturate for a value greater or equal than the maximum disturbance peak value that we are expecting. The maximum peak value of the $\pm 3.5^{\circ}$ doublet is $\omega_{max} = 0.098\ rad$ and we choose to design the safe controller with $\omega_{safe} = 0.1\ rad \geq \omega_{max}$. The intermediate values for the maximum peak disturbances ω_1, ω_2 and ω_3 are chosen by trial and error method in order to obtain a good tracking. Note also that an extra intermediate controller is needed with respect to the previous stable case in order to improve the overall performance of the switching controllers system.

$$\begin{cases} K_{nom} &= \begin{bmatrix} 1.204 \cdot 10^3 & -7.204 \cdot 10^{-1} & 2.889 \cdot 10^1 & 6.177 \cdot 10^1 & 0 \\ -2.4098 \cdot 10^6 & 9.187 \cdot 10^2 & -5.897 \cdot 10^4 & -1.360 \cdot 10^5 & 0 \end{bmatrix} \\ \omega_{nom} &= 2.511 \cdot 10^{-3}\ rad \end{cases} \tag{5.39}$$

$$\begin{cases} K_1 &= \begin{bmatrix} 5.048 & 1.569 \cdot 10^{-2} & 2.669 & 4.244 & -1.232 \cdot 10^{-1} \\ -1.775 \cdot 10^6 & -4.937 \cdot 10^2 & -4.923 \cdot 10^4 & -1.019 \cdot 10^5 & 4.077 \end{bmatrix} \\ \omega_1 &= 1.5 \cdot 10^{-2}\ rad \end{cases} \tag{5.40}$$

$$\begin{cases} K_2 &= \begin{bmatrix} 2.039 \cdot 10^{-1} & 2.273 \cdot 10^{-3} & 1.103 & 1.336 & -5.930 \cdot 10^{-2} \\ -6.561 \cdot 10^{5} & -3.262 \cdot 10^{2} & -2.513 \cdot 10^{4} & -5.011 \cdot 10^{4} & 2.883 \cdot 10^{2} \end{bmatrix} \\ \omega_2 &= 2.6 \cdot 10^{-2}\ rad \end{cases} \tag{5.41}$$

$$\begin{cases} K_3 &= \begin{bmatrix} 8.197 \cdot 10^{-1} & 1.606 \cdot 10^{-3} & 8.081 \cdot 10^{-1} & 8.965 \cdot 10^{-1} & -4.311 \cdot 10^{-2} \\ -2.408 \cdot 10^{5} & -2.485 \cdot 10^{2} & -1.903 \cdot 10^{4} & -3.171 \cdot 10^{4} & 6.380 \cdot 10^{2} \end{bmatrix} \\ \omega_3 &= 3.2 \cdot 10^{-2}\ rad \end{cases} \tag{5.42}$$

$$\begin{cases} K_{safe} &= \begin{bmatrix} -1.410 \cdot 10^{-2} & -1.489 \cdot 10^{-4} & 7.773 \cdot 10^{-2} & 4.929 \cdot 10^{-2} & -4.387 \cdot 10^{-3} \\ -5.603 \cdot 10^{2} & -5.032 & 1.884 \cdot 10^{3} & 1.249 \cdot 10^{3} & -1.062 \cdot 10^{2} \end{bmatrix} \\ \omega_{safe} &= 1 \cdot 10^{-1}\ rad \end{cases} \tag{5.43}$$

As in the previous case, different conditions are checked by tracking reference signals of different amplitude. We start by introducing a reference signal of $\pm 1.5°$ to check the performance of the nominal controller K_{nom}. The results are shown in figure (5.16). The tracking is accurate and there is no saturation of the nominal controller, therefore there is no need to switch to the lower-gain controllers.

Following the same steps as in the stable case, we increase the amplitude of the reference signal to $\pm 3°$. Figure (5.17) shows the response of the aircraft using only the nominal controller: saturation occurs and the system gets unstable.

At this point, figures (5.18) and (5.19) justify the use of intermediate controllers instead of just switching between the K_{nom} and K_{safe} (the one designed to stand the predicted worst case disturbance). On one hand, figure (5.18) shows the nonlinear response of the aircraft by only switching between K_{nom} and K_{safe}. On the other

hand, figure (5.19) shows the nonlinear response by using the 5 controllers introduced before. Although saturation does not occur in any of the two situations, it can be clearly seen that the tracking in the second situation is much better than in the first one. More than tracking, in the plot with only K_{nom} and K_{safe} we make sure that the system does not get unstable.

Finally, figure (5.20) shows the response of the nonlinear aircraft to a $\pm 3.5^{\circ}$ doublet as the reference flight path angle, which is the worst-case scenario considered in the controllers design. We can see that the safe controller is not required and the tracking is good. This shows the conservatism of using the maximum peak value as an indication of the worst-possible disturbance: we are guaranteed that the controller will not saturate for this maximum value, but actually it may not saturate for a larger value. This scheduling technique takes advantage of this fact and does not switch until the controllers saturate, not when they are theoretically supposed to saturate.

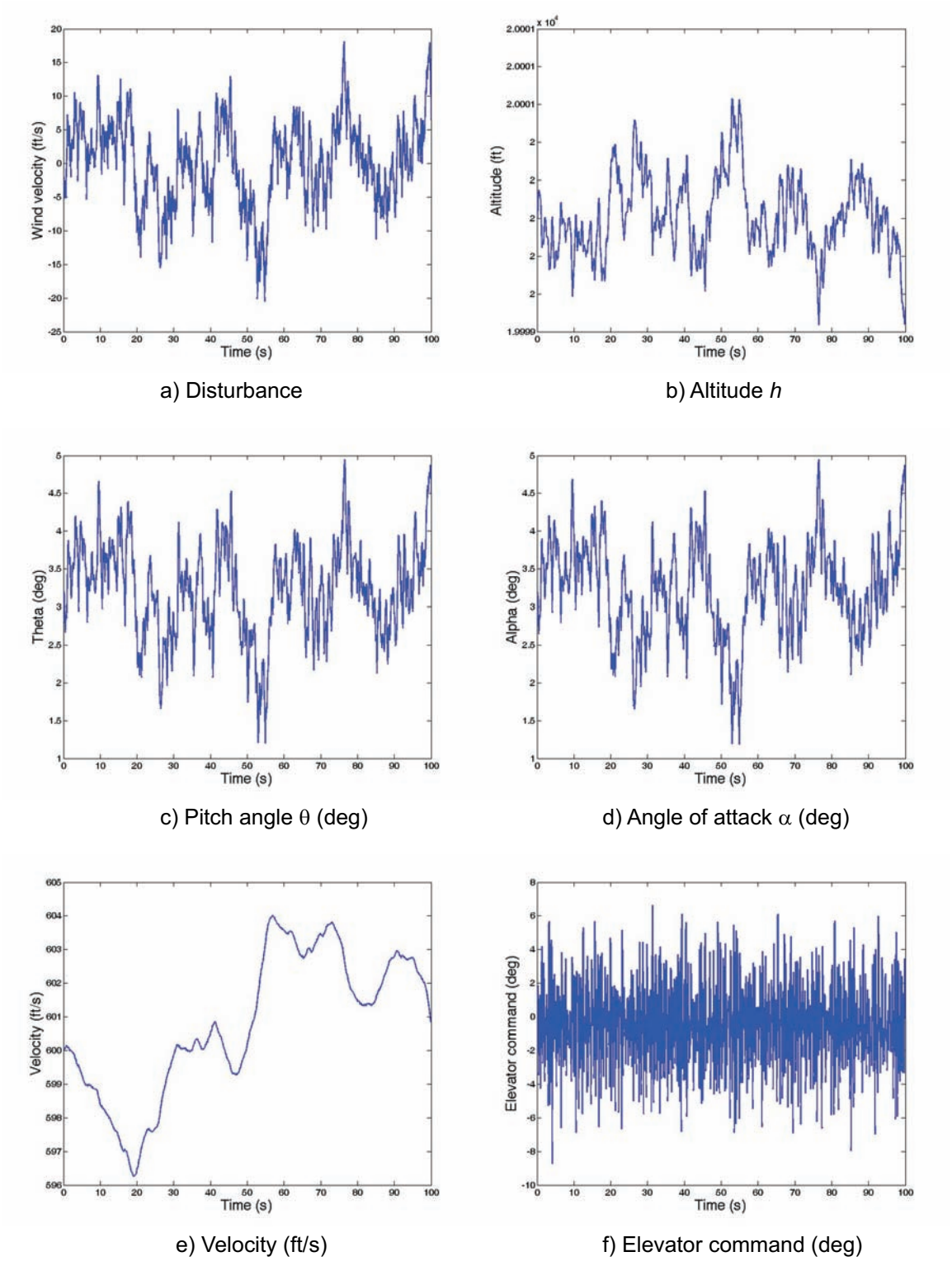

Figure 5.6: Plot of the wind velocity obtained from a moderate disturbance and the closed loop response (altitude) of the linear model of the aircraft to this disturbance

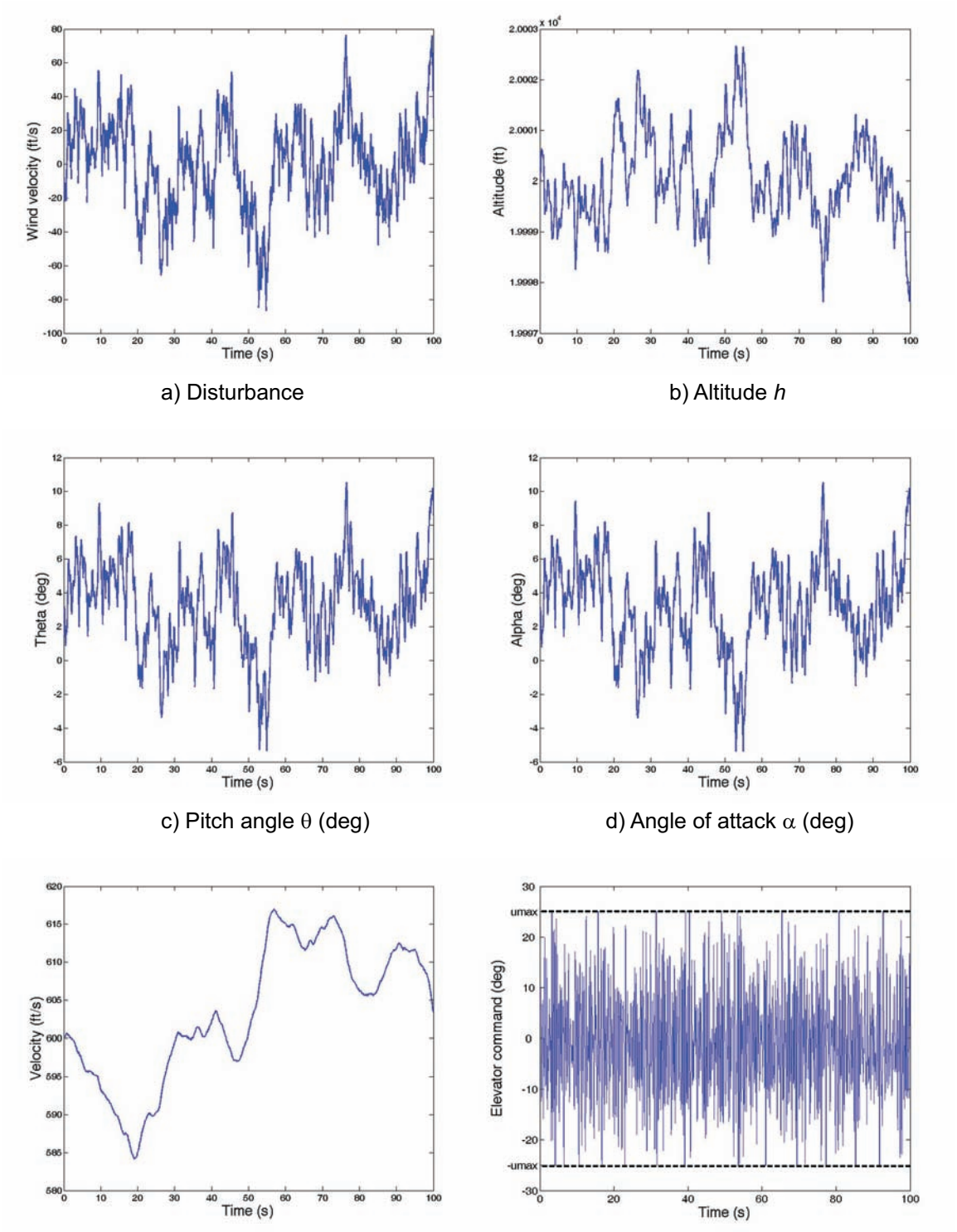

Figure 5.7: Plot of the wind velocity obtained from an extreme disturbance and the closed loop response (altitude) of the linear model of the aircraft to this disturbance

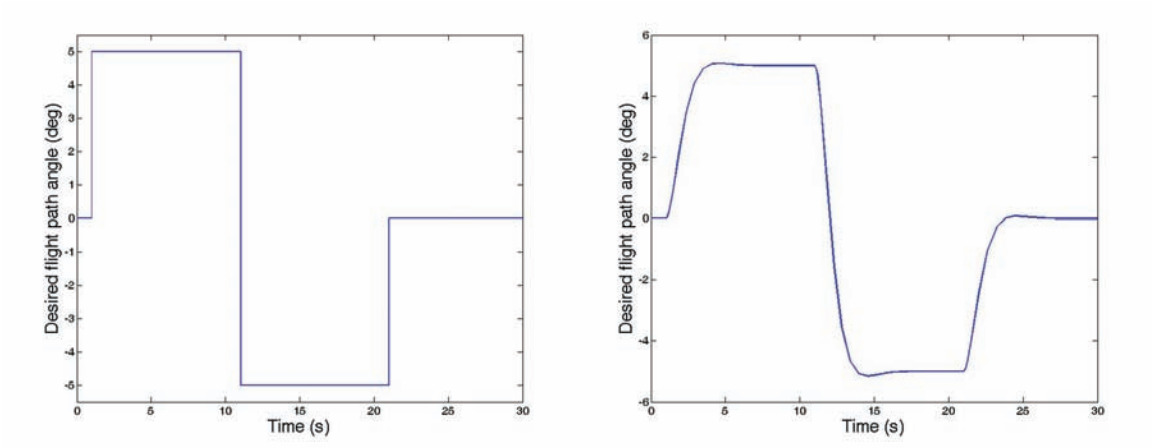

a) Commanded flight path angle γ_{cmd} B) Ideal flight path angle γ_{ideal}

Figure 5.8: Effect of the transfer function in (5.27) to the commanded flight path angle γ_{cmd} (the amplitude of γ_{cmd} may vary depending on the case of study)

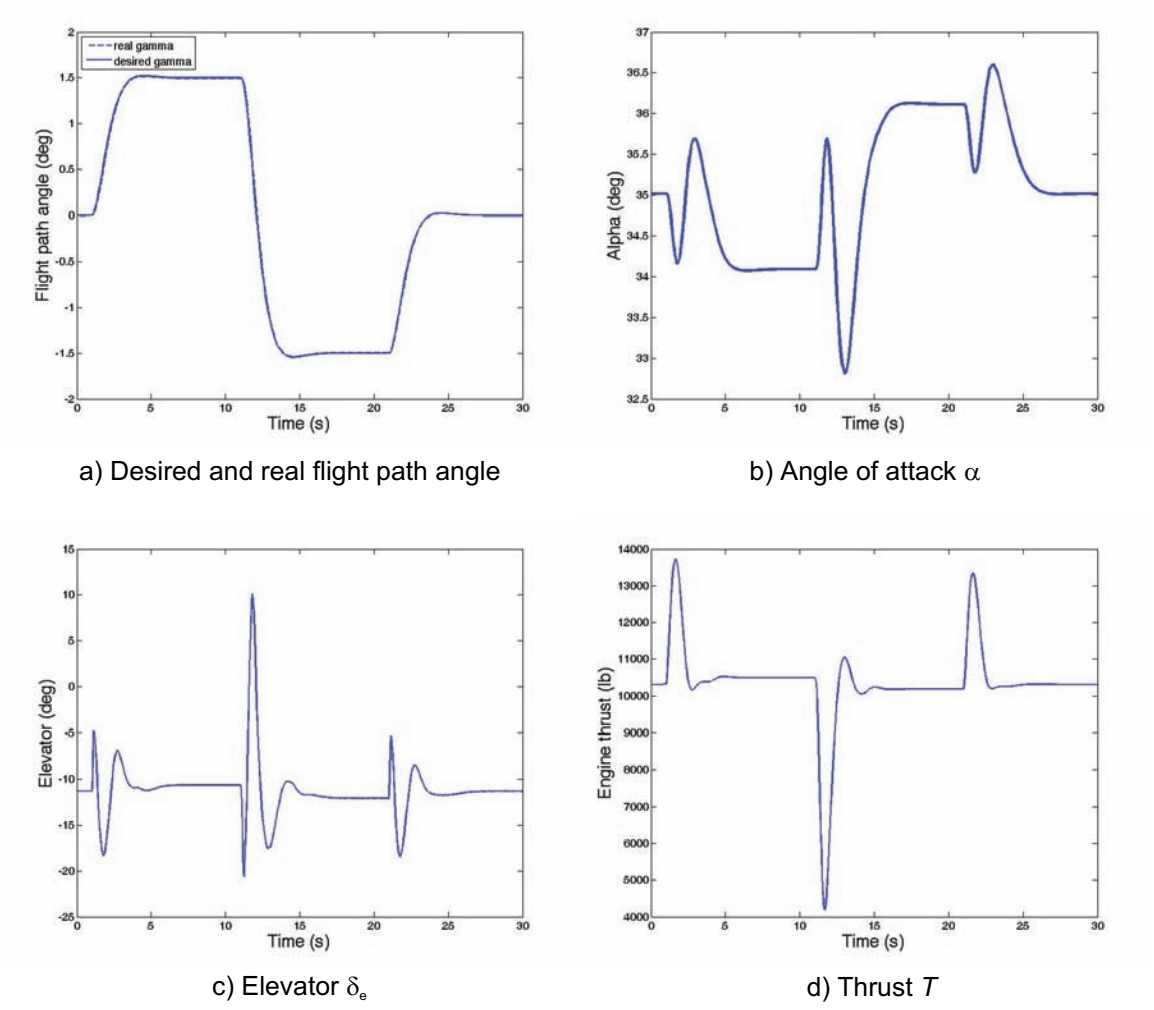

a) Desired and real flight path angle

b) Angle of attack α

c) Elevator δ_e

d) Thrust T

Figure 5.9: Nonlinear $\pm 1.5^\circ$ doublet response (stable case) with K_{nom}

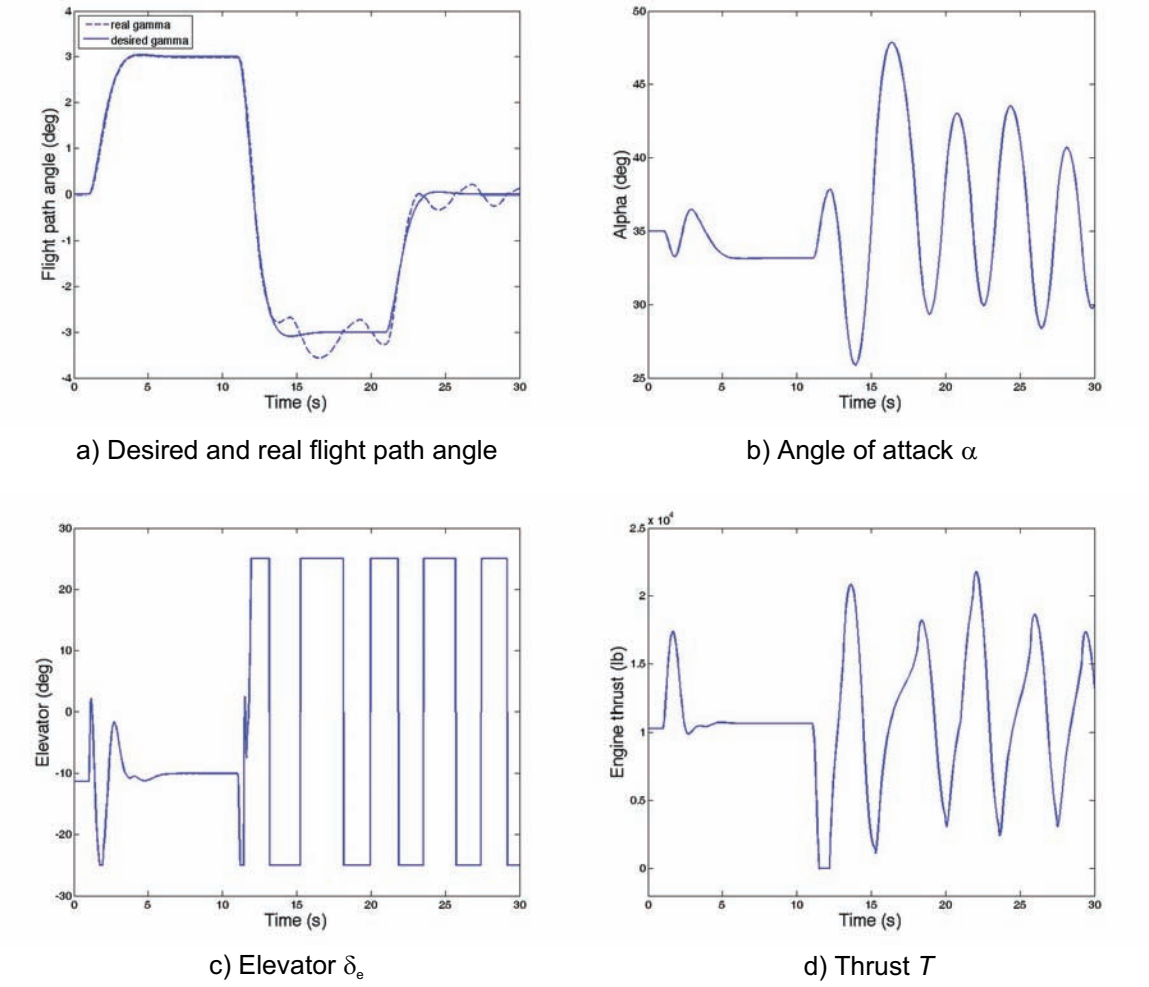

a) Desired and real flight path angle

b) Angle of attack α

c) Elevator δ_e

d) Thrust T

Figure 5.10: Nonlinear $\pm 3^\circ$ doublet response (stable case) with K_{nom}

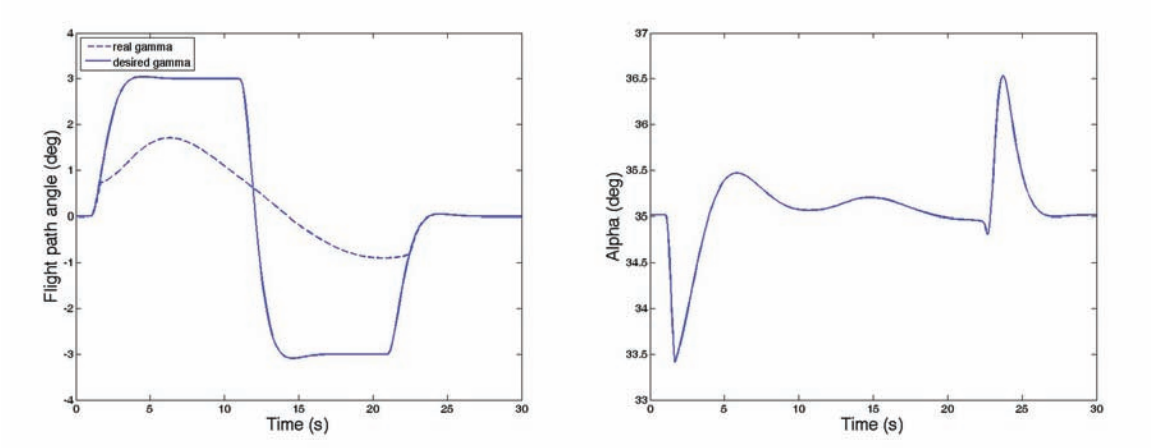

a) Desired and real flight path angle

b) Angle of attack α

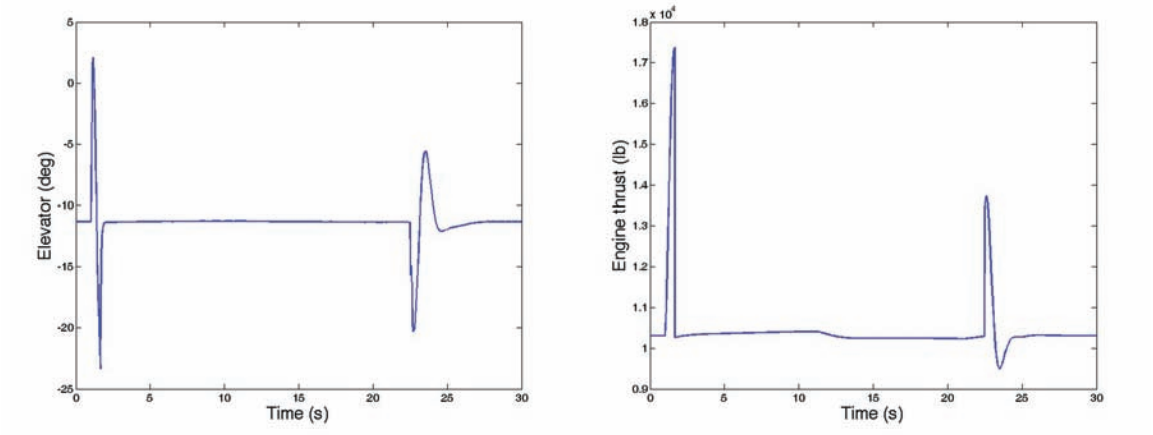

c) Elevator δ_e

d) Thrust *T*

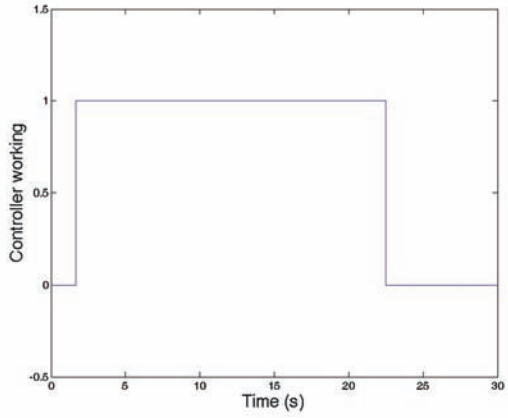

e) Controller working
(0=K_{nom}, 1=K_{safe})

Figure 5.11: Nonlinear $\pm 3^\circ$ doublet response (stable case) with K_{nom} and K_{safe}

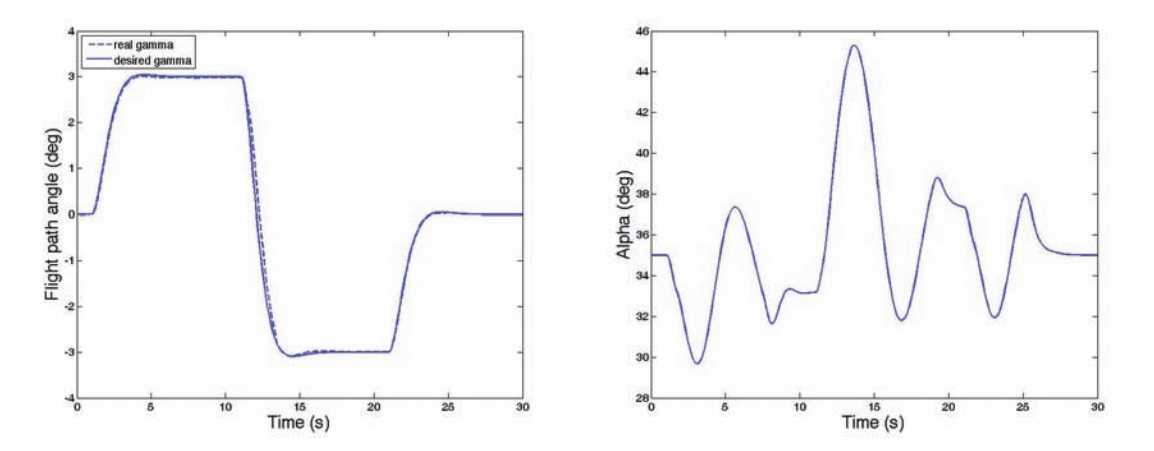

a) Desired and real flight path angle

b) Angle of attack α

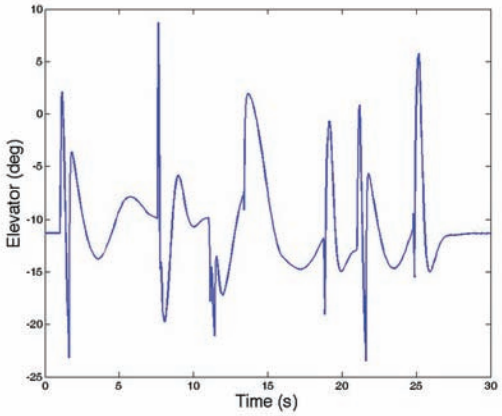

c) Elevator δ_e

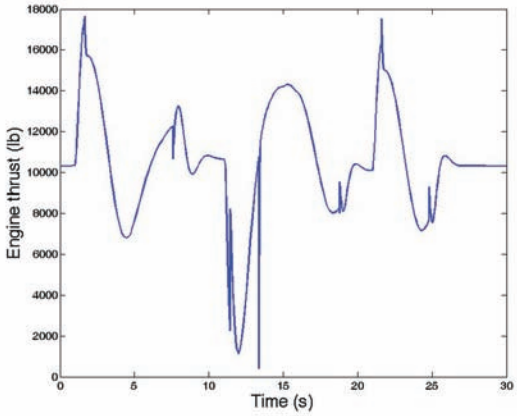

d) Thrust *T*

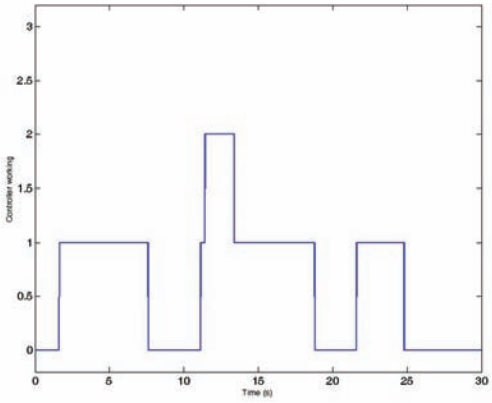

e) Controller working
(0=K_{nom}, 1=K_1, 2=K_2, 3=K_{safe})

Figure 5.12: Nonlinear $\pm 3^\circ$ doublet response (stable case) with K_{nom}, K_1, K_2 and K_{safe}

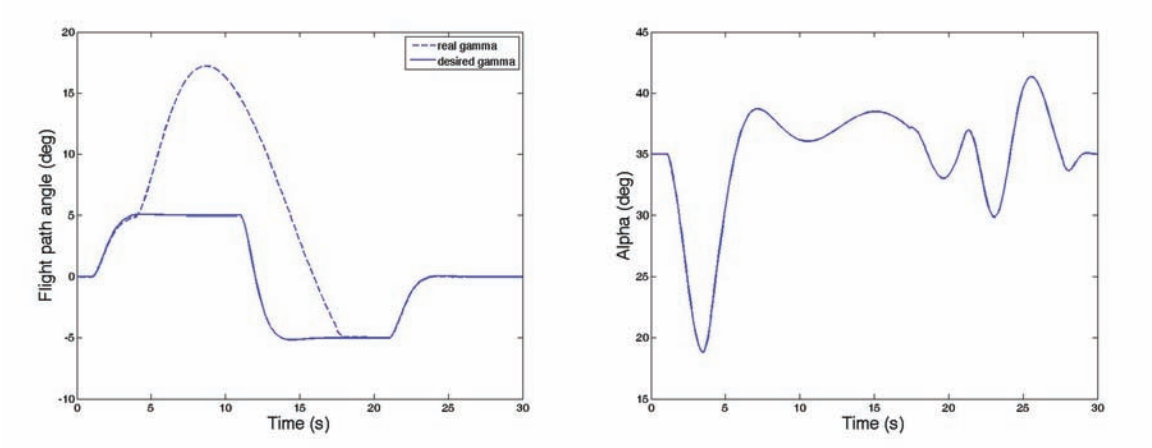

a) Desired and real flight path angle

b) Angle of attack α

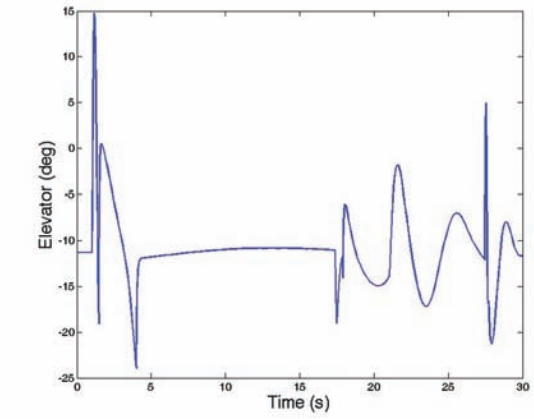

c) Elevator δ_e

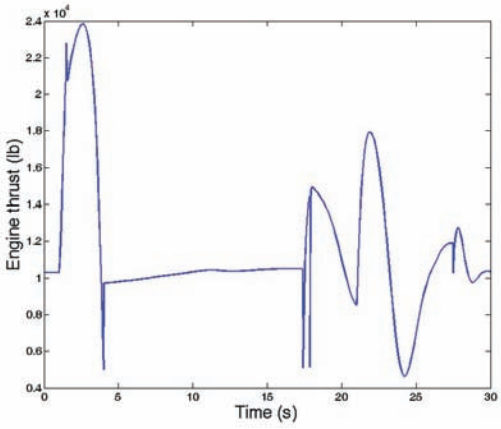

d) Thrust *T*

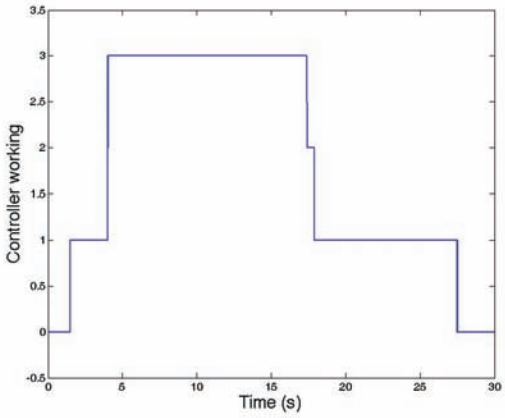

e) Controller working
(0=K_{nom}, 1=K_1, 2=K_2, 3=K_{safe})

Figure 5.13: Nonlinear $\pm 5^\circ$ doublet response (stable case) with K_{nom}, K_1, K_2 and K_{safe}

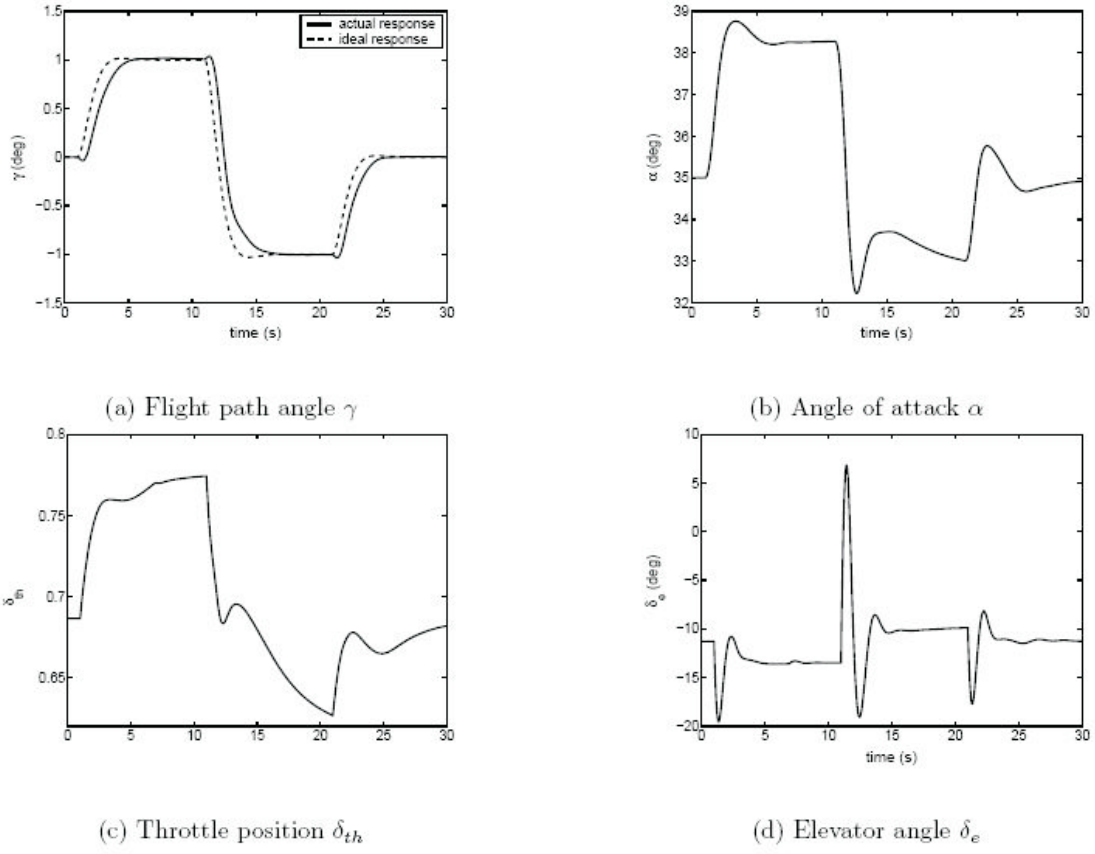

(a) Flight path angle γ

(b) Angle of attack α

(c) Throttle position δ_{th}

(d) Elevator angle δ_e

Figure 5.14: For comparison purposes: nonlinear $\pm 1^\circ$ doublet response (stable case) with an LTI nominal controller (extracted from [13])

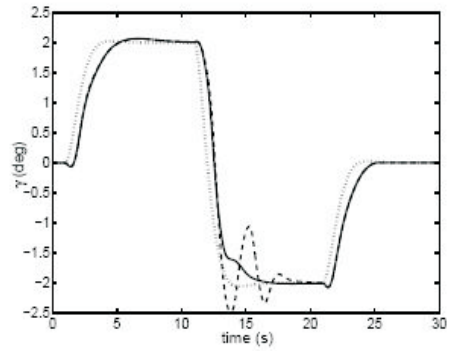

(a) Flight path angle γ

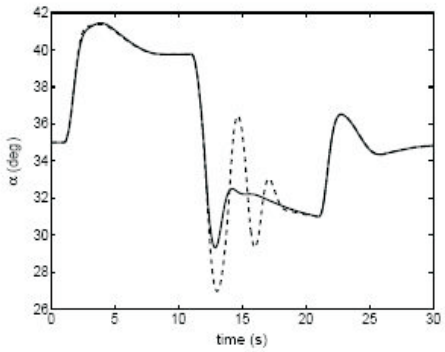

(b) Angle of attack α

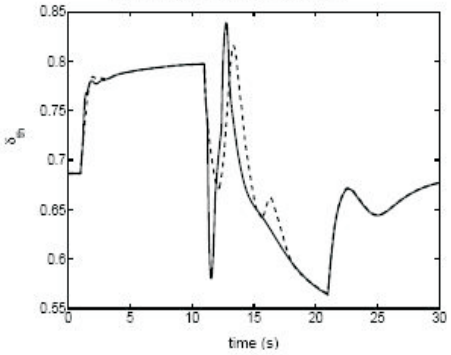

(c) Throttle position δ_{th}

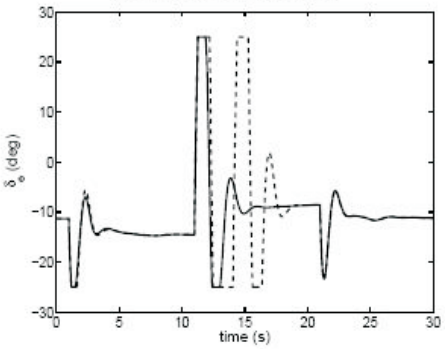

(d) Elevator angle δ_e

Figure 5.15: For comparison purposes: nonlinear $\pm 2^\circ$ doublet response (stable case) with/without an LTI antiwindup compensator (extracted from [13])

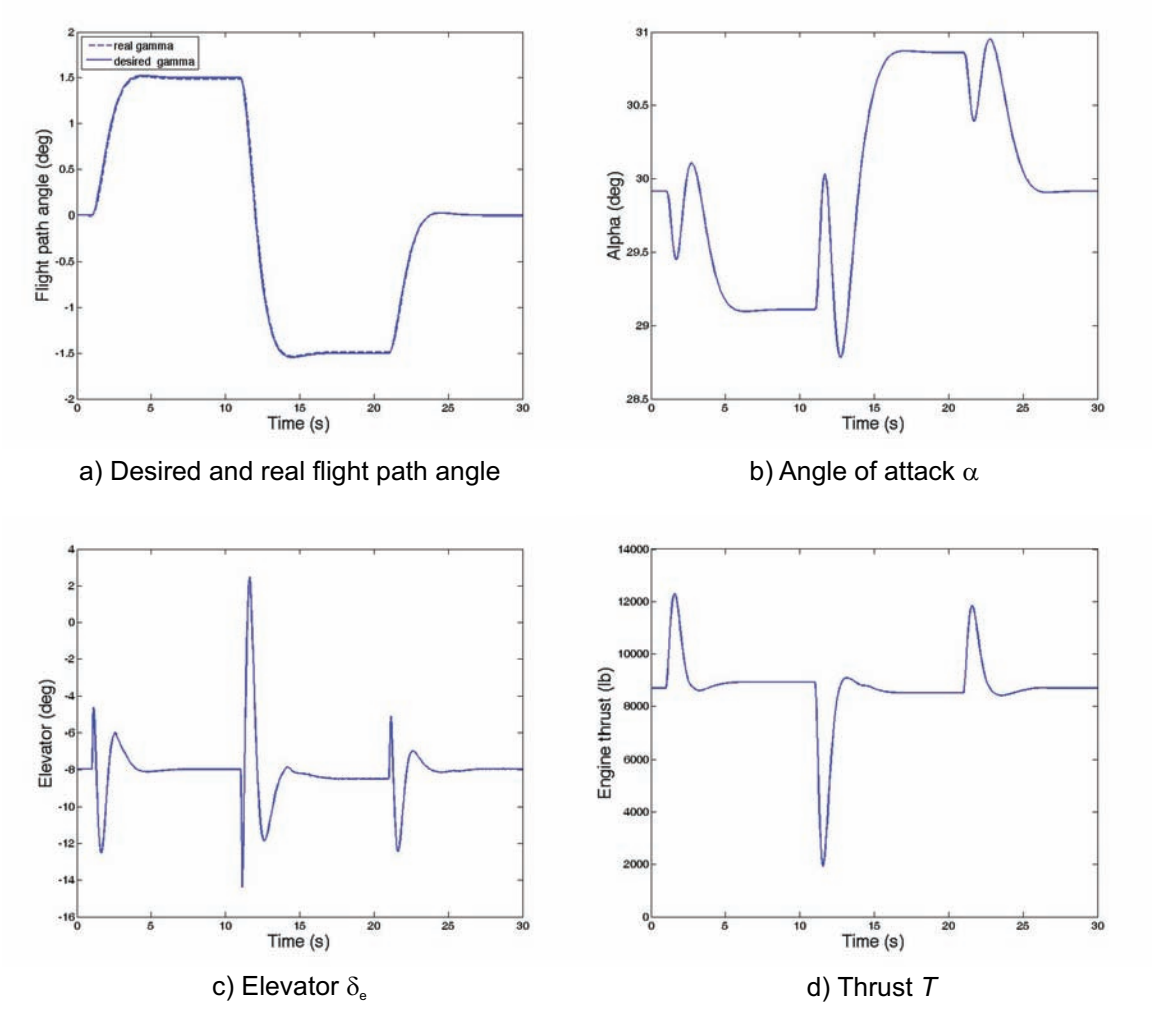

a) Desired and real flight path angle

b) Angle of attack α

c) Elevator δ_e

d) Thrust T

Figure 5.16: Nonlinear $\pm 1.5°$ doublet response (unstable case) with K_{nom}

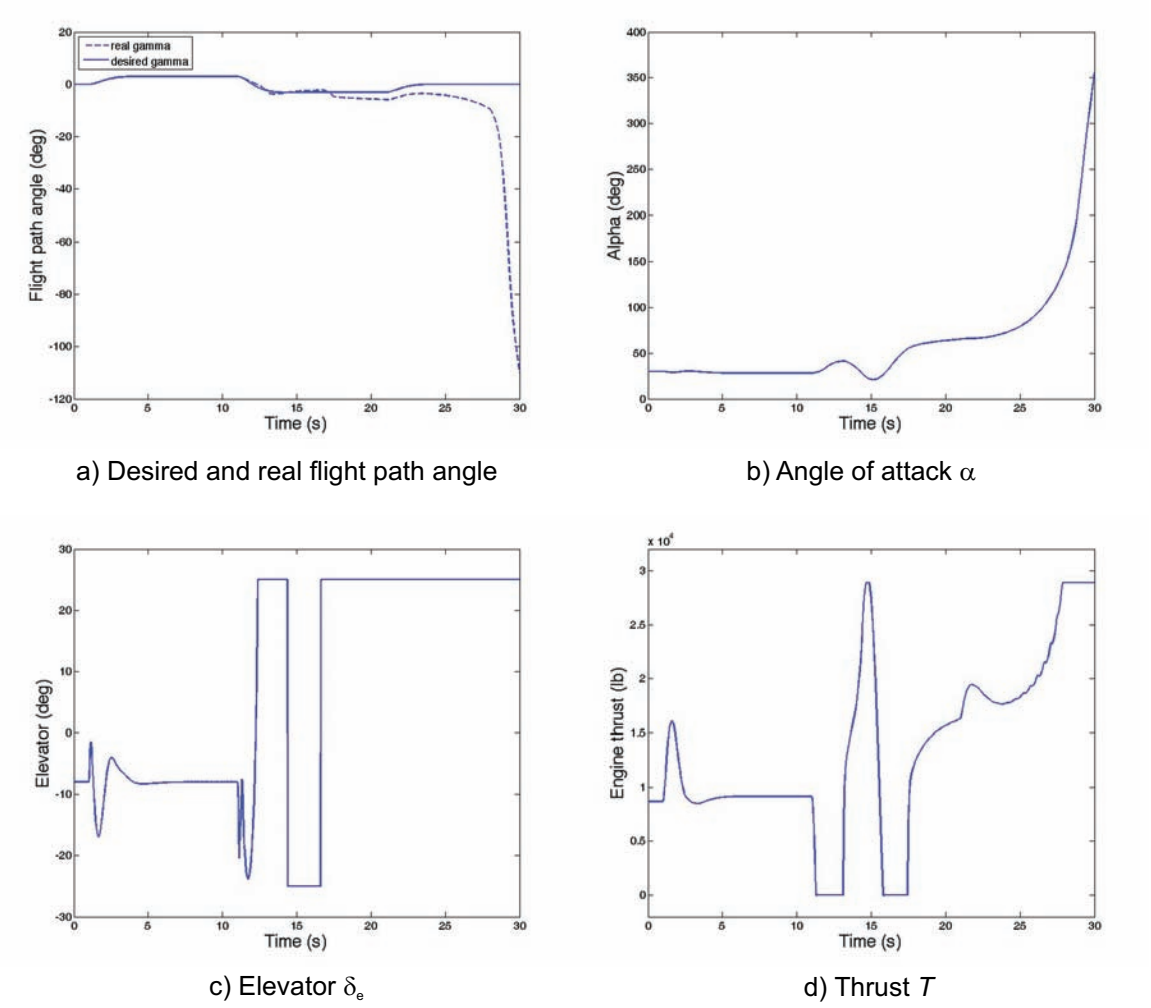

a) Desired and real flight path angle

b) Angle of attack α

c) Elevator δ_e

d) Thrust *T*

Figure 5.17: Nonlinear $\pm 3^\circ$ doublet response (unstable case) with K_{nom}

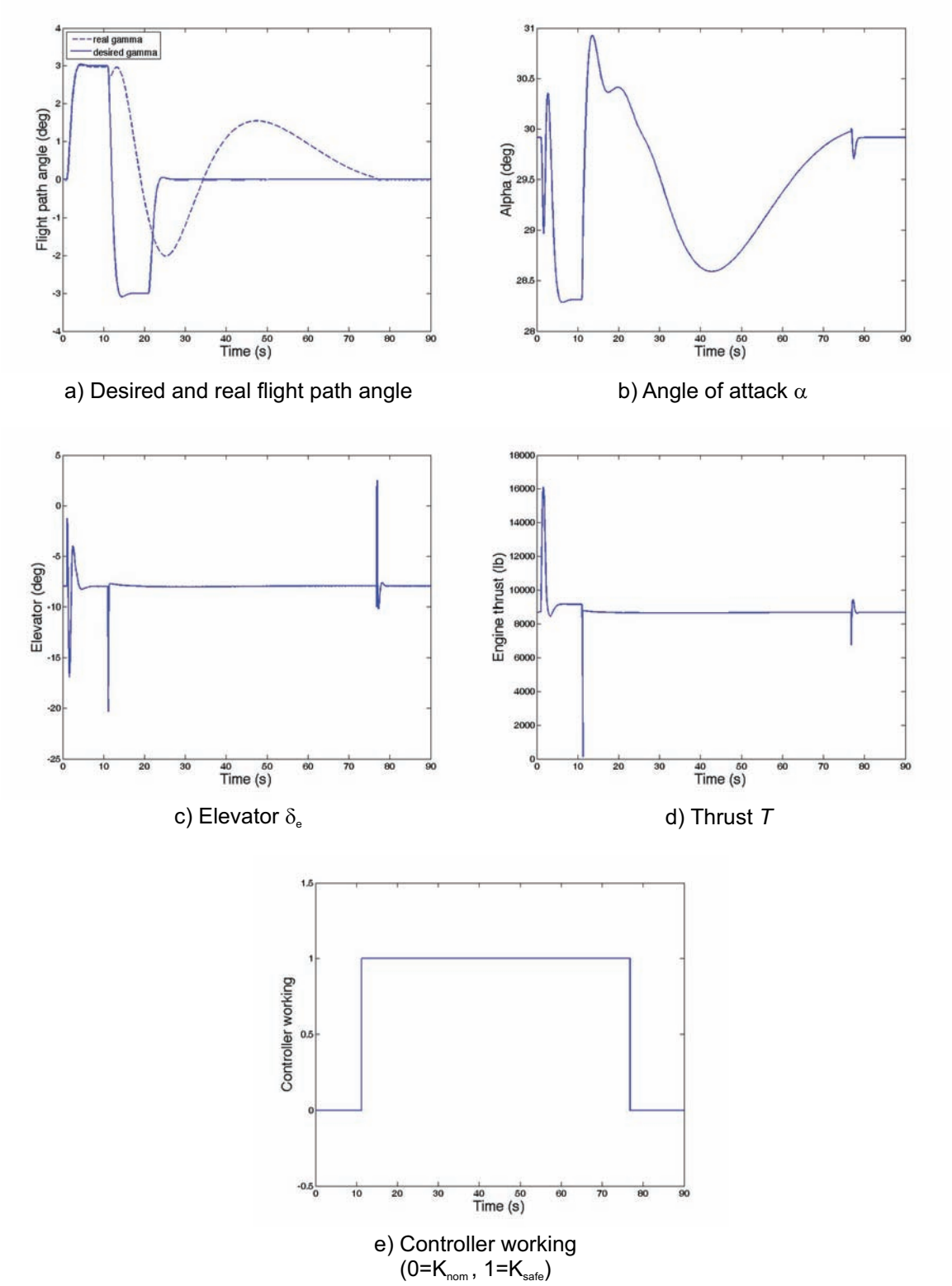

a) Desired and real flight path angle

b) Angle of attack α

c) Elevator δ_e

d) Thrust T

e) Controller working
(0=K_{nom}, 1=K_{safe})

Figure 5.18: Nonlinear $\pm 3^\circ$ doublet response (unstable case) with K_{nom} and K_{safe}

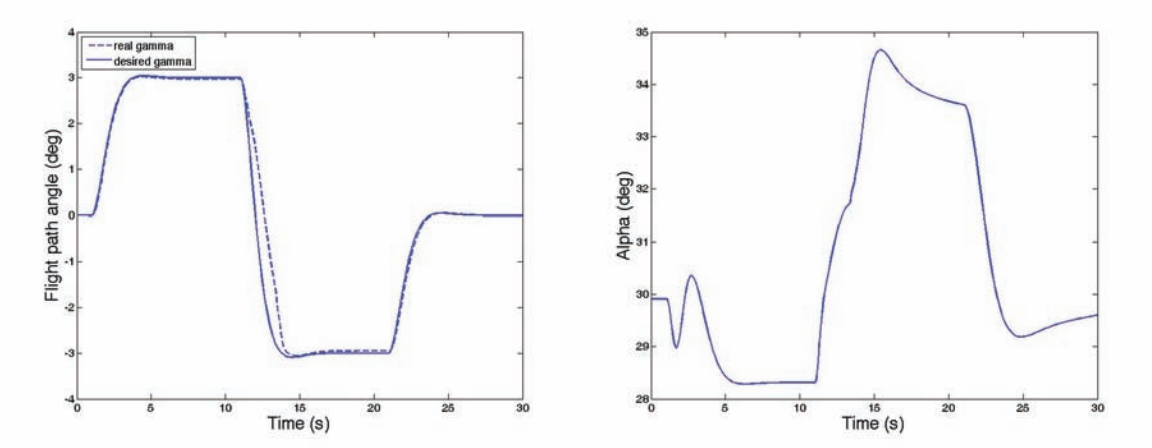

a) Desired and real flight path angle

b) Angle of attack α

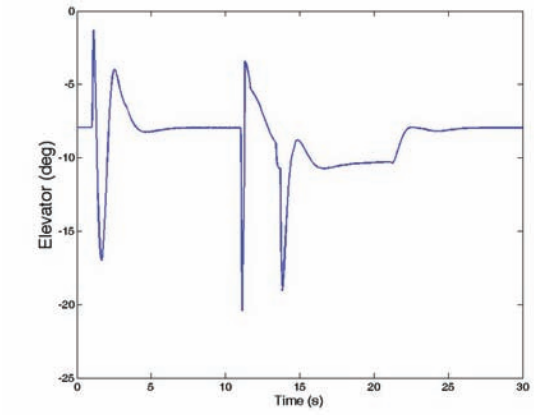

c) Elevator δ_e

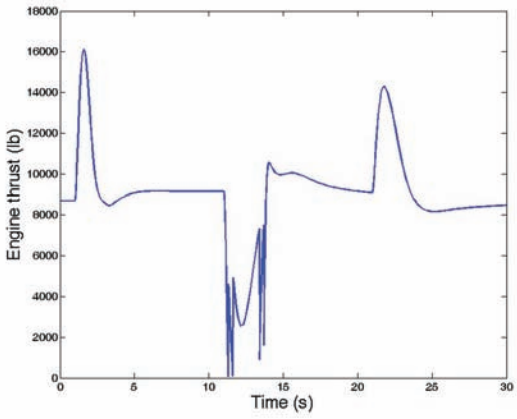

d) Thrust *T*

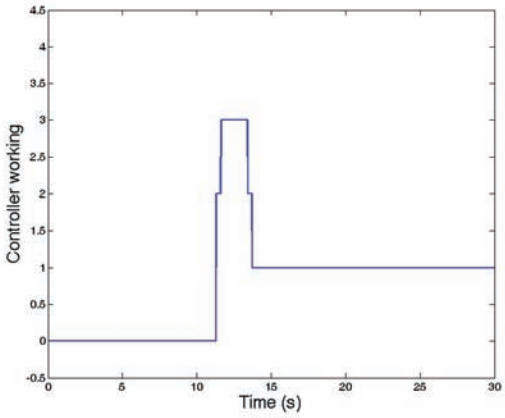

e) Controller working
(0=K_{nom}, 1=K_1, 2=K_2, 3=K_3, 4=K_{safe})

Figure 5.19: Nonlinear $\pm 3^\circ$ doublet response (unstable case) with K_{nom}, K_1, K_2 and K_{safe}

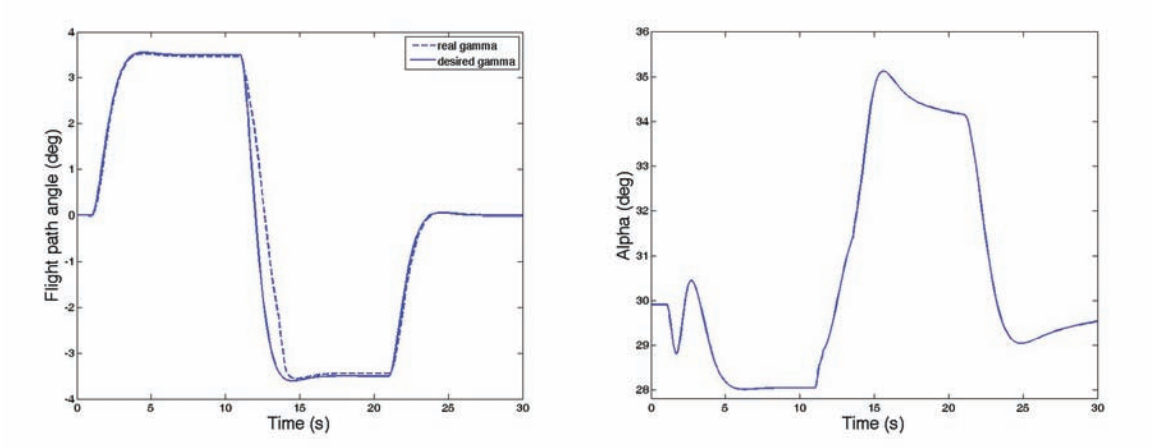

a) Desired and real flight path angle

b) Angle of attack α

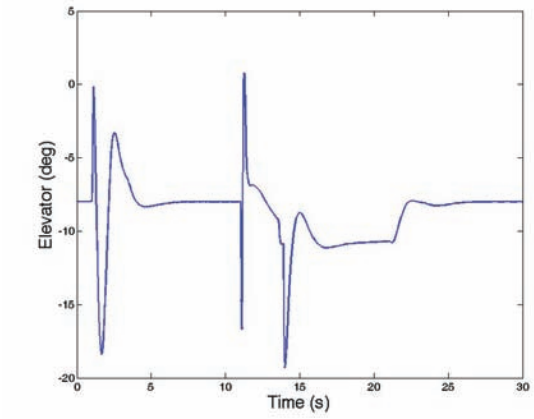

c) Elevator δ_e

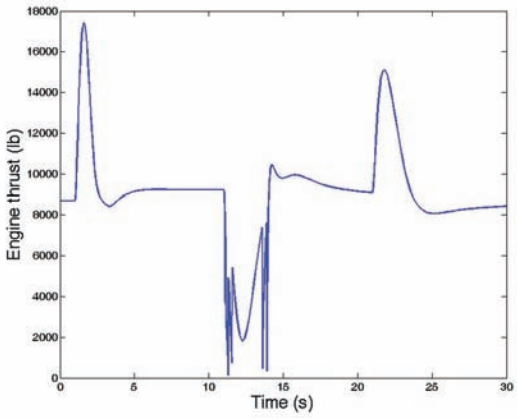

d) Thrust *T*

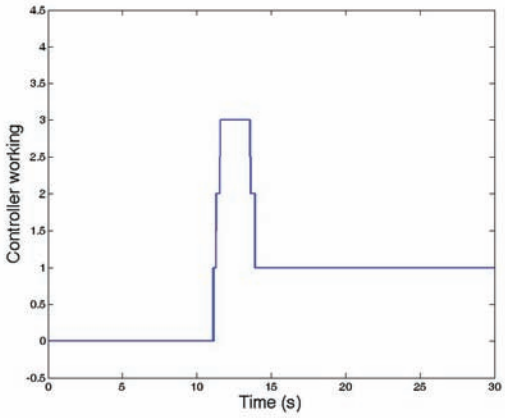

e) Controller working
(0=K_{nom}, 1=K_1, 2=K_2, 3=K_3, 4=K_{safe})

Figure 5.20: Nonlinear $\pm 3.5^\circ$ doublet response (unstable case) with K_{nom}, K_1, K_2 and K_{safe}

Chapter 6

Conclusions

The structure of this study has mainly followed the structure of [13] to be able to qualitatively compare the results obtained using a regular anti-windup approach and the new technique combining both anti-windup and direct approach methods.

The nonlinear longitudinal model of an $F-16$ aircraft has been developed and implemented in this thesis. Although it has not been used, the model includes the possibility to vector the thrust, which probably can improve the performance of the aircraft in the high angle of attack region. To be able to use linear techniques in the design of the controller, this model has been linearized and validated about different equilibrium conditions. The results of the validation process showed that the linear model is a good representation of the nonlinear model as long as changes in the aerodynamic behavior of the aircraft are small, that is, as long as changes in the angle of attack are small and the aircraft stays outside the transient region between low and high angle of attack behavior (around $20°$).

The main problem of using linear methods to design the controllers is that they will only work while the linear model accurately represents the real nonlinear model, which is basically in a small region about the equilibrium condition used in the linearization process. This drawback is especially important in flight control system design since

the aircraft must operate in very different conditions (low-high altitude, low-high angle of attack) in which the behavior of the aircraft can dramatically change. One option to overcome this problem may be the concept of linear parameter varying systems (LPV). In this thesis it has been shown that an approximated LPV model of the aircraft can be easily obtained about a small region defined by different equilibrium points and that this approximated LPV model adequately represents the behavior of the nonlinear model inside that zone. By adequately choosing the equilibrium points that define the LPV region in which the aircraft can operate, e.g. by choosing more points where the behavior of the aircraft changes the most and less points where the behavior of the aircraft is quite constant, probably most of the operating range of the aircraft can be covered. That may simplify the controller design process since we can design the controllers for the whole LPV region instead of designing them point by point.

Also, the method combining the anti-windup and the direct approach methods has been discussed. The main source of conservatism in the direct approach has been pointed out: designing the controller taking into account the worst case scenario (worst case disturbance) even though it may never occur produces very conservative results with a poor performance. To solve this problem a scheduling approach has been used, designing different controllers taking into account different levels of disturbance up to the worst case disturbance. Therefore, the system is always using the highest gain controller available for the level of disturbance that the aircraft is facing and performance is greatly improved. In addition, an extension of the combined method to include the tracking problem has been shown.

Different results have been obtained from the simulations. In the altitude hold case, we have not been able to apply the combined technique to design the safe controllers because of the conservatism associated to the use of the worst peak value as a measure of the disturbance. The predicted value of the disturbance (using LMI analysis) that the nominal controller was able to stand was much smaller than the value at which the nominal controller actually saturated. This actual value of the disturbance was almost the maximum disturbance level that can be obtained from the wind disturbance model used, which means that increasing it would lead to unrealistic

results (exaggerated velocity of the wind). This case was then dropped in order to focus the efforts on the tracking case.

The results on the tracking case have been very positive. The anti-windup concept included in the combined technique allows the nominal controller to work most of the time, since we do not switch until it is saturated. Given the fact that this controller has the desired performance and properties, the more we use it the better the overall performance. Also, the scheduling concept has been very useful to improve the overall performance of the system, since it allowed to use more aggressive controllers depending on the level of the disturbance instead of just using a low-gain safe controller anytime that the nominal controller was saturated. The results obtained from the stable case can be compared to the ones in [13] showing a similar degree of performance. In addition, using this technique has allowed us to check an unstable case showing that the results are also quite desirable.

Further work in this area would be to use output feedback instead of state feedback, which would take into account that not all the states of the system may be available. In addition, using output feedback would allow to consider also rate limits in the controller signal, specially important since the results obtained in this thesis show steep command signals that may be problematic when considering rate saturation.

Bibliography

[1] Francesco Amato. *Robust Control of Linear Systems Subject to Uncertain Time-Varying Parameters*. Springer, first edition, 2005.

[2] Francesco Amato, Raffaele Iervolino, Stefano Scala, and Leopoldo Verde. Category ii pilot-in-the-loop oscillations analysis from robust stability methods. *Journal of Guidance, Control and Dynamics*, pages 531–538, 2001.

[3] Gary Balas and Andres Marcos. Linear parameter varying modeling of the boeing 747-100/200 longitudinal motion. AIAA Guidance, Navigation, and Control Conference and Exhibit, Montreal, Canada, 2001.

[4] C. Barbu, R. Reginatto, A.R. Teel, and L. Zaccarian. Anti-windup design for manual flight control. Proceedings of the American Control Conference San Diego, California, 1999.

[5] Stephen Boyd, Laurent El Ghaoui, Eric Feron, and Venkataramanan Balakrishnan. *Linear Matrix Inequalities in System and Control Theory*. Society for Industrial and Applied Mathematics (SIAM), first edition, 1994.

[6] Stacey Gage. Creating a unified graphical wind turbulence model from multiple specifications. AIAA Modeling and Simulation Technologies Conference and Exhibit, Austin, TX, 2003.

[7] Pascal Gahinet, Arkadi Nemirovski, Alan J. Laub, and Mahmoud Chilali. *LMI Control Toolbox*, first edition, 1995.

[8] Faryar Jabbari and Jin-Hoon Kim. A scheduling approach for tracking of general signals. 2006.

[9] Vikram Kapila and Karolos M. Grigoriadis et altri. *Actuator Saturation Control*. Control Engineering Series, first edition, 2002.

[10] Emre Köse and Faryar Jabbari. Scheduled controller for linear systems with bounded actuators. *Automatica*, 39:1377–1387, 2003.

[11] I. Emre Köse. Parameter-varying control techniques applied to nonlinear systems: a general framework. 2000.

[12] Nguyen L.T., Ogburn M.E., Gillert W.P., and et altri. Simulator study of stall/post-stall characteristics of a fighter airplane with relaxed longitudinal static stability. NASA Technical Paper 1538, 1979.

[13] Bei Lu. *Linear Parameter-Varying Control of An F-16 Aircraft at High Angle of Attack*. PhD thesis, North Carolina State University, 2004.

[14] Eric F. Mulder, Mayuresh V. Kothare, and Manfred Morari. Multivariable anti-windup controller synthesis using linear matrix inequalities. *Automatica*, pages 1407–1416, 2001.

[15] William C. Reigelsperger and Siva S. Banda. Nonlinear simulation of a modified f-16 with full-envelope control laws. *Control Engineering Practice*, pages 309–320, 1998.

[16] Jan Roskam. *Airplane flight dynamics and automatic flight controls*. Roskam Aviation and Engineering Corporation, first edition, 1979.

[17] Solmaz Sajjadi-Kia and Faryar Jabbari. Use of scheduling for anti-windup controller design. 2007.

[18] Brian L. Stevens and Frank L. Lewis. *Aircraft Control and Simulation*. John Wiley and Sons INC., second edition, 2003.

[19] Fen Wu, Ashok Gopalarathnam, and Sungwan Kim. Post-stall aerodynamic modeling and gain-scheduled control design. AIAA Guidance, Navigation, and Control Conference and Exhibit, San Francisco, CA, 2005.

[20] Zhongwei Yu, Huitang Chen, and Peng yung Woo. Gain scheduled linear parameter varying h_∞ control based on lmi approach for a robotic manipulator. *Journal of Robotic Systems*, pages 585–593, 2002.